A STUDY OF MESOSCALE EDDIES, THE AGULHAS CURRENT AND THE EVOLUTION OF ITS MEANDERS USING SATELLITE OBSERVATIONS AND NUMERICAL MODELLING EXPERIMENTS

Laura Braby

January 2019

Thesis presented for the degree of

DOCTOR OF PHILOSOPHY

In the Department of Oceanography

UNIVERSITY OF CAPE TOWN

SUPERVISORS

Dr Björn Backeberg

EGI Foundation, Amsterdam, Netherlands

Nansen-Tutu Centre for Marine Environmental Research, Department of Oceanography, University of Cape Town, Cape Town, South Africa

Nansen Environmental and Remote Sensing Center, Bergen, Norway

Dr Marjolaine Krug

Department of Oceanography, University of Cape Town, Cape Town, South Africa

Nansen-Tutu Centre for Marine Environmental Research, Department of Oceanography, University of Cape Town, Cape Town, South Africa

Earth Observation Research Group, Council for Scientific and Industrial Research, Natural Resources and the Environment, Cape Town, South Africa

Prof. Chris Reason

Department of Oceanography, University of Cape Town

PLAGIARISM DECLARATION

Except where I have otherwise stated, the work presented here is my own.

Signed by candidate

Laura Braby

08 January 2019

DECLARATION: INCLUSION OF PUBLICATION

I confirm that I have been granted permission by the University of Cape Town's Doctoral Degrees Board to include the following publication in my PhD thesis, and where co-authorships are involved, my co-authors have agreed that I may include the publication:

Braby, L., B. C. Backeberg, I. Ansorge, M. J. Roberts, M. Krug, and C. J. C. Reason (2016), Observed eddy dissipation in the Agulhas Current, *Geophys. Res. Lett.*, 43, 8143–8150, doi:10.1002/2016GL069480.

Signed by candidate

Laura Braby

08 January 2019

ACKNOWLEDGEMENTS

Firstly, I am extremely grateful to my supervisors Dr Björn Backeberg, Dr Marjolaine Krug and Prof. Chris Reason for their support throughout my Ph.D. Björn, thank you for the many, many hours you have given up to ensure that I finish my Ph.D. Your guidance, time, and enthusiasm for my thesis have been invaluable to me! Marjolaine, your ideas and constructive feedback have challenged me to produce results of a much higher quality than I ever thought possible. Thank you for always being available to meet with me! Chris, I have really respected your opinion and input into my thesis, particularly in the writing up of my manuscript. I am so thankful to have received direction from someone so experienced.

Over the past few years I have received advice and assistance from so many people, which has hugely impacted the outcome of my thesis. I am especially appreciative of the help I received from Dr Julie D'eshayes, Dr Serena Illig, Emeline Cadier, Dr Pierrick Penven, Dr Jenny Veitch, Dr Issufo Halo, Prof. John Field, Dr Luke Gregor and Marc de Vos.

I am so thankful to my office mates Dr Fehmi Dilmahamod, Dr Neil Malan, Daniel Schilperoort, Michael Hart-Davis, Herman Luyt and Bafana Gweba for all of the coffee breaks, for your suggestions and influence over my work, and for your understanding of just how difficult Ph.D. can be! Thank you for your friendship and for putting up with me!

I am grateful to the Centre for Renewable and Sustainable Energy Studies, Stellenbosch, for their funding of my Ph.D. This work is based on research supported in part by the National Research foundation of South Africa (Grant Number 11205). I would also like to acknowledge the Nansen-Tutu Centre for their support during my Ph.D.

The simulations in this thesis were performed on resources provided by UNINETT Sigma2 - the National Infrastructure for High Performance Computing and Data Storage in Norway.

Finally, this would not have been possible without the unconditional support of my friends and family. I am exceedingly grateful for your encouragement and patience. Thank you!

ABSTRACT

The Agulhas Current is the strongest western boundary current in the Southern Hemisphere and plays an important role in the exchange of heat and salt between the Indian and South Atlantic Ocean basins, thereby affecting global climate. The variability in the northern Agulhas Current is influenced by both cyclonic and anti-cyclonic mesoscale eddies, originating from the Mozambique Channel and south of Madagascar (known as source region eddies) and which propagate toward the offshore edge of the Agulhas Current. Using a combination of an eddy-tracking data set with *in-situ* surface drifter observations and altimetry-derived geostrophic currents, it is shown that source region eddies dissipate upon approaching the Agulhas Current. Their entrainment into the Agulhas Current affects its mean velocity and offshore position through a transfer of momentum, with anti-cyclonic eddies consistently increasing the Agulhas Current's velocity by 0.16 ± 0.17 $m.s^{-1}$. In contrast, entrainment of cyclonic eddies results in a decrease in velocity by 0.13 ± 0.16 $m.s^{-1}$ and shifting the current up to 144 ± 85 km offshore. These velocity anomalies propagate downstream at rates of 44 $km.d^{-1}$ (anti-cyclonic eddies) and 23 $km.d^{-1}$ (cyclonic eddies). Whilst existing numerical models are successfully able to capture many aspects of the Agulhas Current, many models are unable to accurately represent the observed eddy dissipation and interaction processes, affecting our understanding of mesoscale variability within in the current. In this study, we compare two simulation experiments in a regional Hybrid Coordinate Ocean Model (HYCOM), where we change the wind forcing, and using an eddy tracking algorithm assess the local effect of the changed wind stress on source region eddies and their interaction with the northern Agulhas Current. There is an overall reduction in eddy kinetic energy (EKE) of 33% over the Agulhas Current domain. Changes in eddy pathways, properties and energy conversion terms, resulting from the change in forcing from absolute to relative winds (the wind speed relative to the current speed) have resulted in significantly different mesoscale eddies in the regional HYCOM. The effects of the change in wind forcing on the variability within the Agulhas Current were examined and the differences between the two simulations

were found to be very small. Finally, the evolution of meanders in the Agulhas Current, including the properties and dissipation of smaller meanders as well as mesoscale Natal Pulses type meanders, were assessed using both HYCOM experiments and compared to satellite observations. The representation of smaller meanders (under 50km in size) improved with the changed in wind forcing. However, larger Agulhas Current meanders (greater than or equal to 50km) which previously occurred too frequently in the regional HYCOM, are now too infrequent in the regional HYCOM, with an average of 1.1 meanders occurring each year. A decrease in the frequency of larger meanders was observed from the location offshore of Port Edward (30.22° E, 31.05° S) to the region of the ACT array (27.48° E, 33.35° S), in the satellite data as well as both model experiments, indicating that some of the meanders have dissipated and that both regional HYCOM models are able to resolve this.

TABLE OF CONTENTS

LIST OF FIGURES **11**

LIST OF TABLES **18**

CHAPTER 1: **INTRODUCTION** **19**

1.1 The Role of the Agulhas Current 20

1.2 Mozambique Channel Eddies...22

1.3 Madagascar Eddies 23

1.4 Natal Pulses...25

1.5 Mesoscale Variability in Numerical Models 26

1.6 Objectives 27

1.7 Structure of Thesis 28

CHAPTER 2: COMPARISON OF EDDY TRACKING METHODS AND MODEL DESCRIPTION... **29**

2.1 A comparison of two eddy-tracking algorithms in the source region of the Agulhas Current 29

2.1.1 Introduction 29

2.1.2 Data and Methods 29

2.1.2.1 The Chelton eddy-tracking algorithm 30

2.1.2.2 The Penven eddy-tracking algorithm..32

2.1.3 Results..35

2.1.3.1 Case Studies 38

2.1.3.2 Eddy properties...40

2.1.4 Discussion and Conclusion 43

2.2 The Hybrid Coordinate Ocean Model **44**

2.2.1 Absolute and relative wind forcing experiments 49

CHAPTER 3: OBSERVED EDDY DISSIPATION IN THE AGULHAS CURRENT................ **51**

3.1 Introduction 51

3.2 Data and Methods 53
3.3 Results and Discussion 58
3.4 Conclusion..68

CHAPTER 4: UNDERSTANDING THE IMPACT OF CHANGING WIND STRESS ON SIMULATED AGULHAS CURRENT SOURCE REGION EDDY CHARACTERISTICS IN HYCOM 69
4.1 Introduction 69
4.1.2 Thermal Feedback...71
4.1.3 The Impact of Current Feedback on Coupled Models 71
4.1.4 The Effects of Current Feedback on the Agulhas Current System 73
4.2 Data..76
4.2.1 The Hybrid Coordinate Ocean Model 76
4.2.2 Absolute and Relative Wind Forcing Experiments 76
4.2.3 Satellite altimetry data...76
4.2.4 Eddy tracking algorithm 77
4.3 Methods..78
4.3.1 Kinetic energy 78
4.3.2 Energy Conversion Terms 80
4.3 Results..81
4.3.1 Winds and wind stress 81
4.3.2 Kinetic energy 85
4.3.3 Eddy pathways 95
4.3.4 Energy Conversion terms 108
4.4 Discussion 110
4.5 Summary and Conclusion..115

CHAPTER 5: THE EVOLUTION OF MEANDERS IN THE AGULHAS CURRENT FROM HYCOM AND SATELLITE OBSERVATIONS.. 119
5.1 Introduction 119
5.1.1 The interaction of Natal Pulses with shelf topography...........................120
5.1.2 The downstream impacts of Agulhas Current meanders........................120

5.1.3 Improving the simulation of Natal Pulses in numerical models..............121
5.2 Data..........123
5.2.1 The Hybrid Coordinate Ocean Model..........123
5.2.2 Observations (in-situ and satellite data)..........124
5.2.2.1 ACT data..........124
5.2.2.2 ADCP data..........125
5.2.2.3 Aviso Data..........127
5.2.2.4 GlobCurrent Data..........127
5.3 Methods..........128
5.3.1. Principal Component Analysis..........128
5.3.2 Transects..........128
5.3.3 Identifying the position of the Agulhas Current core to characterize meanders..........129
5.3.4 Composite plots..........131
5.4 Results..........131
5.4.1 Variability within the Agulhas Current..........131
5.4.2 The evolution of meanders in the Agulhas Current..........134
5.5 Discussion..........139
5.6 Conclusion..........143

CHAPTER 6: SYNTHESIS..........144
6.1 Key Findings..........144
6.1.1 Chapter 3..........144
6.1.2 Chapter 4..........144
6.1.3 Chapter 5..........146
6.2 Summary..........146

REFERENCES..........151

LIST OF FIGURES

Figure 1.1: A schematic of the ocean circulation surrounding southern Africa. The South Equatorial Current and anti-cyclonic circulation of the Comoros Basin are indicated. The southern branch of the East Madagascar Current, known as the South East Madagascar Current (SEMC) retroflects south of Madagascar. Both cyclonic and anti-cyclonic eddies forming south of Madagascar and in the Mozambique Channel propagate towards the Agulhas Current, which retroflects south of the African continent to form the Agulhas Return Current. At the Agulhas retroflection, large Agulhas Rings are spawned into the south Atlantic Ocean. The anti-cyclonic circulation of the South-West Indian Ocean sub-gyre and the Benguela Current, on the west coast of southern Africa, are also shown. The contours indicate the depth in thousands of meters (Source: Lutjeharms and Ansorge, 2001). 20

Figure 1.2: The mean position of the northern Agulhas Current core (solid black line) and standard deviation (error bars). Thin black lines indicate the bathymetry. The Natal bight is the region between Durban and Cape St. Lucia where the continental shelf (grey shading) widens (Source: Lutjeharms: 2007). 26

Figure 2.1: Sea level anomaly data (shading) with the shapes of eddies tracked by three different eddy-tracking algorithms overlaid in coloured lines. The CHE11 eddies (C11 eddies) are shown with red lines, HAL13 eddies (H14 eddies) are shown by green circles and the NEN10 eddies (Nencioli eddies) are shown by yellow lines. (Source: Escudier et al., 2016). 32

Figure 2.2: The origin (circles) and termination sites (x's) of all cyclonic and anti-cyclonic eddies tracked through the black box by the a) C11 and b) H14 eddy tracking algorithms between 1993 and 2012, overlaid on the mean Geostrophic velocity ($cm.s^{-1}$). Histograms show the frequency of cyclonic (C) and anti-cyclonic (AC) eddies forming and dissipating at each latitude and longitude. The

colours of the eddies in the legends of the histograms also correspond to the colours used in the maps. 37

Figure 2.3: A histogram showing the frequency of cyclonic and anti-cyclonic eddy lifespans from 1993 to 2012, in the C11 and H14 eddy tracking algorithms. 38

Figure 2.4: The trajectory of an eddy as tracked by a) the C11 algorithm and b) the H14 algorithm, overlaid on the corresponding SLA map of the last date the eddy was tracked. 39

Figure 2.5: The trajectory of an eddy as tracked by a) the C11 and b) H14 eddy-tracking algorithms, overlaid on the corresponding SLA map of the first date the eddy was tracked for each algorithm...40

Figure 2.6: The radii (km) of all a) C11 and b) H14 eddies which are tracked through the black box. 41

Figure 2.7: The amplitudes (cm) of all a) C11 and b) H14 eddies which are tracked through the black box. 42

Figure 2.8: A schematic showing the vertical coordinate systems used by HYCOM. (Source: Griffies et al., 2000) 45

Figure 2.9: The latitudinal variation in HYCOM grid resolution. The coarser resolution of the parent INDIA grid is evident in the zonal colour bands. The finer resolution of the regional AGULHAS model is visible in the two darkest shades of blue (5 − 10 km and 10 − 15 km resolution ranges). (Source: de Vos et al., 2016). 47

Figure 3.1: AVISO Sea level anomaly (cm) with a) a green circle showing the origin of an eddy which travels through the black box as tracked by the Chelton algorithm and b) a green line and circle depicting the eddy trajectory and termination point as tracked by the Chelton algorithm. 55

Figure 3.2: AVISO Sea level anomaly (cm) with c) a green circle showing the origin on an eddy which travels through the black box as tracked by the Chelton algorithm and d) a green line and circle depicting the eddy trajectory and termination point as tracked by the Chelton algorithm. 56

Figure 3.4: a) The trajectories of surface drifters (colour) passing through the black box between October 1992 and April 2002. b) Formation (circles) and termination (x's) sites of all cyclonic (blue) and anti-cyclonic eddies (red) passing through the black box overlaid on the mean geostrophic current derived from the satellite altimetry observations between October 1992 and April 2012......59

Figure 3.5: The meridional mean of 28° − 29.5 S° and standard deviation of the radii (red) and amplitudes (blue) of eddies as they approach the Agulhas Current meridional mean of 28° − 29.5 S° indicated by the black line. Thin grey lines show annual meridional mean velocities of the Agulhas Current. 61

Figure 3.6: Stages of dissipation of a) an anti-cyclonic eddy and b) a cyclonic eddy shown by geostrophic velocities ($cm.s^{-1}$) derived from satellite altimetry SSH means. Arrows indicate the direction of flow in regions with velocities over 50 $cm.s^{-1}$..63

Figure 3.7: The time-averaged velocity anomaly of the Agulhas Current core (black), with the distance of the Agulhas Current core from the coast (grey) and cyclonic (blue) and anti-cyclonic (red) eddies interacting with the Agulhas Current core from a) 1992 − 1997, b) 1997 − 2002, c) 2002 − 2007 and d) 2007 − 2012. The position of 0 velocity anomaly is shown (black dotted line), as well as the mean distance of the Agulhas Current core from the coast (grey dotted line). 65

Figure 3.8: a) A time-series of Agulhas Current core velocities across the transect, 30° S, 30.95° E to 32.4° S, 34.4° E. b) A wavelet power spectrum with the 95% significance level shown by bold, black contours. A thin black line shows the cone-of-influence. c) A global wavelet spectrum (blue). The red dashed line indicates significance. 66

Figure 3.9: a1) The mean velocity anomaly of the Agulhas Current when an anti-cyclonic eddy is present based on 61 anti-cyclonic eddies detected from 1992 − 2012 and a2) the resulting effect on the Agulhas Current 1 week and a3) 3 weeks later. (b1) The mean velocity anomaly of the Agulhas Current when a cyclonic eddy is present based on 71 cyclonic eddies detected from 1992 − 2012 and b2) the resulting effect on the Agulhas Current 6 weeks and b3) 15 weeks later. The transect across which the Agulhas Current core properties were studied, 30° S, 30.95° E to 32.4° S, 34.4° E, is shown by a thin black line. The black vectors indicate absolute geostrophic velocity greater than 10 $cm.s^{-1}$ and show the direction of flow. 67

Figure 4.1: Weekly surface velocities from a) a numerical model and b) AVISO satellite altimetry (Source: Backeberg et al., 2008). 70

Figure 4.2: Mean ERA-interim winds at 10 m for a) Summer, b) Autumn, c) Winter and d) Spring from 1993− 2013. Shading denotes the speed of the wind, whilst the blue arrows indicate the direction of flow. The scale for the vectors is given in red. 82

Figure 4.3: Mean wind stress ($N.m^{-2}$) for the simulation with absolute wind forcing in a) Summer, b) Winter, c) Autumn and d) Spring from 1993 − 2013. Arrows indicate the direction of the stress, with the scale of the arrows shown in red. 83

Figure 4.4: Mean wind stress ($N.m^{-2}$) for the simulation with relative wind forcing from 1993− 2013. Arrows indicate the direction of the stress, with the scale for the arrows shown in red. 84

Figure 4.5: The difference in mean wind stress ($N.m^{-2}$) between the model forced by absolute winds and the model forced by relative winds for a) Summer, b) Autumn, c) Winter and d) Spring. 85

Figure 4.6: The mean surface EKE for a) the model forced by absolute winds b) the model forced by relative winds and c) AVISO data; the mean surface MKE for d) the model with a absolute wind forcing, e) the model with relative wind forcing and f) AVISO data from 1993 − 2013. 88

Figure 4.7: Differences in the mean surface a) EKE and b) MKE between the experiment forced by absolute winds and the experiment forced by relative winds from 1993 − 2013. 89

Figure 4.8: A 0.5° by 0.5° grid of the mean energy within the eddies ($cm^2.s^{-2}$) for a) AVISO, b) the model forced by absolute winds and c) the model forced by relative winds from 1993 − 2013. 92

Figure 4.9: A 0.5° by 0.5° grid of the mean residual EKE ($cm^2.s^{-2}$) for a) AVISO, b) the model forced by absolute winds and c) the model forced by relative winds from 1993 − 2013. 93

Figure 4.10: Differences in the mean surface a) energy within the eddies and b) residual EKE ($cm^2.s^{-2}$) between the absolute and relative winds models from 1993 − 2013. 94

Figure 4.11: Trajectories of all eddies which pass through the black box (32 − 50° E and 25 − 31° S) from 1993−2013 overlaid on the mean EKE ($cm^2.s^{-2}$) for a) the model forced by absolute winds and b) the model forced by relative winds. Anti-cyclonic eddy trajectories are shown in red and cyclonic eddy trajectories are shown in blue. Black dots indicate locations of eddy dissipation. 96

Figure 4.12: Eddy trajectory roses showing directions of all eddy trajectories, within 32 − 50° E and 25 − 31° S, from 1993 − 2013 for a) the model forced by absolute winds and b) the model forced by relative winds. C_S is the current speed in $m.s^{-1}$. 97

Figure 4.13: A 1° by 1° grid showing the frequency of a) ABS, b) REL and c) AVISO eddy formations, d) ABS, e) REL and f) AVISO eddy terminations and, the number of g) ABS, h) REL and i) AVISO eddy occurrences per year. 99

Figure 4.14: A 1° by 1° grid showing the means Amplitudes (cm) of a) ABS and b) REL eddies occurring in each grid cell. 101

Figure 4.15: A 1° by 1° grid showing the mean radii (km) of a) ABS and b) REL eddies occurring in each grid cell. 102

Figure 4.16: A 1° by 1° grid showing the mean circum-averaged speed ($cm.s^{-1}$) of a) ABS and b) REL eddies occurring in each grid cell. 103

Figure 4.17: Q-Q plots of eddies occurring within 32 − 50° E and 25 − 31° S, from 1992 − 2013, showing a) anti-cyclonic eddy lifespans, b) cyclonic eddy lifespans, c) anti-cyclonic eddy radii, d) cyclonic eddy radii, e) anti-cyclonic eddy radii, f) cyclonic eddy radii, g) anti-cyclonic eddy radii and h) cyclonic eddy radii. AVISO-AVISO plots are indicated in black (along with a thin grey line along the diagonal to show the reference position), AVISO-ABS in red, and AVISO-REL are indicated in blue. 107

Figure 4.18: The depth integrated barotropic energy conversion for a) the model forced with absolute winds and b) the model forced with relative winds. 109

Figure 4.19: The depth integrated baroclinic energy conversion for a) the model forced by absolute winds and b) the model forced by relative winds. 110

Figure 5.1: Weekly geostrophic velocities ($cm.s^{-1}$) for a) the model forced by absolute winds, b) the model forced by relative winds and c) AVISO for the week of 15/02/1993. 122

Figure 5.2: The location of the Agulhas Current Time-Series mooring array. Current meter moorings are indicated by red dots, whereas C-Pies are indicated by magenta dots. The shading indicates the depth of the ocean. The smaller map

insert gives reference to the position of the ACT array along the South African coastline. (Source: Beal et al., 2015) 125

Figure 5.3: The position of the ADCP sites (x's) overlaid on the mean AVISO geostrophic velocity ($cm.s^{-1}$) from 1993 – 2013. 126

Figure 5.4: An example of Agulhas Current core detection applied to the ABS model output. The map shows weekly velocities ($m.s^{-1}$) of the Agulhas Current (colour) with the SSH contour representative of the Agulhas Current core overlaid in red. Black vectors indicate the direction of flow for velocities greater than $0.5m.s^{-1}$. Orange crosses indicate the positions of the Port Edward (north) and ACT (south) transects. 130

Figure 5.5: Time averaged GlobCurrent velocities (colour) overlaid with current ellipses from ADCP data (white), GlobCurrent (red), the HYCOM experiment forced by absolute winds (black) and HYCOM data from the experiment forced by relative winds (green) for a) Cape Morgan b) East London and c) Fish River. 132

Figure 5.6: Mean Current velocities from April 2010 to February 2013 across the ACT transect ($m.s^{-1}$) of a) the *in-situ* mooring data b) the regional HYCOM simulation forced by absolute winds and c) the regional HYCOM simulation forced by relative winds. d) The differences in mean velocities between ABS and REL. .. 134

LIST OF TABLES

Table 2.1: A comparison of the number of eddies tracked from 1993 to 2012 by the C11 and H14 eddy-tracking algorithms. 35

Table 4.1: Eddies properties for eddies passing within 32 − 50° E and 25 − 31° S between 1993 − 2013 for both anti-cyclonic (AC) and cyclonic (C) eddies, including the number of eddies with lifespans greater than 4 weeks, mean lifespans of the eddies (weeks), mean eddy radii (km), mean eddy amplitudes (cm) and mean eddy circum-averaged speeds (cm.s^{-1}). 104

Table 5.1: The locations and times at which the RDI 300 ADCP measurements of Agulhas Current velocities were collected. 126

Table 5.2: Table showing the smallest and largest eigenvalues (m.s^{-1}) of ADCP, GlobCurrent, ABS and REL data at the Cape Morgan, Fish River, and East London locations. 133

Table 5.3: Mean meander properties off the coast of Port Edward for AVISO, ABS and REL data from January 1993 to December 2013. 136

Table 5.4: Mean meander Properties in the region of the ACT array for AVISO, ABS and REL data from January 1993 to December 2013. 137

CHAPTER 1.

INTRODUCTION

The wind fields above the Indian Ocean bring about the strongest western boundary current in the Southern Hemisphere, the Agulhas Current, which flows southwestwards along the east coast of southern Africa (Renell, 1832; Lutjeharms, 2006). Transports of 30 Sv from the South-West Indian Ocean sub-gyre, 25 Sv from the South East Madagascar Current (Stramma and Lutjeharms, 1997), as well as 15 Sv from the southward flow in Mozambique Channel all contribute to the flow of the Agulhas Current (de Ruijter et al., 2002). Eddies, which form in the Mozambique Channel and south of Madagascar and propagate towards the Agulhas Current (Figure 1), are important contributors to the Current's total volume transport (de Ruijter et al., 2002; Schouten et al., 2002; Siedler et al., 2009). Past studies have shown the total poleward transport of the Agulhas Current to be of 70 ±22 Sv (Bryden et al., 2005) at 32°S and 77 ± 5 Sv at a region close to 34°S (Beal et al., 2015).

South of the African continent, the Agulhas Current begins to move into the open ocean before it retroflects eastwards (Ou and de Ruijter, 1986; Lutjeharms and van Ballegooyen, 1988). Most of the Agulhas Current's waters are retained in the retroflection and continue eastward via the Agulhas Return Current (de Ruijter et al., 1999; Lutjeharms and Ansorge, 2001). Between 2 and 18Sv of the Agulhas Current's water (de Ruijter et al., 1999; Richardson, 2007; Biastoch et al., 2008; Putrasahan et al., 2015; Chen et al., 2016) is lost into the Atlantic Ocean through large Agulhas Rings shed at the Agulhas Current retroflection (Gordon 1986; Lutjeharms and van Ballegooyen, 1988), as well as submesoscale filaments (Lutjeharms and Cooper, 1996), the Goodhope Jet (Gordon et al., 1995) and other non-eddy fluxes (Loveday et al., 2015). This transfer of warm, saline water from the southwest Indian Ocean into the south Atlantic Ocean is termed Agulhas Leakage.

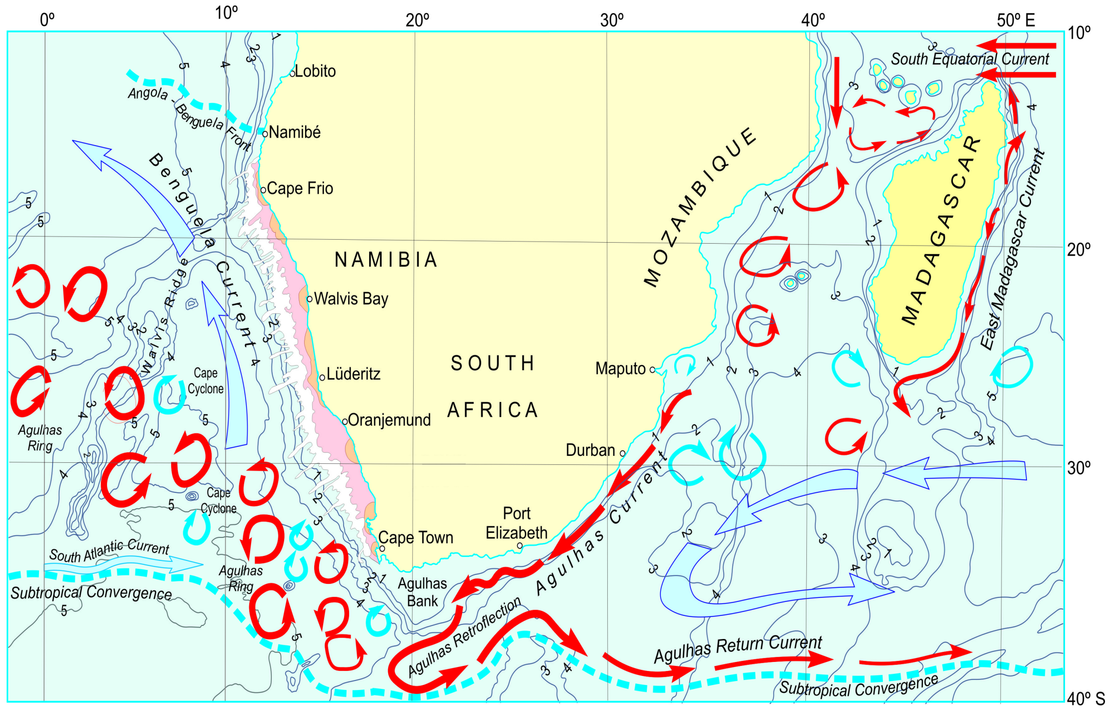

Figure 1.1: A schematic of the ocean circulation surrounding southern Africa. The South Equatorial Current and anti-cyclonic circulation of the Comoros Basin are indicated. The southern branch of the East Madagascar Current, known as the South East Madagascar Current (SEMC) retroflects south of Madagascar. Both cyclonic and anti-cyclonic eddies forming south of Madagascar and in the Mozambique Channel propagate towards the Agulhas Current, which retroflects south of the African continent to form the Agulhas Return Current. At the Agulhas retroflection, large Agulhas Rings are spawned into the south Atlantic Ocean. The anti-cyclonic circulation of the South-West Indian Ocean sub-gyre and the Benguela Current, on the west coast of southern Africa, are also shown. The contours indicate the depth in thousands of meters (Source: Lutjeharms and Ansorge, 2001).

1.1 The Role of the Agulhas Current

The warm Agulhas Current has a global impact. The Atlantic Meridional Overturning Circulation, which transports warm water northwards at the oceans surface and cold water southwards at depth, plays a substantial role in global climate. One of the sources of Atlantic Meridional Overturning Circulation is warm Indian Ocean water which makes its way into the Atlantic Ocean through Agulhas leakage (Weijer et al., 1999). The Agulhas Current system therefore, in part, regulates the strength of the Atlantic Meridional Overturning Circulation (Weijer et al., 1999). The heat and salt resulting from Agulhas leakage into the Atlantic Ocean is vital to the stability of the global Meridional Overturning Circulation and the Agulhas Current system therefore has a significant impact on the global climate (de Ruijter et al., 1999; Beal et al., 2011). It has also been shown that the Agulhas leakage could play an important role in the strengthening of the Atlantic Meridional Overturning Circulation, even though the melting of ice as a result of climate change could slow it down (Beal et al., 2011).

In addition to its influence on global climate, the Agulhas Current also has a defining role in the regional climate. Above warm western boundary currents, very high rates of evaporation often occur (Rouault et al., 2002). The Agulhas Current is one such current, and the resulting latent heat flux and evaporation significantly impacts the Southern African rainfall (Jury et al., 1993). The temperature of the Agulhas Current and its proximity to the coast have been shown to affect the rainfall on the south east cost of Africa (Walker 1990; Jury et al., 1993). Similarly, previous research has shown that warmer (cooler) sea surface temperatures (SST) in the South West Indian Ocean tend to be linked to wetter (dryer) conditions over regions of South Africa (Reason and Mulenga, 1999). Observations have shown that a dipole of cooler SST off Western Australia and warmer SST in the region south of Madagascar results in increased summer rainfall in large parts of south-eastern Africa (Reason, 2001). Model results from Reason (2001) suggest that this increase in rainfall occurs due to a significant increase in the convergence of moist air in the region which has been advected towards the coast from the low pressure anomaly which occurs above the warm SST pole as a result of increased evaporation. Over the source regions of the Agulhas Current, and the South West Indian Ocean, Easterly wind anomalies have been shown to occur before and during warm SST events that occur simultaneously with increased rainfall (Walker, 1990). The Agulhas Current also has been shown to have an effect on the occurrence of severe flooding events and storms whereby the low-level advection of moisture from the Agulhas Current onshore can intensify the local storm systems (Rouault et al., 2002).

Regionally, the variability of the Agulhas Current has potential to impact several large industries; including but not limited to the shipping, renewable energy and fishing industries. The fast flowing Agulhas Current is a potentially viable source for energy extraction that could contribute significantly to the South African electricity grid (Meyer et al., 2017). In the study by Meyer et al. (2017) it was found that the satellite and model data used were only able to accurately capture the variability in the Agulhas Current at time scales longer than 1 month. Meanders, which occur in the Agulhas Current, would therefore present a unique challenge to renewable energy developers. Meanders are also critical to cross-shelf exchanges in the region (Bryden et al., 2005; Jackson et al., 2012; Krug et al., 2014; Malan et al., 2018). They have been shown to influence shelf waters by the formation of upwelling and downwelling fronts along the shelf edge (Malan et al., 2018). These cross-shelf exchanges transport vital nutrients onto the shelf (Roberts, 2005; Roberts et al., 2010), particularly in the region of the Agulhas Bank where many fish species are spawned, several of which are critically important to fisheries in South Africa (Hutchings et al., 2002). A significant amount of Agulhas Current variability can be linked to upstream forcing by deep ocean eddies in the source regions of the current.

1.2 Mozambique Channel Eddies

The flow in the Mozambique Channel is dominated by mesoscale anti-cyclonic eddies (Gordon et al., 1983; Saetre and da Silva, 1984; Schouten et al., 2002; Quartly and Srokosz, 2004; Halo et al., 2014a). The two most favourable sites for anti-cyclonic Mozambique Channel eddy formation are in the Comoros basin near 12° S, and further south in the eastern sector of the channel near 20° S, 43° E (Halo et al., 2014a). Approximately 4 to 6 anti-cyclonic eddies pass through the narrows of the northern Mozambique Channel each year (at 17° S), with a mean diameter of 300–400 km (Schouten et al., 2002; Ridderinkhof and de Ruijter, 2003; Schouten et al., 2003; Backeberg et al.,2008). It was suggested by Ridderinkhof and de Ruijter (2003) that these northern anti-cyclonic eddies form when an unstable, strong, eastward flowing current moves over the Davie Ridge (17° 10’ 00” S, 41° 45’ 00” E). Other studies show that positive vorticity anomalies as well as shear instabilities, caused by friction between the Madagascan coastline and the South Equatorial Current, contribute towards eddy generation (Biastoch and Krauss, 1999; Backeberg and Reason, 2010; Halo et al,. 2014a). Furthermore, these eddies are primarily generated through barotropic instabilities (Collins et al., 2014). Using altimetry data, an average of 17.1 anticyclonic eddies have been recorded in the Mozambique Channel annually, between 14 and 24° S, with a mean radius of 157 km and an average lifespan of 101 days (Halo et al., 2014a). Anti-cyclonic Mozambique Channel eddies propagate polewards at a speed of 7 ±2 $km.day^{-1}$, and move into the northern Agulhas Current with approximately 4−6 of the eddies propagating as far the Agulhas retroflection region (Schouten et al., 2002; Backeberg et al., 2008).

As anti-cyclonic Mozambique Channel eddies are so prevalent, with signals easily identified in satellite data, many studies tend to neglect cyclonic Mozambique Channel eddies. Some studies have even suggested that no cyclonic eddies occur within the Mozambique Channel (de Ruijter et al., 2002). Although cyclonic eddies are smaller than their counterparts, with a mean radius of 139 km, they are even more abundant (Halo et al., 2014a). On average, altimetry data indicates that 22.1 cyclonic eddies form within the Mozambique Channel each year, between 14 and 24° S, with an average duration of 85 days (Halo et al., 2014a). Halo et al. (2014a) show that cyclonic eddies form throughout the Mozambique Channel with more favourable regions of formation along the eastern side of the channel at 16° S, 44° E and 24° S, 44° E. The formation of the cyclonic eddies at the southern site is influenced by the turbulence associated with current-shelf interactions (Halo et al., 2014a). Cyclonic eddies also form along the western side of the Mozambique Channel at 17° S (Lutjeharms, 2006; Halo et al., 2014a) through baroclinic instabilities (Collins et al., 2014). Drifter trajectories reveal that flow on the western side of the channel is predominantly anti-cyclonic whilst the eastern side of the channel has more cyclonic eddy activity (Hancke et al., 2014).

1.3 Madagascar Eddies

Several distinctive explanations have emerged to explain the complex circulation south of Madagascar. Originally, it was thought that the South East Madagascar Current (SEMC) flowed directly into the Agulhas Current (Grunglingh, 1985). Many studies, however, suggest that the SEMC retroflects south of Madagascar (Lutjeharms, 1988; Quartly and Srokosz, 2002) in a manner that is thought to be similar to the retroflection of the Agulhas Current. Inertia is thought to separate the SEMC from the Madagascan shelf. The Madagascar ridge, which is as shallow as 1000 m in parts, then causes the current to retroflect south of the Madagascan island (de Ruijter et al., 2004; Quartly and Srokosz, 2004; Halo, 2008). The retroflection of the SEMC is thought to trigger anti-cyclonic eddy formation (de Ruijter et al., 2004; Halo, 2008; Halo et al., 2014b). In contrast, cyclonic eddies form on the inshore edge of the SEMC as a result of the friction between the SEMC and the continental shelf (de Ruijter et al., 2004; Ridderinkhof et al., 2013). Further studies suggest that the SEMC retroflection is not permanent or alternatively that the current bifurcates; with one branch of the current retroflecting, and the other continuing towards the Agulhas Current (de Ruijter et al., 2004; Siedler et al., 2009; Halo et al., 2014b). One further description of the SEMC system, is that the westward flowing current, breaks down south of Madagascar, forming 4–6 pairs of contra-rotating, symmetric eddies annually (de Ruijter et al., 2004; Ridderinkhof et al., 2013). These eddies, known as dipoles, are approximately equal in size and have radii of approximately 50 to 200 km (de Ruijter et al., 2004; Ridderinkhof et al., 2013).

Halo et al. (2014b) investigated two regions for eddy formation, south of Madagascar, one to the southeast (45.10° E to 51.10° E and 32° S to 23° S) and one to the southwest (39° E to 45° E and 32° S to 23° S), and found that the different regions had different mechanisms for eddy generation. Eddies occuring in the southeast region, were formed by barotropic instabilities, whereas those occuring in the southwest were formed by barotropic and baroclinic instabilities (Halo et al., 2014b). Their study shows that eddies in the southwest region are larger than those in the southeast region, with mean anti-cyclonic eddy radii of 145 ± 37 km and 141 ± 32 km, respectively. Cyclonic eddies occuring in the southwest had a mean radius of 140 ± 37 km comparative to the mean southeast cyclonic eddy radius of 129 ± 34km (Halo et al., 2014b). The similarity in sizes of the southwest anti-cyclonic and cyclonic eddies are comparative to the dipoles observed by de Ruijter et al. (2004) and Ridderinkhof et al. (2013). Both cyclonic and anti-cyclonic eddies form south of

Madagascar and propagate westwards towards the Agulhas Current (Schouten et al., 2002; de Ruijter et al., 2004).

A study by Zhai et al. (2010) shows that western boundary currents are sinks for ocean-eddy energy, whereby the potential energy associated with westward propagating eddies is converted into kinetic energy of smaller eddies and short Rossby waves. As observed in other western boundary current systems, the interaction of source region eddies (forming in the Mozambique Channel and south of Madagascar) with the Agulhas Current has a direct impact on the Agulhas Current's variability. In this way, western boundary currents act as an eddy "graveyard" (Zhai et al., 2010).

1.4 Natal Pulses

The arrival of anti-cyclonic eddies at the offshore edge of the Agulhas Current, near to the Natal Bight (at approximately 29° S, shown in Figure 1.2), will often cause a large cyclonic meander in the current which propagates down the coast (de Ruijter et al., 1999; van Leeuwen et al., 2000; Schouten et al., 2002, Backeberg et al., 2008, Tsugawa and Hasumi, 2010). Between one and two large meanders, known as Natal Pulses, propagate to the southern Agulhas Current region each year (Rouault and Penven, 2011; Elipot and Beal, 2015). They can cause and early retroflection of the Agulhas Current, south of the African continent (Lutjeharms and van Ballegooyen, 1988; Krug et al., 2012). Natal Pulses are considered to play a significant role in the variability of the southern Agulhas Current and thus the number of large Agulhas Rings that are shed into the South Atlantic Ocean (de Ruijter et al., 1999; Schouten et al., 2002). Other studies, however, have shown that a Natal Pulse is not required in order to generate an Agulhas Ring (Rouault and Penven, 2011; Elipot and Beal, 2015). In addition, Leber and Beal (2014) suggest that the transport of the Agulhas Current is maintained during a meander and a study by Biastoch et al., (2008) shows using a numerical model that Natal Pulses do not significantly influence Agulhas leakage, therefore further questioning the link between Natal Pulses and Agulhas Leakage variability.

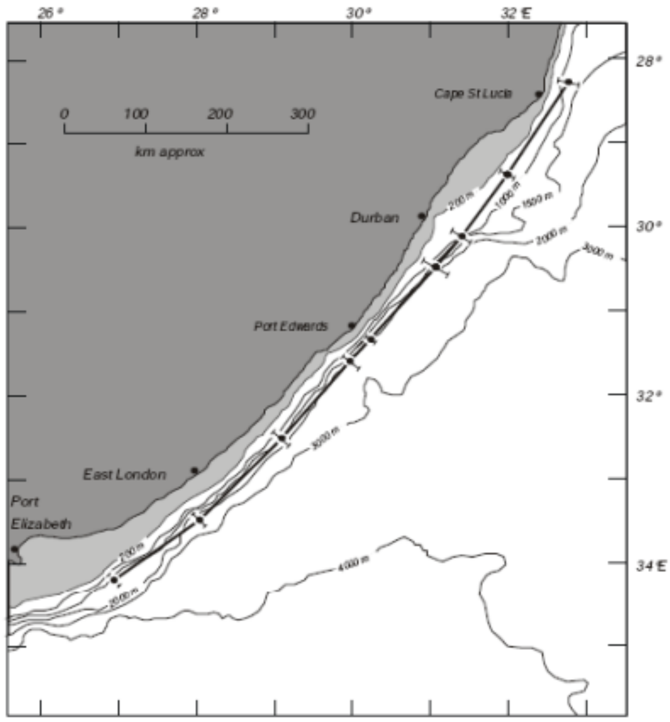

Figure 1.2: The mean position of the northern Agulhas Current core (solid black line) and standard deviation (error bars). Thin black lines indicate the bathymetry. The Natal bight is the region between Durban and Cape St. Lucia where the continental shelf (grey shading) widens (Source: Lutjeharms: 2007).

1.5 Mesoscale Variability in Numerical Models

As the downstream impacts of source region eddies on the Agulhas Current are so important, and *in-situ* data in the region is so sparse, it is necessary to precisely capture the complex mesoscale circulation with numerical models. Whilst existing numerical models are successfully able to capture many aspects of the Agulhas Current, they tend to overestimate or underestimate the frequency and size of the source region eddies and the associated eddy kinetic energy (EKE) levels (Backeberg et al., 2014; Durgadoo et al., 2013; Loveday et al., 2014).

Studies have shown that coupled ocean-atmosphere models are better able to simulate mesoscale variability than uncoupled models (McClean et al., 2011; Putrashan et al., 2015; Chen et al., 2016; Renault et al., 2016a; Renault et al., 2016b; Renault et al., 2017). This is because coupled models are able to incorporate important air-sea interactions through the inclusion of small-scale processes in the ocean that enable the atmosphere to be more realistically forced (Renault et al., 2017). Two of the most commonly studied ocean-atmosphere feedbacks are thermal and current feedbacks, whereby the influences of SST and sea surface velocity on the atmosphere are investigated.

Surface ocean currents can affect the atmosphere, this is known as current feedback (Renault et al., 2017). A study by Dewar and Flierl (1987) showed that including the effect of sea surface velocity in wind stress calculations caused Gulf Stream rings to weaken. Since then, several studies (Duhaut and Straub, 2006; Dawe and Thompson, 2006; Eden and Dietze, 2009; Renault et al., 2016a; Renault et al., 2016b; Renault et al., 2017) have shown that the inclusion of surface currents in wind stress calculation caused a significant reduction in the energy of the ocean though "mechanical dampening". More recently, current feedback to the atmosphere has been shown to reduce the work done by the wind on the ocean and hence the EKE (Hughes and Wilson, 2008; Scott and Xu, 2009; Renault et al., 2016a; Renault et al., 2016b; Renault et al., 2017). Consequently, current feedback is often referred to as an "eddy killer" (Renault et al., 2016a; Renault et al., 2016b; Renault et al., 2017). A study on the Agulhas Current System by Renault et al. (2017) showed that surface ocean current feedback the atmosphere reduced the wind work and caused a mean energy decrease over the domain of 25%.

1.6 Objectives

There are 3 main objectives of this thesis. Firstly, this study aims to build on previous eddy dissipation studies using a global dataset of automatically tracked eddies in combination with *in-situ* surface drifter data and altimetry-derived geostrophic currents to study the interaction and dissipation of source region eddies in the Agulhas Current.

Next, the ability of a regional Hybrid Coordinate Ocean Model (HYCOM) to accurately capture these processes will be determined. The local effect of the current feedback on mesoscale eddies forming in the Mozambique Channel and South of Madagascar and their interaction with the northern Agulhas Current will be investigated by comparing two simulation experiments, where we change the wind forcing, and use an eddy-tracking algorithm. It is anticipated that through the process of "mechanical dampening", a reduced EKE will enable a more accurate representation of cyclonic and anti-cyclonic eddy dynamics in the source region of the Agulhas Current and that eddy-current dissipation processes will be better simulated.

The final objective of this study is to assess the evolution of meanders in the Agulhas Current using both HYCOM experiments and then comparing the results with satellite observations. The influence of deep ocean eddies on the downstream variability of the Agulhas Current will be investigated.

1.7 Structure of Thesis

The structure of this thesis is as follows. Firstly, the data and methods used in this study are discussed. Chapter 2 contains a detailed comparison of the eddy tracking algorithms used in this thesis as well as the set up of the regional Hybrid Coordinate Ocean Model. Thereafter, three results chapters based on the objectives of this study follow. Each of these chapters is written in a paper type format and the relevant literature for each of the chapters is therefore included in the introduction of the three results chapters of this thesis. Chapter 6 contains a summary and conclusion of the main findings of this work.

CHAPTER 2.

COMPARISON OF EDDY TRACKING METHODS AND MODEL DESCRIPTION

2.1 A comparison of two eddy-tracking algorithms in the source region of the Agulhas Current

2.1.1 Introduction

The mesoscale eddy-tracking algorithm used in the following chapter was developed by Dudley Chelton and Michael Schlax (described in Chelton et al., 2011 and hereafter referred to as C11). It enables a quantitative investigation of the dynamics of source region eddies, from the time they form until they dissipate. However, many existing numerical models are unable to accurately capture eddy dissipation processes, impacting our understanding of the Agulhas Current.

In order to study the eddy-current interactions captured by numerical models, it is necessary to apply an eddy-tracking algorithm to the model data. Unfortunately it is not possible to apply the C11 algorithm to model data as only the output from the algorithm is available to use and not the algorithm itself. Therefore, in this chapter we compare the results of the C11 algorithm with the eddy-tracking scheme used by Halo et al. (2014a) (hereafter referred to as H14) to understand the differences between the two algorithms and the eddy dynamics that they are able to capture. The H14 algorithm will later be applied to model data.

2.1.2 Data and Methods

The first algorithm for tracking eddies in altimeter data was developed by Isern-Fontanet et al. (2003) and identified eddies by calculating the Okubo-Weiss parameter (W) (Okubo, 1970; Weiss, 1991) and selecting areas where the flow is dominated by vorticity (W is negative). W is defined by the following set of equations, where S_n is the normal component of the strain, S_s is the shear component of the strain and ξ is the relative vorticity. u and v are the velocity components in the x and y directions.

$$W = S_n + S_s - \xi^2 \tag{2.1}$$

$$S_n = \frac{\partial u}{\partial x} - \frac{\partial v}{\partial y} \tag{2.2}$$

$$S_s = \frac{\partial v}{\partial x} + \frac{du}{dy} \tag{2.3}$$

$$\xi = \frac{\partial v}{\partial x} - \frac{\partial u}{\partial y} \tag{2.4}$$

Many W-based algorithms have since been developed (Isern-Fontanet et al., 2004; Isern-Fontanet et al., 2006a; Isern-Fontanet et al., 2006b; Penven et al., 2005; Chelton et al., 2007). Chelton et al. (2011) however, observed three major problems with this method. Firstly, this method requires a threshold value of W to be set. Because there is no suitable value that can be used for the global ocean, too few or too many eddies might be tracked. Secondly, W is calculated from the second derivative of sea surface height (SSH). Each differentiation of SSH increases the noise in the SSH field and can intensify tracking errors in the algorithms (Chelton et al., 2011; Halo et al., 2014a). Lastly, Chelton et al., (2011) realised that the closed W contours often did not match closed SSH contours indicating that the eddy properties calculated from the W method were not always correct. They concluded that the eddy-tracking methodology needed to be improved and they developed a new geometric algorithm for tracking mesoscale eddies in noisy SSH fields.

2.1.2.1 The Chelton eddy-tracking algorithm

The C11 algorithm was applied to gridded satellite altimeter maps of SSH (Chelton et al., 2011). The gridded data from which eddies were tracked was produced every 7 days and has a 0.25° resolution (Chelton et al., 2011). The C11 eddy-tracking algorithm defines eddies as having an amplitude of at least 1cm, and in each SSH map an eddy consists of closed SSH loops containing a minimum of 8 and a maximum of 1000 pixels (1 pixel represents an area of approximately 25 km x 25 km, making the minimum area of an eddy equal to 5000 km^2 and the maximum area of a detected eddy equal to 625 000 km^2) with the distance between connected pixels being less than a specified amount which is dependent on the eddies' latitude. SSH must fall between -100cm and +100cm. For anti-cyclonic eddies, which have a positive sea level anomaly (SLA), the SSH threshold of the pixels must be greater than -100cm with a local SSH maximum (Chelton et al., 2011). A cyclonic eddy would have a negative SLA and is therefore defined as having a SSH threshold less than 100cm, with a local SSH minimum (Chelton et al., 2011). One downfall of the C11 tracking method is that more than one maximum or minimum per eddy can sometimes be identified. This is observed in a study by Escudier et al., (2016), where the C11 algorithm is shown to detect several large elongated eddies, as opposed to two smaller eddies as tracked by other algorithms (Figure 2.1). The methodology to split these eddies became too complicated and was therefore not incorporated into the C11 algorithm (Chelton et al., 2011). The other two algorithms analysed by Escudier et al. (2016) include the H14 method, which is investigated in this chapter, and the method developed by Necioli et al. (2010). The Necioli et al. (2010) method uses the geometry of surface velocity vectors to detect eddies, whereby the algorithm detects velocities rotating around the center of an eddy. This method is not explored in this study.

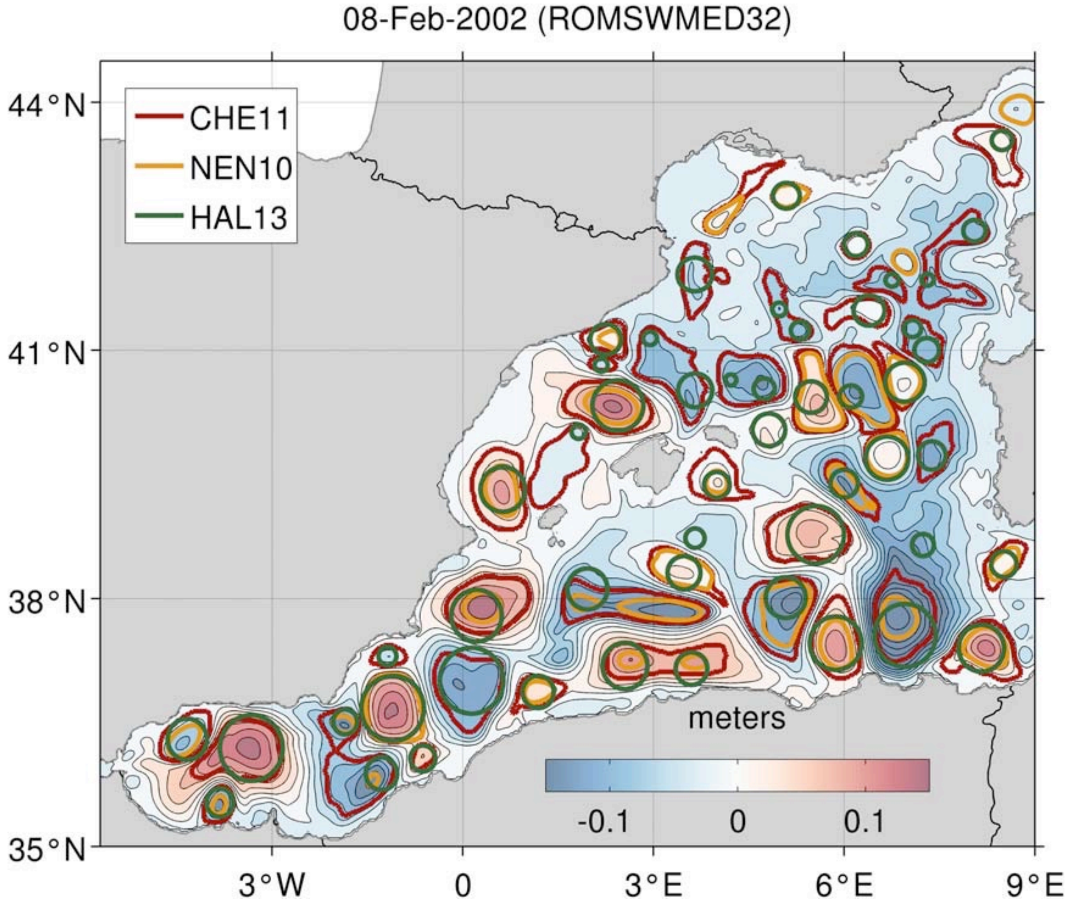

Figure 2.1: Sea level anomaly data (shading) with the shapes of eddies tracked by three different eddy-tracking algorithms overlaid in coloured lines. The CHE11 eddies (C11 eddies) are shown with red lines, HAL13 eddies (H14 eddies) are shown by green circles and the NEN10 eddies (Nencioli eddies) are shown by yellow lines. (Source: Escudier et al., 2016).

Once an eddy is identified, the algorithm calculates different properties associated with the eddy at 7–day intervals. These include their longitude and latitude positions, the directions of rotation, the amplitudes, radii and circum-averaged speeds. This distance is dependent on latitude and needs to be less than 400 km for latitudes greater than 25°, and increases equatorwards to a maximum of 1200 km (Chelton et al. 2011). To reduce the risk of fake eddies being identified from noise in the SSH fields, only eddies with lifetimes greater than 4 weeks were retained.

2.1.2.2 The Penven eddy-tracking algorithm

The second eddy-tracking algorithm used in this study was developed by Pierrick

Penven. It is best described by Halo et al. (2014a) but follows the method originally proposed by Penven et al. (2005), and is able to detect if an eddy is present in successive frames. The H14 algorithm uses a combination of both the geometric method (the closed SSH contours) and the W-based method to track mesoscale eddies. Combining the regions where W was negative, along with closed SSH contours, prevented the detection of multiple cores and elongated closed loops (Halo et al., 2014a).

Halo et al. (2014a) noted that the W-based method is very sensitive and eddy-tracking methods based on geometric criteria are easier. The geometric method, however, requires certain thresholds and requirements to be met based on eddy shapes. As this eddy-tracking algorithm was intended to be used on multiple data sets, it was necessary to combine both the geometric and W-based methods in order to create a more adaptable algorithm less dependent on specified criteria. The H14 eddy-tracking algorithm has only 3 tunable parameters; the number of Hanning filter passes, the maximum eddy size and the interval between closed SSH contours which form a loop. The number of eddies tracked is not very sensitive to these parameters. The H14 algorithm was therefore a good choice for this study.

In order to create the most accurate comparison possible with the C11 algorithm, the H14 algorithm was applied to AVISO Maps of Absolute Dynamic Topography (MADT) at the same weekly interval selected for the C11 algorithm. An advantage of applying the algorithm to MADT data rather than MSLA data is that it prevents the detection of current meanders as eddies (Halo et al., 2014a).

Where possible, the criteria were set to match the C11 eddy-tracking algorithm as accurately as possible. Two passes of the Hanning filter were applied to the W Parameter to help eliminate grid-scale noise, the effect of which can be seen in Figure 2 of the study by Halo et al. (2014a). Regions inside a closed loop of SSH which were less than 400 km in radius were then selected. The interval between the contours for closed loop detection was set to 2 cm. In order to better match the C11 algorithm, only eddies with a lifetime of 28 days or more were selected. For both methods an eddy radius is defined by the equation:

$$R = \sqrt{S/\pi} \tag{2.5}$$

where S is the shape of the eddy detected by the algorithm. However, the H14 algorithm does not provide a shape, and therefore a circle of the detected radius is used instead (Figure 2.1).

This H14 algorithm was used to identify all eddies globally from January 1993 until April 2012. In this study only eddies tracked in the Mozambique Channel and south of Madagascar that reach the northern Agulhas Current are examined. For both the C11 and H14 tracking algorithms, only eddies passing through the region 28 − 29.5° S and 31 − 35° E were considered, which is the approximate location where the Agulhas Current becomes well defined (Grundlingh, 1983; Lutjerharms, 2006). The data were further reduced by separating cyclonic eddies from anti-cyclonic eddies in order to observe the abundance of dipole eddy pairs (Table 2.1). These subsets of data were used for the remainder of the comparison.

To illustrate how ocean eddies evolve upon reaching the Agulhas Current in the different eddy-tracking algorithms, the formation and termination positions of all cyclonic and anti-cyclonic eddies passing through the black box (Figures 2.2a and 2.2b) were overlaid on the mean geostrophic current derived from altimetry observations. AVISO MADT was used to calculate the mean for the period of October 1992 until April 2012 (Figures 2.2a and 2.2b). Histograms were used to display the most dominant latitudes and longitudes for eddy formation and dissipation in the different algorithms.

To compare the lifespans of the eddies tracked by the C11 and H14 eddy-tracking algorithms, the frequencies of both cyclonic and anti-cyclonic lifespans were calculated for each algorithm (Figure 2.3). To better observe the accuracy of the eddy lifetimes recorded by the algorithms, eddy tracks were checked against MSLA data. Two eddies were selected as case studies to contrast the trajectories recorded by each eddy-tracking algorithm (Figures 2.4 and 2.5).

The subsets of data were used in Figures 2.6 and 2.7 to observe any differences between the eddy amplitudes and radii calculated by the C11 and H14 methods. This was done by comparing how the radii and amplitudes of all the eddies in both subsets of data evolved from the formation of the eddies, until their dissipation. It is necessary to understand the similarities and differences between the properties of C11 and H14 eddies before we apply the H14 algorithm to model data and compare the results with those in Chapter 3 of this thesis.

2.1.3 Results

An investigation of the C11 and H14 eddy-tracking algorithms, in the region 28 − 29.5° S and 31 − 35° E, showed that on average the C11 algorithm detected 6.9 eddies per year in comparison to the 6.0 eddies tracked annually by the H14 algorithm (Table 1). Out of the 132 eddies tracked using C11 method, 46% were anti-cyclonic where as 54% were cyclonic. Results from the H14 algorithm however, showed a bias towards anti-cyclonic eddy formation where 62% of the 115 tracked eddies were anti-cyclonic and 38% were cyclonic.

Tracking algorithm	C11	H14
Number of eddies/year	6.9	6.0
% Anti-cyclonic	46.2	61.7
% Cyclonic	53.8	38.3

Table 2.1: A comparison of the number of eddies tracked from 1993 to 2012 by the C11 and H14 eddy-tracking algorithms.

Results from the C11 algorithm indicate that both anti-cyclonic and cyclonic eddies are generated in the Mozambique Channel and south of Madagascar. They propagate towards the Agulhas Current and dissipate as they reach the current, or very shortly after that (Figure 2.2a). Whilst the H14 algorithm appears to yield similar results, the trajectories of the eddies were much shorter (Figure 2.2b) and show H14 eddies forming much closer to the Agulhas Current in contrast to C11 eddies. The histograms in Figure 2.2 show the dominant region of formation in the C11 algorithm is 27° S, 36° E (Figure 2.2a) compared to the H14 eddies that form closer to the Agulhas Current, and most frequently at 28° S, 35° E (Figure 2.2b). Interestingly, the region of most frequent eddy dissipation in both algorithms is the same at 29° S, 34° E (within the black box).

Further investigation into the formation and dissipation times of individual eddies revealed that eddies tracked by the H14 algorithm have a shorter lifespan than C11 eddies, with over 80% of eddies having a lifetime of 4 - 12 weeks (Figure 2.3). In contrast, only 32% of eddies tracked by C11 have a life span of 4 - 12 weeks (Figure 2.3). Eddies tracked by C11 can have a life span of up to 60 weeks, where as the longest lifespan of a H14 eddy is 28 weeks. The mean lifespan of a C11 eddy is 19 ± 12 weeks, compared to the mean lifespan of a H14 eddy which is 8 ± 5 weeks. For both algorithms, the mean lifespan of cyclonic eddies is between 1 and 3 weeks longer than the mean lifespan of anti-cyclonic eddies.

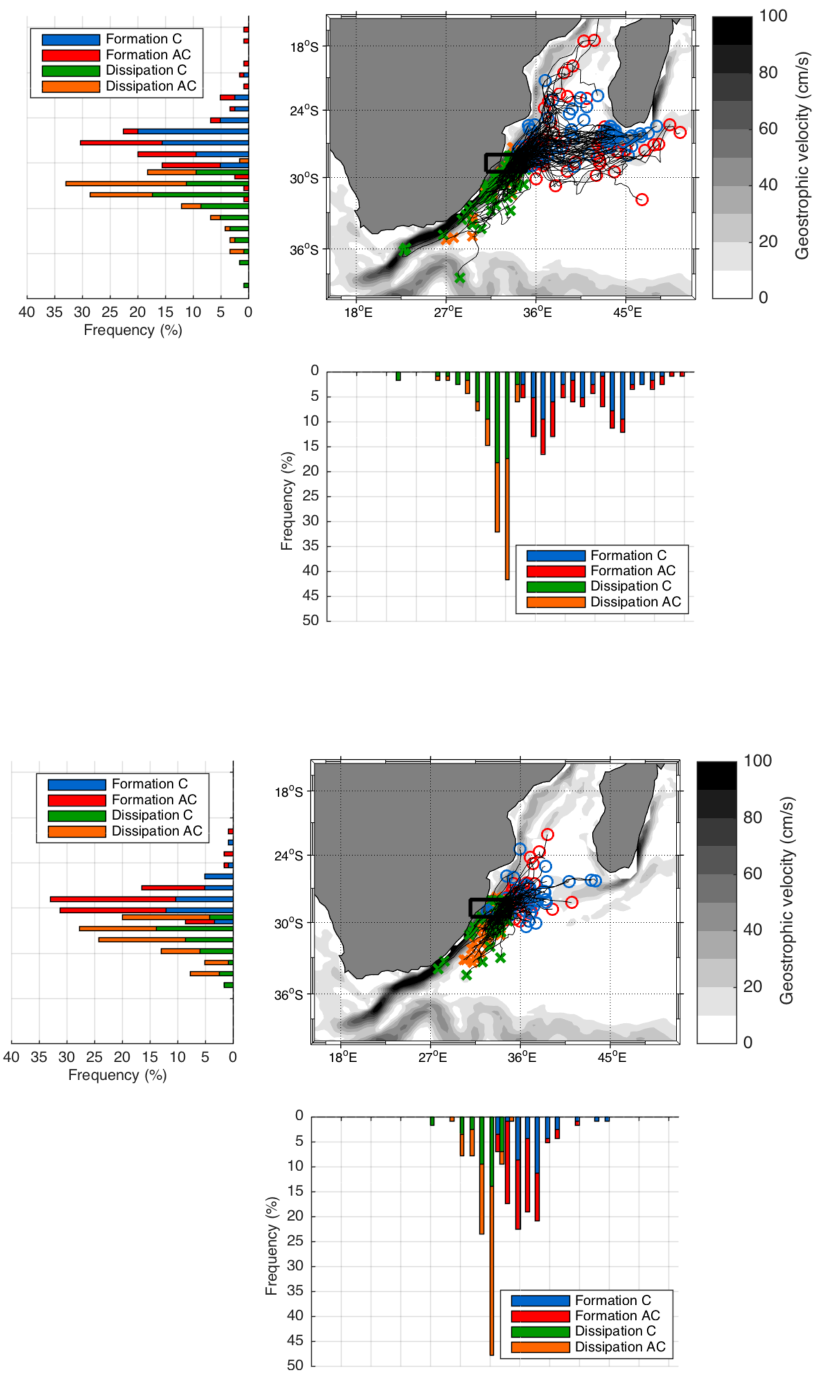

Figure 2.2: The origin (circles) and termination sites (x's) of all cyclonic and anti-cyclonic eddies tracked through the black box by the a) C11 and b) H14 eddy tracking algorithms between 1993 and 2012, overlaid on the mean Geostrophic velocity ($cm.s^{-1}$). Histograms show the frequency of cyclonic (C) and anti-cyclonic (AC) eddies forming and dissipating at each latitude and longitude. The colours of the eddies in the legends of the histograms also correspond to the colours used in the maps.

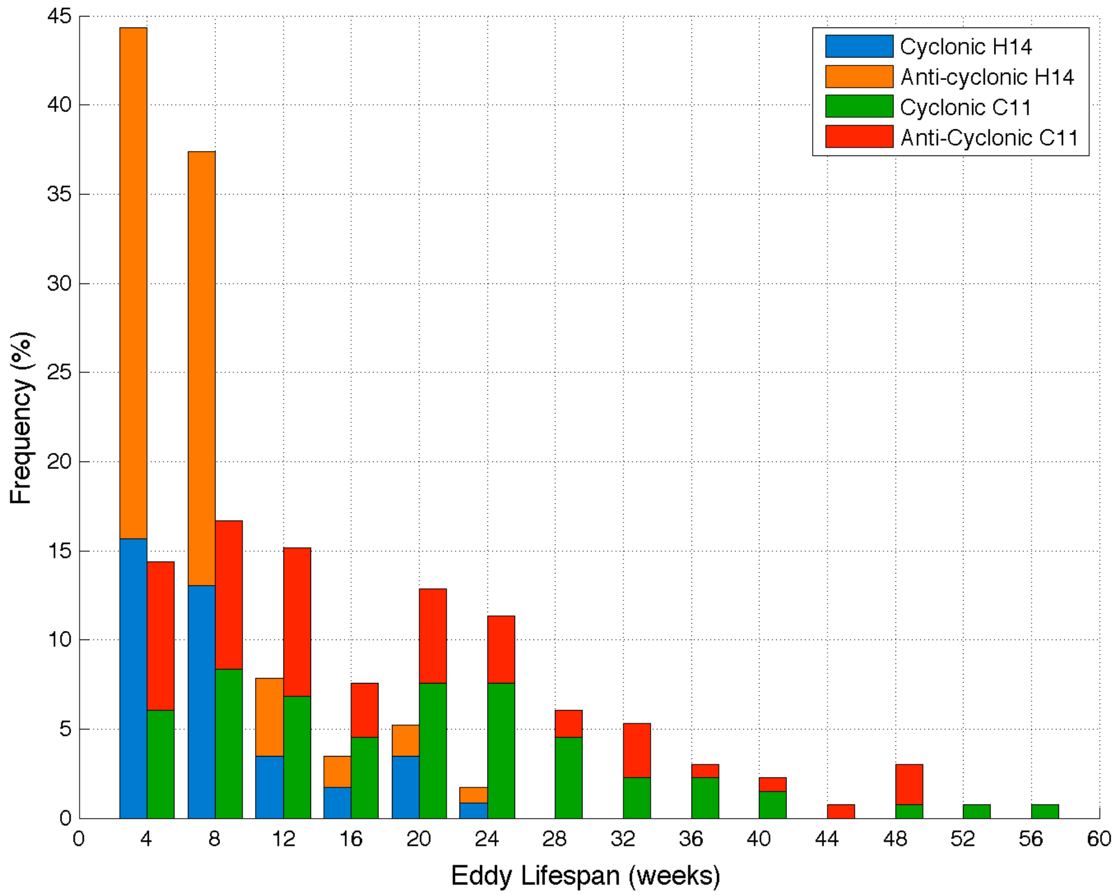

Figure 2.3: A histogram showing the frequency of cyclonic and anti-cyclonic eddy lifespans from 1993 to 2012, in the C11 and H14 eddy tracking algorithms.

2.1.3.1 Case Studies

Two eddies were chosen as case studies to illustrate the differences in the tracking algorithms. In both examples, the trajectories of the C11 eddies were far longer than the H14 eddies. In Chapter 3 it will be shown that the C11 algorithm is not completely accurate because of erroneous changes in eddy identification numbers and eddies did in fact exist for longer than they were tracked by the algorithm. In these examples however, the C11 algorithm is shown to track eddies for longer than the H14 algorithm. In the first example (Figure 2.4) the C11 algorithm was able to track an eddy from 27/11/2002 until 02/07/2003 whereas this same eddy was tracked for just 4 weeks by the H14 algorithm from 18/06/2003 until 09/07/2003.

The second example yielded a very similar result (Figure 2.5). The C11 algorithm tracked an eddy from south of Madagascar across the Mozambique Channel from 13/10/1993 until 30/03/1994, whereas the H14 algorithm only tracked this eddy from 09/02/1994 until 09/03/1994. Both algorithms do cease to track both of these eddies shortly after they propagate into the Agulhas Current.

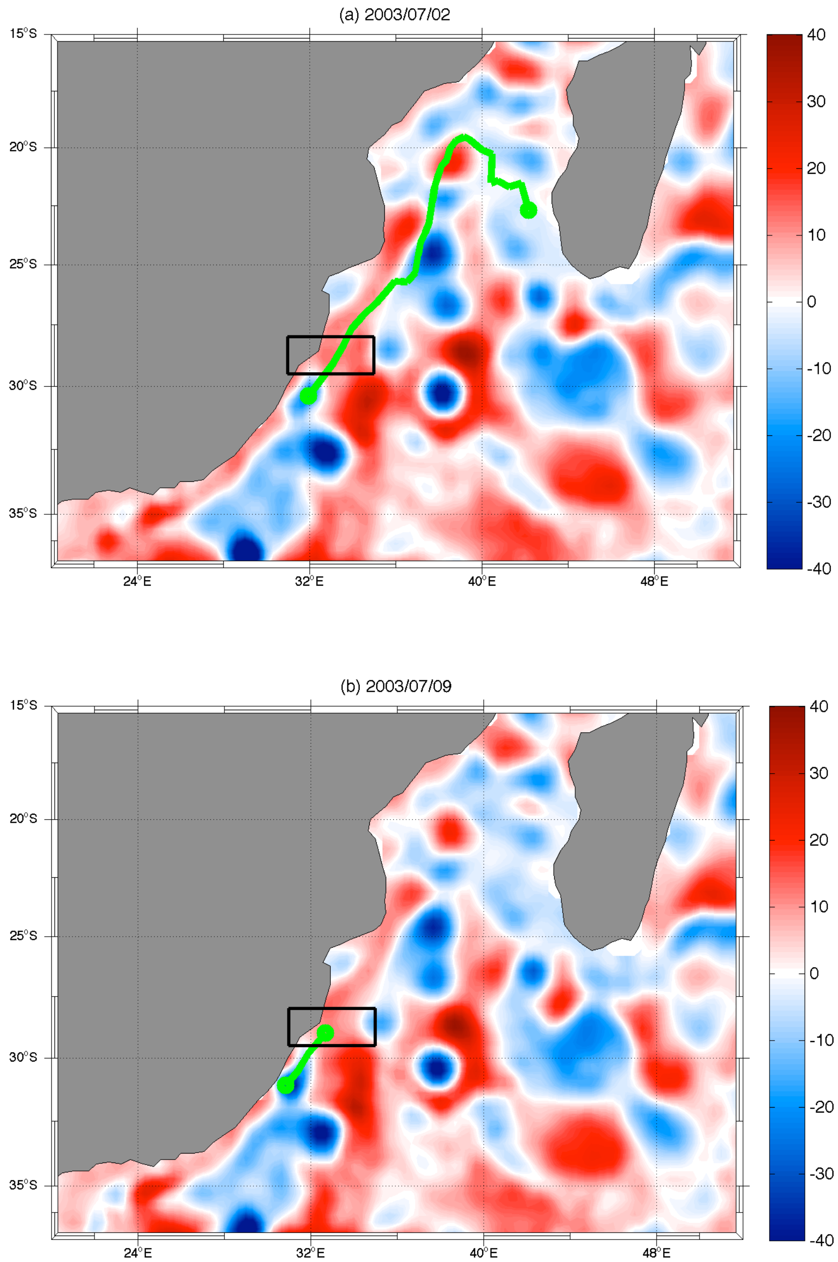

Figure 2.4: The trajectory of an eddy as tracked by a) the C11 algorithm and b) the H14 algorithm, overlaid on the corresponding SLA map of the last date the eddy was tracked.

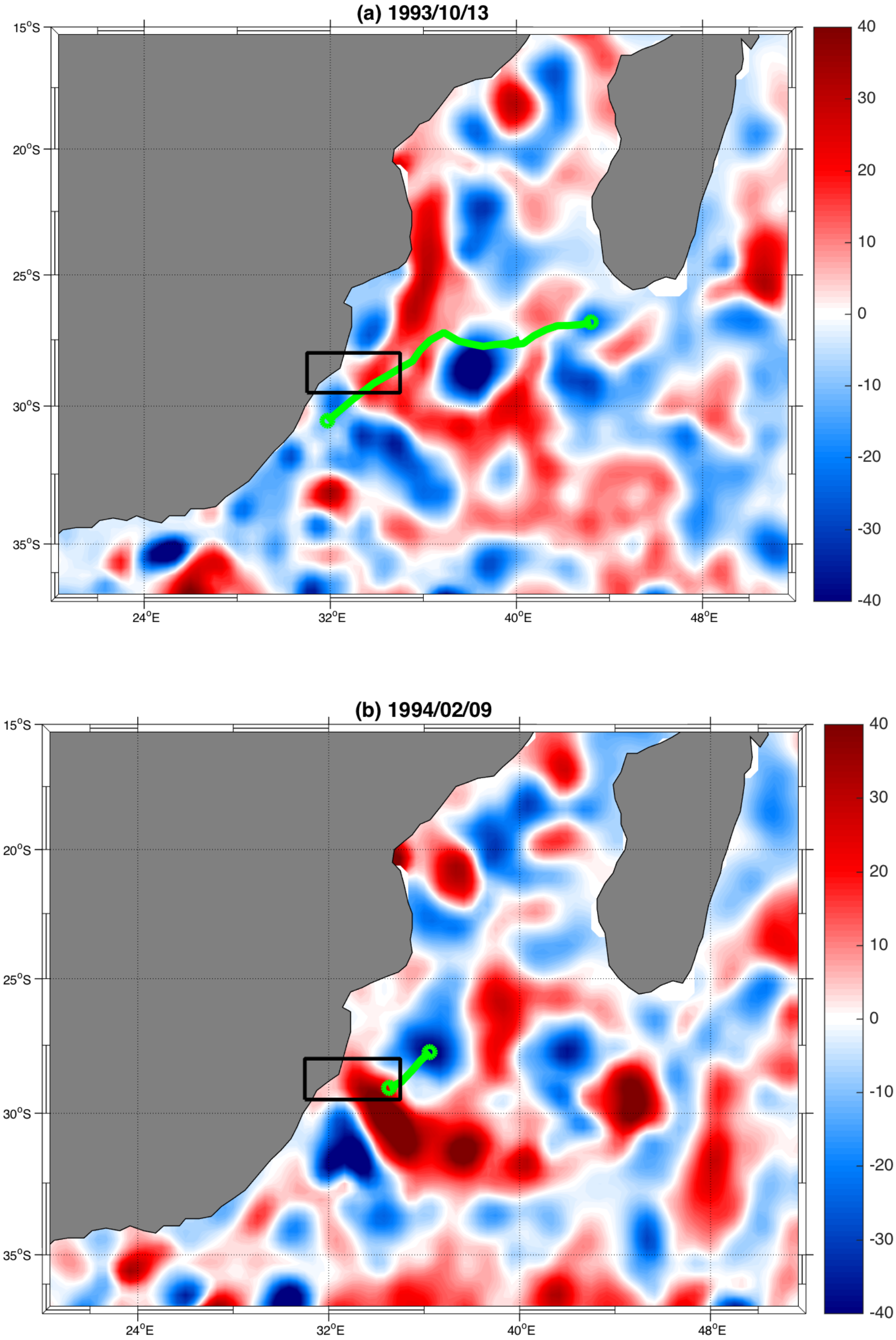

Figure 2.5: The trajectory of an eddy as tracked by a) the C11 and b) H14 eddy-tracking algorithms, overlaid on the corresponding SLA map of the first date the eddy was tracked for each algorithm.

2.1.3.2 Eddy properties

A comparison of the properties of the subsets of eddies revealed a similar trend in both eddy size and the amplitude. In both the C11 and the H14 eddies, the radii and the amplitudes of the tracked eddies decrease as eddies propagate into the Agulhas Current. The radii of the C11 eddies are larger with maximum sizes of approximately 100 – 160 km (Figure 2.6a). The H14 eddies reach a maximum radius of approximately 70 – 100 km (Figure 2.6b). The radii of both sets of eddies decrease as the eddies propagate into the Agulhas Current until the eddies are no longer tracked by the algorithms.

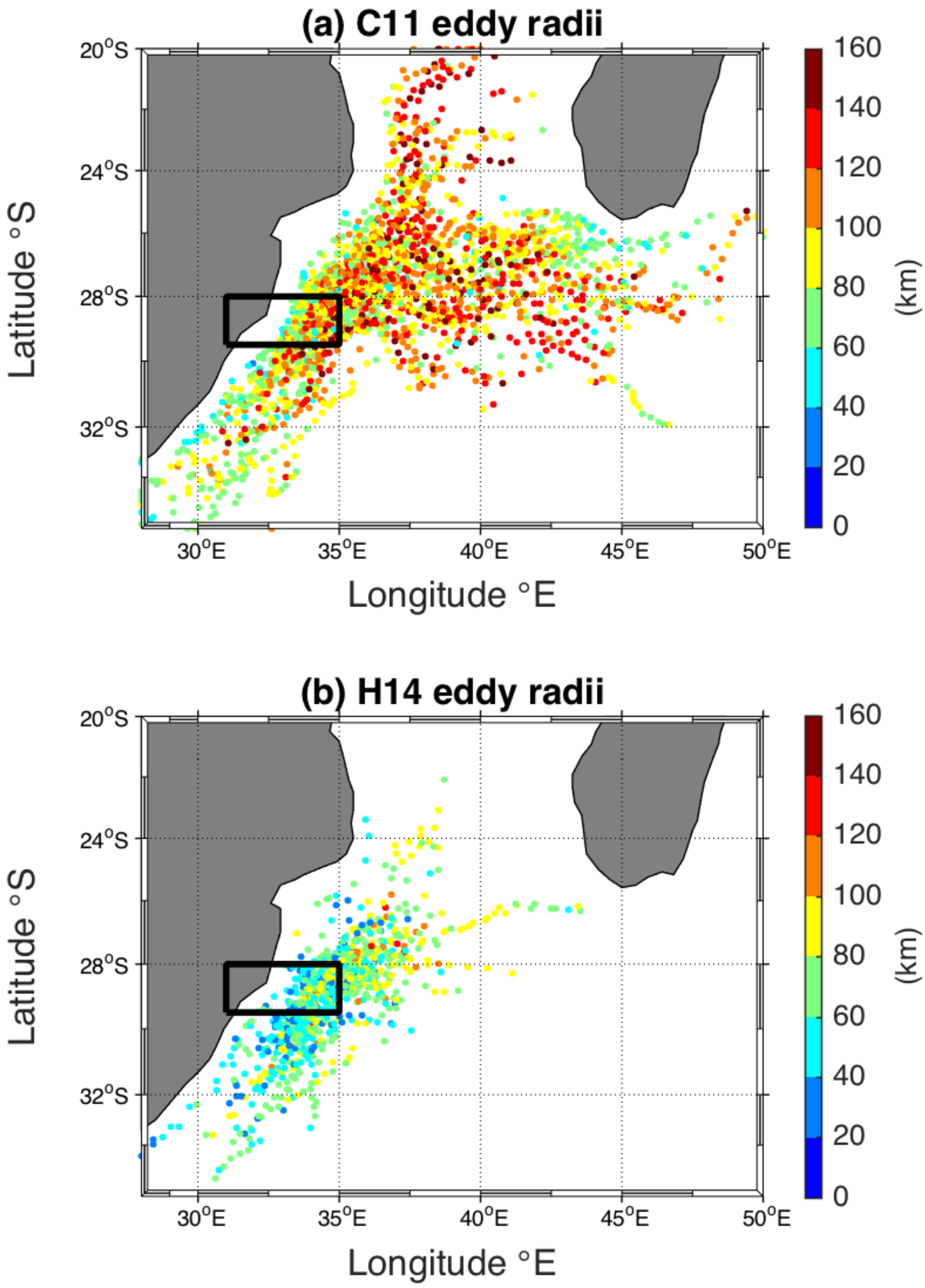

Figure 2.6: The radii (km) of all a) C11 and b) H14 eddies which are tracked through the black box.

The amplitudes of the eddies from both algorithms are comparable (Figure 2.7). Both sets of eddies have a maximum amplitude of approximately 30 − 40 cm in the central Mozambique Channel but reach a minimum of 0 – 15 cm as they propagate into the Agulhas Current. These results are consistent with those of Chapter 3. Both tracking algorithms show that eddies decrease in size as they propagate into the Agulhas Current.

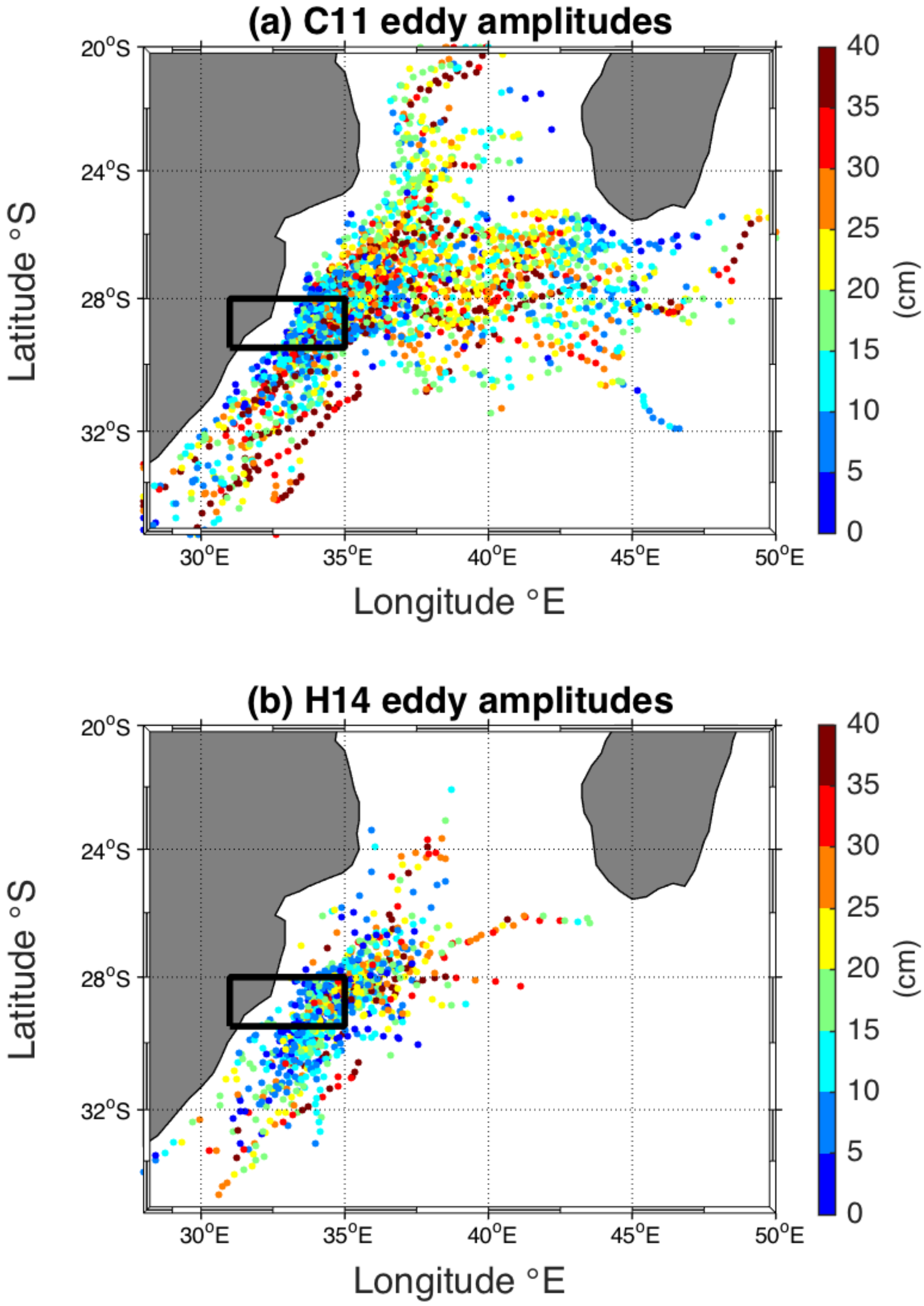

Figure 2.7: The amplitudes (cm) of all a) C11 and b) H14 eddies which are tracked through the black box.

2.1.4 Discussion and Conclusion

In this study, the properties of eddies, occurring between 1993 and 2012, and propagating through the region of 28 − 29.5° S and 31 − 35° E (the approximate location where the Agulhas Current begins) were analysed using the C11 and the H14 eddy-tracking algorithms. A comparison showed more C11 eddies moving into the source region of the Agulhas Current than the H14 algorithm, with an average of 6.85 C11 eddies tracked annually in contrast to the 5.97 eddies.year^{-1} detected by the H14 algorithm (Table 2.1). Both algorithms cease to track eddies shortly after they propagate into the Agulhas Current, accurately capturing the eddy dissipation described in Chapter 3 (Figure 2.2). The most frequent region for eddy dissipation is the same for both algorithms at 29° S, 34° E. This location is within the region of the subsets of data, suggesting that the Agulhas Current strongly influences eddy dissipation. In Figure 2.2, the trajectories of the H14 eddies were considerably shorter than the C11 trajectories. It was found that the C11 eddy-tracking algorithm is able to track eddies for up to 60 weeks, where as the H14 eddies have a maximum lifespan of 28 weeks (Figure 2.3). The mean lifespan of a C11 eddy is 19 ± 12 weeks in contrast to the mean lifespan of a H14 eddy of only 8 ± 5 weeks.

Although the trajectories of the H14 eddies are much shorter than the C11 eddies (Figures 2.4 and 2.5), both algorithms show that eddies dissipate as they propagate into the Agulhas Current. The differences in the results of the C11 and H14 eddy-tracking algorithms are a result of the differences in the selection criteria for eddy identification. Whilst both eddy-tracking algorithms similarly use closed SSH contours to detect eddies, the H14 eddies are also selected by calculating the Okubo-Weiss parameter and selecting regions dominated by vorticity. The H14 criteria are arguably stricter than those of the C11 algorithm and as a result, eddies are fewer and shorter lived. However, as the SSH fields used in the C11 algorithm are not publicly available (Mason et al., 2014), it is not possible to say which algorithm better captures the eddy dynamics in the source region of the Agulhas Current.

One possible explanation for the shorter eddy lifespans of the H14 eddies is the difference in size between the eddies. Previous studies have shown that smaller eddies tend to have shorter lifespans (Chelton et al., 2011; Halo et al., 2014a). The tracked C11 eddies are larger than the H14 eddies by up to 90 km in radius, with the maximum sizes of C11 eddies reaching approximately 100 – 160 km (Figure 2.6a). The H14 eddies reach a maximum radius of approximately 70 – 100 km (Figure 2.6b). These results compare favourably with a study by Escudier et al., (2016), where it was noted that the C11 algorithm tracked larger eddies than the H14 algorithm. This is due to differences in the surface shape detection of eddies between the algorithms (Escudier et al., 2016). The radii of the eddies captured by both algorithms equate well with existing literature, with studies recording eddy radii of 50 − 200 km in the Mozambique Channel and south of Madagascar (Schouten et al., 2002, de Ruijter et al., 2004; Ridderinkhof et al., 2013).

Although there are significant differences between the algorithms in the lifespan and radii of the eddies captured, there are also many similarities. Both the C11 and H14 algorithms capture maximum eddy amplitudes of 30 − 40 cm (Figure 2.7). Both the C11 and H14 algorithms show eddies decrease in amplitude and radius as they approach the Agulhas Current, and that eddies dissipate as they reach the Agulhas Current or very shortly after that (Figures 2.6 and 2.7).

This study has shown that both the C11 and H14 algorithms are able to capture eddy dissipation in the Agulhas Current. Using the knowledge of the differences between the algorithms in tracking eddies using satellite altimetry data, we will be better equipped to understand the capabilities of the H14 algorithm to track eddies in model data and the models' abilities to accurately capture eddy dissipation processes.

2.2 The Hybrid Coordinate Ocean Model

The Hybrid Coordinate Ocean Model (HYCOM) used in this study is a primitive equation model derived from the Miami Isopycnal Coordinate Model (Griffies et al., 2000). It uses a combination of isopycnic vertical co-ordinates (ρ) in the stratified open ocean, fixed-grid co-ordinates (z) in the upper ocean mixed layer or the unstratified ocean and sigma coordinates (σ) which are terrain following and used in shallow coastal regions (Figure 2.8) (Bleck, 2002; Wallcraft et al., 2009). The layered continuity equation is used to make the transition from ρ co-ordinates to z or σ co-ordinates (Wallcraft et al., 2009). The structure of the vertical layer discretisation is contingent on the dominant processes at each time-step, in every layer of the simulation (Bleck, 2002). The minimum and maximum layer thickness for transition to z-levels are 3 m and 450 m, respectively (Backeberg et al., 2014). HYCOM is able to interchange its vertical co-ordinates efficiently to accurately simulate the water column, with importance being placed on restoring the grid to ρ co-ordinates during the interchanges (Bleck, 2002).

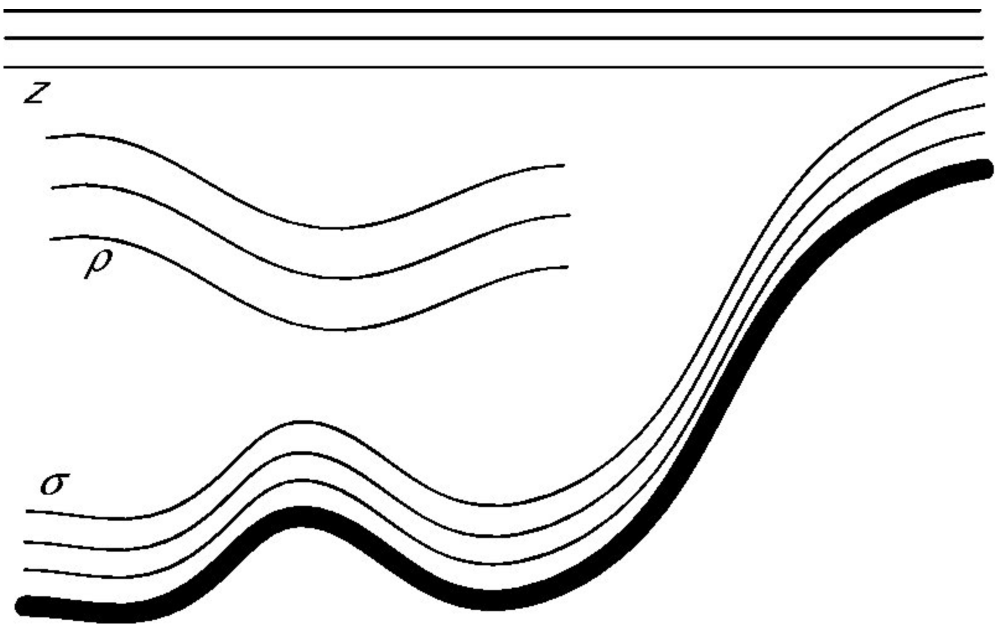

Figure 2.8: A schematic showing the vertical coordinate systems used by HYCOM. (Source: Griffies et al., 2000)

The domain of the regional HYCOM (AGULHAS) model used in this study covers the entire the Agulhas Current system from 0° to 60° E and 10° to 50° S, including the Mozambique Channel and East Madagascar Current (Figure 2.9). It has a resolution of approximately 10 km (1/10°) and the Rossby radius of deformation for the region is 30 km (Chelton et al., 1998). The nested model is therefore considered to be sufficient to resolve mesoscale eddies in the region (Backeberg et al., 2008; Backeberg et al., 2009; Backeberg et al., 2014). AGULHAS is nested within a larger basin scale model (INDIA) that spans the Indian and Southern Ocean at a resolution which ranges from 14 km in the northern region of the Indian Ocean to 45 km further south (Figure 2.9) (George et al., 2010). Both models were developed using a conformal mapping tool (Bentsen et al., 1999). Both the inner and outer model have 30 hybrid layers, which have a minimum thickness of 3 m near the surface (Backeberg et al., 2014). The layers have target densities ranging from 21.0 kg.m^{-3} to 28.3 kg.m^{-3}, referenced to σ_0 which is equal to 1000 kg.m^{-3} (Backeberg, 2010).

INDIA contributes unassimilated boundary conditions to the nested model every 6 hours (Backeberg, 2010; de Vos et al., 2018). There is a 20 grid cell buffer zone between the AGULHAS and INDIA models, towards which slow changing variables (including temperature, and salinity) are relaxed, based on the flow relaxation scheme which decreases inwards by a factor of 4 with distance from the boundary, over a maximum time period of 13 hours at the outer most grid cell (Davies, 1983, Backeberg et al., 2014). The method described by Browning and Kreiss (1982; 1986) is applied for faster changing variables including barotropic velocities and pressure.

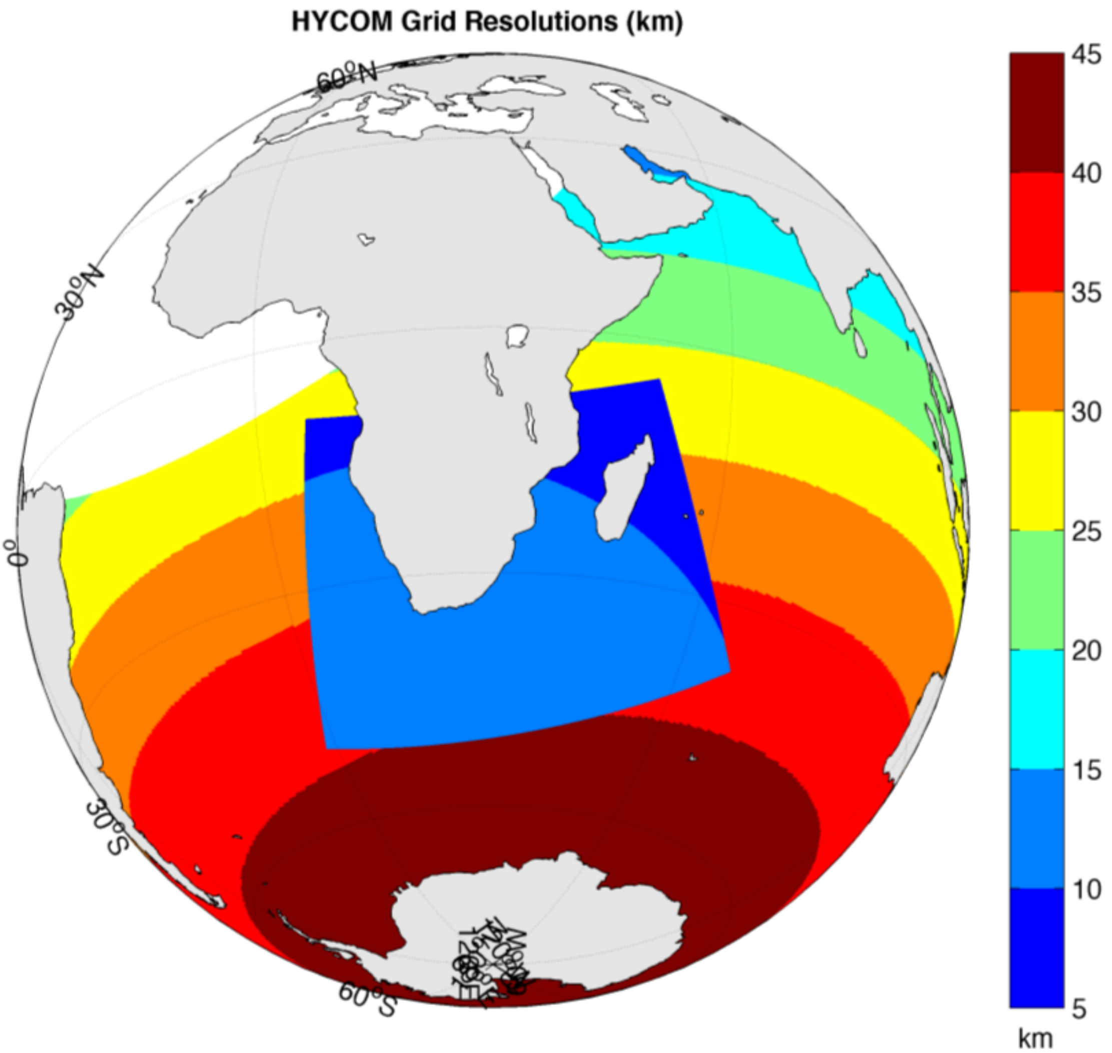

Figure 2.9: The latitudinal variation in HYCOM grid resolution. The coarser resolution of the parent INDIA grid is evident in the zonal colour bands. The finer resolution of the regional AGULHAS model is visible in the two darkest shades of blue (5 − 10 km and 10 − 15 km resolution ranges). (Source: de Vos et al., 2016).

INDIA is initialised from Levitus climatology and spun up for 10 years using ERA40 and ERA-interim forcing, which is produced by the European Centre for Medium-Range Weather Forecasts (ECMWF) (Dee et al., 2011). The nested AGULHAS model is then initialised from the balanced field of INDIA model interpolated onto the higher resolution grid (Backeberg et al., 2014). Both models are run using ERA40 atmospheric forcing from 1980 to 1992, thereafter ERA-interim is used until 2013. Bias corrections schemes have been applied to the some of the ERA-interim data, previously prepared for ERA40 and a bias correction procedures are applied for surface pressure and radiosonde temperature observations (Dee et al., 2011). The ERA-interim product has a 0.7 km spatial resolution and provides a large variety of 3 hourly surface parameters as well as 6 hourly upper air parameters (Dee et al., 2011). The ERA-interim product has increased accuracy over land as a result of more observational data on humidity and rainfall (Dee et al., 2011).

The methods described by Kara et al. (2000) and Drange and Simonsen (1996) are used to calculate the momentum and heat fluxes respectively. The hydrological model: Total Runoff Integrating Pathways (TRIP), which receives river run-off data from ERA-interim, is used to determine monthly river discharges from major catchment areas and their associated river channels at a 1° x 1° resolution (Oki and Sud, 1998). The relaxation of surface salinity, towards monthly climatologies from Hydrographic Climatology, is used to improve the accuracy of river runoff, rainfall and evaporation (Steele et al., 2001; Backeberg et al., 2014).

The bathymetry boundary conditions are set with GEBCO data at a 1' resolution and are optimally interpolated onto the HYCOM grid. Neither the INDIA nor the AGULHAS model includes tides.

In this study version 2.2 of HYCOM was used. One of the main differences between version 2.1 of HYCOM and version 2.2 is that the interpolation scheme of the mixed layer has been improved and now includes the Weighted Essentially Non-Oscillatory Piecewise Parabolic Method for the interpolation of the mixed layer (Wallcraft et al., 2009; Backeberg et al., 2014). Whilst a study by Backeberg et al. (2009) demonstrated a marked improvement in the representation of the Agulhas Current by using a fourth order momentum advection scheme, the fourth order advection scheme is not completely functional in version 2.2 of HYCOM and could not be used in this study. Backeberg et al. (2014) showed that the mean circulation is significantly improved in version 2.2 of HYCOM using the second order momentum advection scheme. The second order momentum advection scheme is therefore used in this model. The vertical mixing scheme used in HYCOM is the K-Profile Parameterisation

(KPP) (Large et al., 1994; Backeberg, 2010; de Vos et al., 2018). Version 2.2 of the regional HYCOM model has been validated and used in studies by Backeberg et al. (2014), Holton et al. (2017), de Vos et al. (2018), Malan et al. (2018) and Vermeulen et al. (2019).

2.2.1 Absolute and relative wind forcing experiments

Two experiments are used in this study. Both of the simulations run for 21 years, from January 1993 until December 2013. The first simulation experiment is forced with absolute winds; the second is forced with relative winds (the wind speed relative to the surface current speed). The model forced by relative winds therefore takes into account the effect of the surface ocean currents on wind velocities.

In the first experiment forced by absolute winds, the forcing speed in the wind stress calculation is determined from wind velocity only. In this model, the wind stress is calculated using the equations

$$W = \sqrt{(U_{10})^2 + (V_{10})^2} \quad (2.6)$$

$$\tau_x = \rho_{air} C_d W U_{10} \quad (2.7)$$

$$\tau_x = \rho_{air} C_d W V_{10} \quad (2.8)$$

where ρ_{air} is the density of air, C_D is the drag coefficient and U_{10}, V_{10} are the wind velocities at 10m in the zonal and meridional directions, respectively.

In comparison, in the model forced by relative winds, the forcing speed in the wind stress calculation is found by taking the difference between the wind velocities at 10 m and the surface current velocities at every time step. In the model forced by relative winds, wind stress is calculated using

$$W = \sqrt{(U_{10} - U_{Ocean})^2 + (V_{10} - V_{Ocean})^2} \tag{2.9}$$

$$\tau_x = \rho_{air} C_d W (U_{10} - U_{Ocean}) \tag{2.10}$$

$$\tau_y = \rho_{air} C_d W (V_{10} - V_{Ocean}) \tag{2.11}$$

where U_{Ocean}, V_{Ocean} are the surface current velocity in the zonal and meridional directions respectively.

When the velocity of the surface currents is equal to 0, there will be no difference between the experiments (Middleton, 2015). However, depending on the direction of the surface currents, the experiment forced with absolute winds would either over estimate or under estimate the wind stress on the ocean (Middleton, 2015). The differences in the wind stress between the 2 experiments are analysed in Chapter 4 of this thesis. Weekly averaged output from January 1993 until December 2013 were used from both simulations.

CHAPTER 3.

OBSERVED EDDY DISSIPATION IN THE AGULHAS CURRENT

This chapter is based on the work published as:

Braby, L., B. C. Backeberg, I. Ansorge, M. J. Roberts, M. Krug, and C. J. C. Reason (2016), Observed eddy dissipation in the Agulhas Current, Geophys. Res. Lett., 43, 8143–8150, doi:10.1002/2016GL069480.

3.1 Introduction

Variability in the northern Agulhas Current is influenced by both cyclonic and anti-cyclonic mesoscale eddies, originating from the Mozambique Channel and south of Madagascar (hereafter referred to as source region eddies) and which propagate towards the offshore edge of the Agulhas Current (Schouten et al., 2002; Harlander et al., 2009; Backeberg and Reason, 2010; Collins et al., 2014). Past studies focused on the influence anti-cyclonic eddies have in destabilising the current's trajectory and thus triggering cyclonic meanders known as Natal Pulses (de Ruijter et al., 1999; Schouten et al., 2002; Tsugawa and Hasumi, 2010). These pulses have been shown to propagate polewards along the offshore edge of the Agulhas Current (van Leeuwen et al., 2000; Backeberg et al., 2008), occasionally affecting the Agulhas retroflection dynamics, by causing an upstream retroflection of the Agulhas Current (Lutjeharms and van Ballegooyen, 1988), thereby affecting the leakage of warm and salty waters into the South Atlantic Ocean (Biastoch et al., 2008; Loveday et al., 2014). In contrast, the impact of cyclonic eddies on the dynamics of the Agulhas Current is less known. Indeed, the need for improved understanding of such interactions has been highlighted by Zhai et al. (2010) and Rouault and Penven (2011).

The mesoscale eddy circulation in the Mozambique Channel and south of Madagascar is complex, and both cyclonic and anti-cyclonic eddies regularly propagate from these source regions towards the Agulhas Current. However, the mechanisms for eddy entrainment and their dissipation in the Agulhas Current is not well understood. The region is poorly observed and numerical models tend to exaggerate the frequency and scales of eddies approaching the Agulhas Current. This is further evident by the eddy kinetic energy (EKE) distribution of eddy resolving models (Backeberg et al., 2014; Durgadoo et al., 2013; Loveday et al., 2014), where higher levels of EKE have been observed further from the coast than satellite altimetry observations suggest (Penven et al., 2006; Biastoch et al., 2008).

Globally, western boundary currents are known to be sinks for ocean-eddy energy (Zhai et al., 2010), and conventionally, anti-cyclonic and cyclonic eddies interacting with a wall are known to propagate poleward and equatorward, respectively, along a continental shelf (Shi and Nof, 1993; Shi and Nof, 1994). These studies did not, however account for the presence of a western boundary current. A study by Nof (1999) shows that as an eddy interacts with a meridional boundary wall, it remains almost stationary and gradually dissipates as a result of an equatorward leakage of water from the eddy until it can no longer be defined as an eddy. Nof (1999) also highlight that an eddy propagating towards such a boundary loses one third of its open ocean velocity as a result of increased bottom friction. Nof (1999) show that eddies slow down as they propagate towards a western boundary but suggest that water leakage from an eddy interacting with a continental boundary would be very difficult to detect because it would be occurring at depth. One might consider that in the case of deep ocean eddies interacting with a western boundary current, the eddy-topography interaction is relatively small, as the western boundary current present a significant barrier through which the eddies need to break in order to feel the bathymetry. Figure 3.4 suggests that eddies passing through the region 28° – 29.5° S and 31° – 35° E have dissipated at 32.9° E, before reaching the landward side of the core of the current which is at 32.2° E. Frequent interactions between deep oceanic eddies and the northern region of the Agulhas Current make this area an ideal natural laboratory to study the evolution of source region eddies as they approach and interact with a major western boundary current.

This paper aims to build on previous eddy dissipation studies using a global (altimetry-based) dataset of automatically tracked eddies in combination with *in-situ* surface drifter data and altimetry-derived geostrophic currents.

3.2 Data and Methods

Eddy characteristics from a global (altimetry-based) dataset of automatically tracked eddies (Chelton et al., 2011 - http://cioss.coas.oregonstate.edu/eddies/) were analysed for the Agulhas Current region between 24° – 52° E and 15° – 35° S for the period October 1992 to April 2012. A detailed description of the eddy-tracking data used in this study is given in Chapter 2. In this study, only eddies passing through the northern sector of the Agulhas Current, defined by Grundlingh (1983) and Lutjeharms (2006) to be 28° − 29.5° S and 31° − 35° E, were considered (black box in Figure 3.1). Surface current velocities in this region are known to often exceed 1.3 ± 0.3 m.s^{-1} (Grundlingh, 1980).

In some instances the Chelton eddy-tracking algorithm fails to accurately track the origin and termination sites of an eddy. One example of this is illustrated in Figures 3.1 and 3.2 below. The algorithm tracked an eddy from 27 November 2002 until 2 July 2003. On 9 July 2003, the same eddy is wrongly given a different identification number and propagates down the Agulhas Current until it dissipates on 1 October 2003. It was found that 41.7% of eddies used in this study were not correctly tracked. Of these eddies, 41.8% were found to dissipate too early as a result of an erroneous change in the eddy identification numbers. As this could impact the outcome of our study, the eddy-tracking dataset used in this study has been thoroughly visually checked against the AVISO Sea Level Anomaly fields. Where necessary, eddy trajectories have been merged to correct eddy formation and termination points, when the algorithm incorrectly identified new eddies. The results and conclusions of this study are based on this corrected data set.

Eddy parameters used in this study were determined from altimetry data – which are known to have limitations near the coast (Bouffard et al., 2010; Chelton et al., 502011). Hence, to further validate the accuracy of eddy characteristics in the northern Agulhas Current where the current flows close to the coastline, the eddy termination sites were compared to *in-situ* surface drifter observations from the Global Drifter Programme (GDP) (Figure 3.4). Nine drogued drifters which were entrained into eddies and subsequently moved into the Agulhas Current, after passing through the black box (Figure 3.4a), were studied. A drifter was identified to have moved into an eddy when its trajectory moved in concentric circles.

To illustrate the effect of the Agulhas Current on approaching eddies, the formation and termination positions of all cyclonic and anti-cyclonic eddies passing through the black box (Figure 3.4) were overlaid on the mean geostrophic current derived from altimetry observations for the period October 1992 to April 2012 (Figure 3.4b).

The long-term and annual mean meridional geostrophic velocity profile from 31° to 35° E, together with the corresponding meridional mean eddy amplitudes and radii are shown in Figure 3.5. To illustrate the mechanism through which eddies are dissipated by interacting with the Agulhas Current, two case studies are presented using satellite altimetry derived geostrophic currents (Figure 3.6).

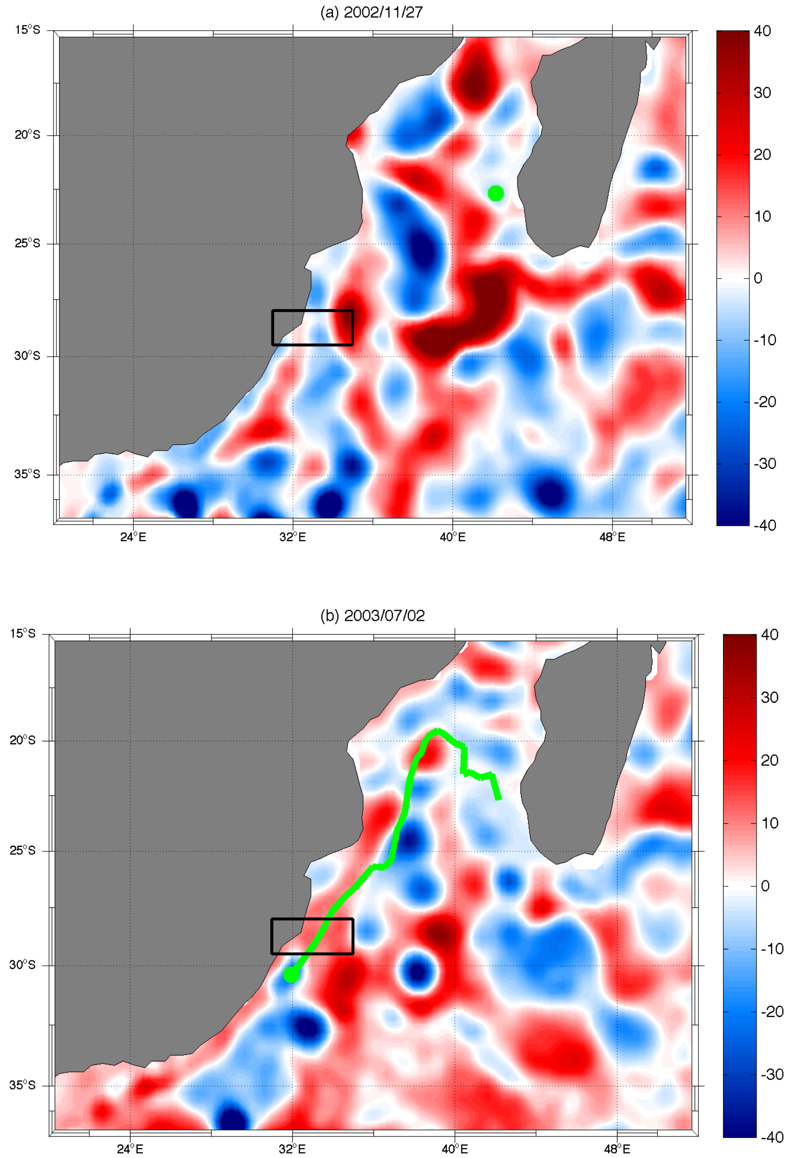

Figure 3.1: AVISO Sea level anomaly (cm) with a) a green circle showing the origin of an eddy which travels through the black box as tracked by the Chelton algorithm and b) a green line and circle depicting the eddy trajectory and termination point as tracked by the Chelton algorithm.

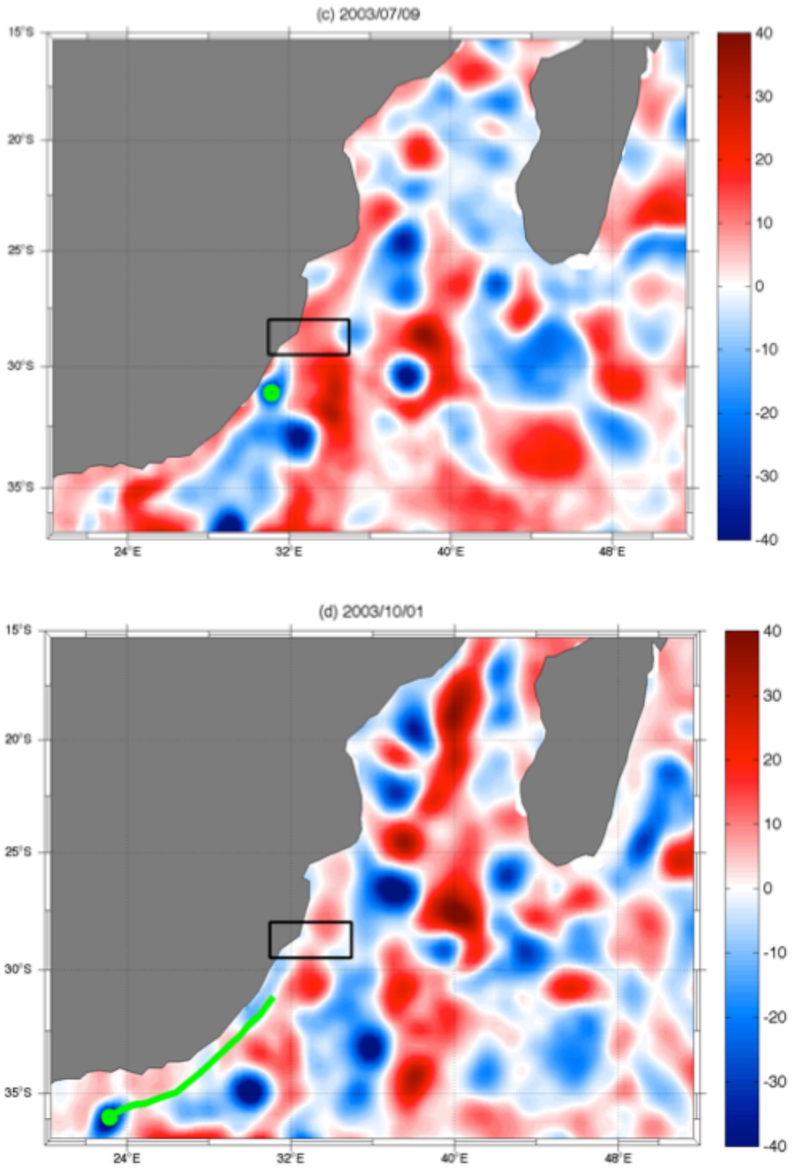

Figure 3.2: AVISO Sea level anomaly (cm) with c) a green circle showing the origin on an eddy which travels through the black box as tracked by the Chelton algorithm and d) a green line and circle depicting the eddy trajectory and termination point as tracked by the Chelton algorithm.

In order to quantitatively analyse how eddies interact with the Agulhas Current, the offshore position and velocity of the Agulhas Current along the transect extending between 30.0° – 32.4° S and 30.95° – 34.4° E (see black line in Figure 3.3) is determined using the method described in Krug et al. (2014). The resultant offshore position and current velocity anomaly time series are shown in Figure 3.7. Observations in the altimetry data where cyclonic and anti-cyclonic eddies interact with the Agulhas Current are represented by the blue and red vertical lines respectively. Events in which an eddy interacted with the Agulhas Current were defined as the minimum distance between the eddy's edge and the concurrent position of the current. In this study, an eddy is considered to interact with the Agulhas Current if its edge was <50 km from the current core (where 50 km is the minimum size used in this study to define a mesoscale ocean eddy). All data used in this chapter is weekly data, with corresponding times.

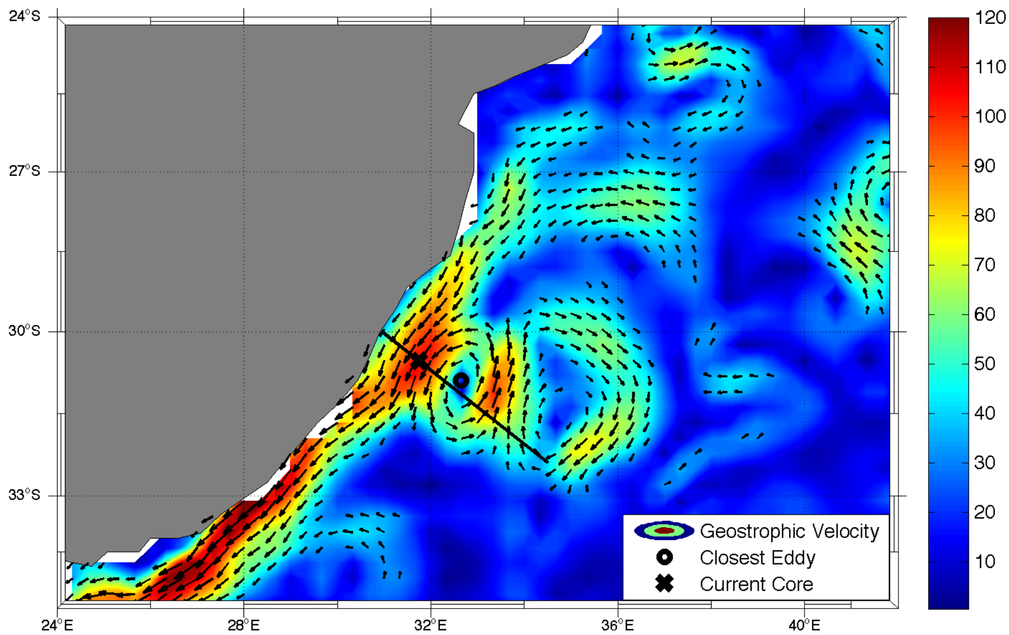

Figure 3.3: Weekly geostrophic velocities (cm.s^{-1})(colour) with the location of an anti-cyclonic eddy (circle) at its closest position to the Agulhas Current core (x) along the transect (30.0° – 32.4° S and 30.95° – 34.4° E). Vectors indicate the direction of flow for velocities greater than 50 cm.s^{-1}.

A wavelet analysis was performed on the time series of Agulhas Current core velocities extracted from the AVISO MADT data if there was any seasonality to the velocity of the Agulhas Current and is shown in Figure 3.8. The method used was initially developed by Torrence and Compo (1998) (available online at http://paos.colorado.edu/research/wavelets/), with the bias of their method corrected by Liu et al. (2007). The chi- squared method was used to calculate significance. Previously, wavelet analyses of the Agulhas Current core have been carried out further south in the Agulhas Current (Krug et al., 2012). In this way, it is also possible to ensure that the composite analysis that follows is not biased by a potential seasonal variability.

A composite analysis was performed so as to quantify the average change to the current during an Agulhas Current – eddy interaction event (Figure 3.9). The mean velocity anomaly where all anti-cyclonic (Figure 3.9(a1)) and cyclonic (Figure 3.9(b1)) eddies interact with the Agulhas Current was calculated and composite maps for the weeks following the eddy–current interaction events calculated for weeks 1 and 3 (anti-cyclonic eddy interaction, Figures 3.9(a2, a3)) and as a result of slower propagation speeds for weeks 6 and 15 (cyclonic eddy interaction, Figures 3.9(b2, b3)). These weeks were chosen to best show a sequence of the velocity anomalies propagating down the Agulhas Current

3.3 Results and Discussion

Surface drifters were used to highlight the entrainment of mesoscale eddies into the Agulhas Current (Figure 3.4a). On approaching the Agulhas Current, rotating drifter trajectories very quickly become linear indicating their entrainment into the fast flowing Agulhas Current. The position of the eddy termination sites for eddies moving through the same region (red x's, Figure 3.4b) shows that eddies forming in the Mozambique Channel and south of Madagascar (blue circles) are no longer tracked, shortly after arriving at the Agulhas Current – providing evidence of eddy dissipation. This also indicates that the eddy characteristics dataset (Chelton et al., 2011) is able to accurately determine eddy characteristics as they approach the Agulhas Current.

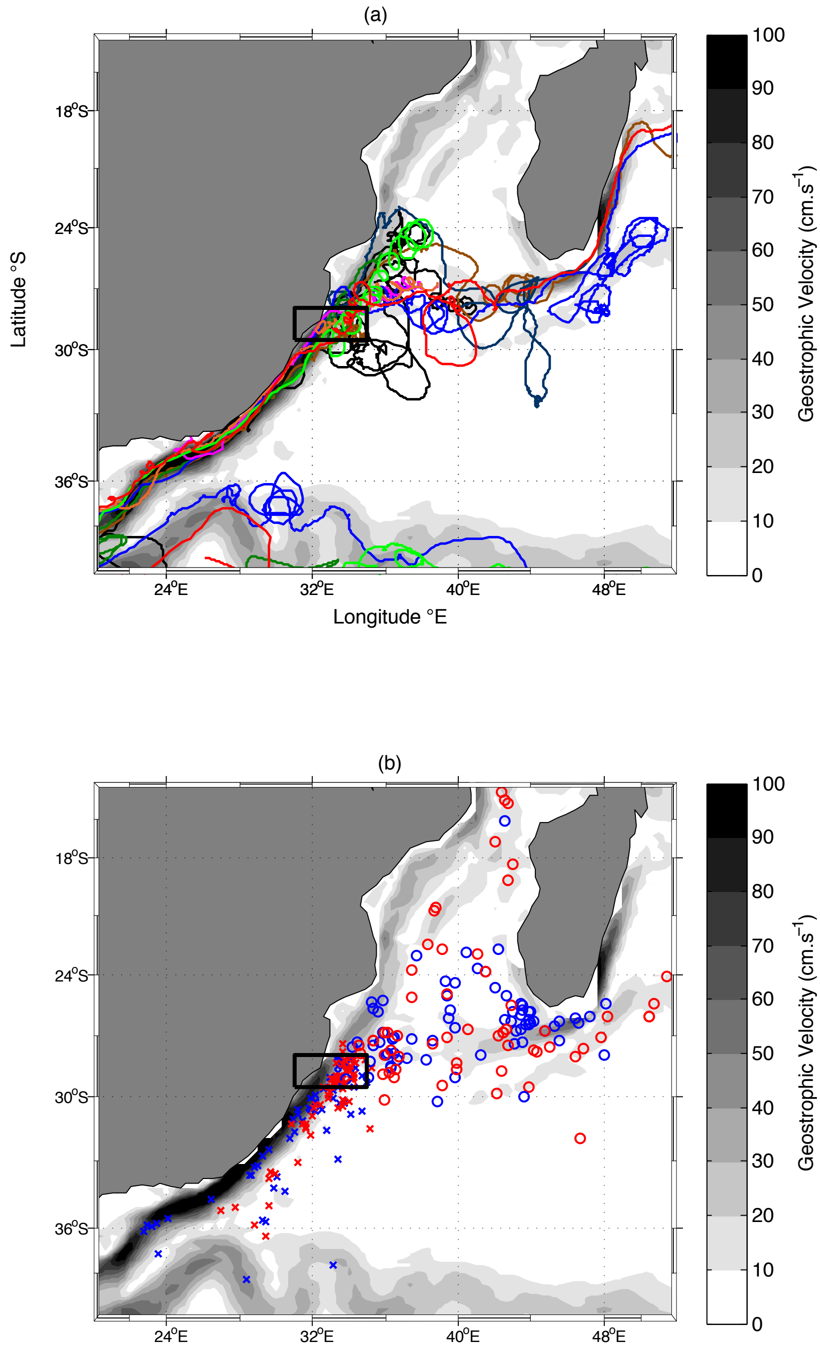

Figure 3.4: a) The trajectories of surface drifters (colour) passing through the black box between October 1992 and April 2002. b) Formation (circles) and termination (x's) sites of all cyclonic (blue) and anti-cyclonic eddies (red) passing through the black box overlaid on the mean geostrophic current derived from the satellite altimetry observations between October 1992 and April 2012.

Considering all eddies that pass through the black box between 1992 and 2012 (Figure 3.4a), it is evident that those arriving at the Agulhas Current originate predominantly from the Mozambique Channel and the South East Madagascar

Current (Figure 3.4b). Approximately 5 eddies propagate into the black box annually. A maximum of 22% of the eddies reach further south each year. Increasing the width of the black box, to capture these offshore eddies, does not alter the results of our study. Although more eddies are captured in a bigger box, it is still found that the eddies still dissipate upon approaching the Agulhas Current further south. Additionally, a larger box also captured eddies that did not interact with the Agulhas Current – many of these eddies propagate southwestward before dissipating upon interaction with other eddies. We chose to keep the box small as we wanted to examine only those eddies that propagated into the Agulhas Current.

A total of 132 source region eddies approached the Agulhas Current at the black box between October 1992 and April 2012 of which 61 eddies were anti-cyclonic and 71 eddies were cyclonic. Before they interacted with the Agulhas Current, eddies have radii of 50 – 200 km, in agreement the existing literature (Schouten et al., 2002l de Ruijter et al., 2004; Ridderinkhof et al., 2013; Halo et al., 2014a; Halo et al., 2014b). The dissipation of eddies upon approaching the Agulhas Current is evident in the mean zonal geostrophic velocity profile, the zonal mean eddy amplitudes and radii from 31° to 35° E (Figure 3.5). Eddies decrease in amplitude and radius upon approaching the Agulhas Current between 28° and 29.5° S. They reach their minimum dimensions at around 33° E where Agulhas Current velocities are approximately 45 $cm.s^{-1}$. Between 35° E and 33° E, the mean radius of the eddies decreases from 98 ± 23 km to 65 ± 10 km and the mean amplitude of decreases from 21 ± 12 cm to 8 ± 6 cm. The mean decrease in amplitude and radii is most pronounced when eddies are within ± 100 km proximity of the Agulhas Current. These results suggest that eddies dissipate upon approaching the Agulhas Current due to eddy-current interactions. While we are confident that the eddy characteristics are accurately captured in the dataset (Figure 3.5), it should be noted that the dataset does not necessarily track eddies close to the coast and that eddies may exist for longer than the automated eddy tracking algorithm suggests.

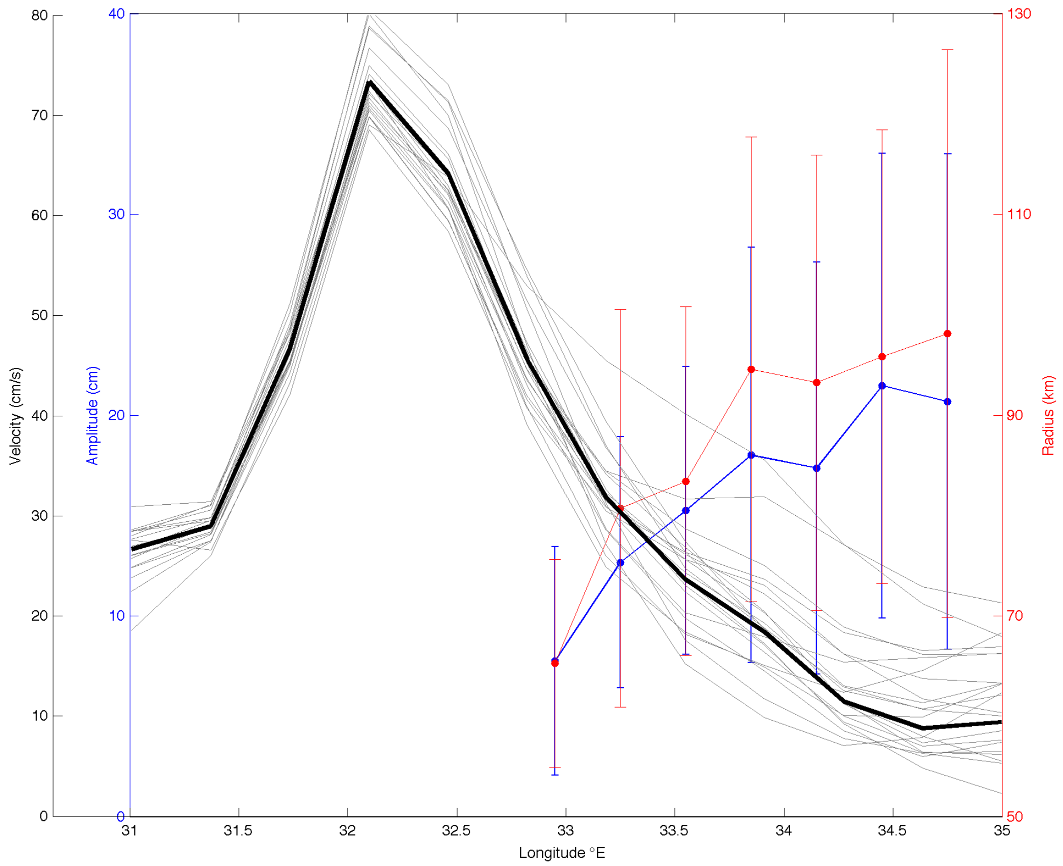

Figure 3.5: The meridional mean of 28° – 29.5 S° and standard deviation of the radii (red) and amplitudes (blue) of eddies as they approach the Agulhas Current meridional mean of 28° – 29.5 S° indicated by the black line. Thin grey lines show annual meridional mean velocities of the Agulhas Current.

To illustrate the mechanism through which eddies are dissipated by interacting with the Agulhas Current, two case studies are presented using satellite altimetry derived geostrophic currents (Figure 3.6). Figure 3.6(a) shows an anti-cyclonic eddy approaching the Agulhas Current. The leading edge of the anti-cyclonic eddy is flowing in the same poleward direction as the Agulhas Current and the interaction of the eddy with the fast flowing Agulhas Current causes the eddy to become elongated (Figure 3.6(a2)) until it eventually becomes entrained in the current.

The results showing eddy dissipation are in agreement with previous findings (Zhai et al., 2010) which show western boundary currents to be eddy energy sinks. An investigation into the influence of all eddies on the velocities and position of the Agulhas Current core was also undertaken for the transect 30° S, 30.95° E to 32.4° S, 34.4° E (Figure 3.9) by tracking the maximum current velocity and its offshore position (red vertical lines in Figure 3.7). The time mean satellite-derived geostrophic current velocity and distance offshore at this latitude was found to be 0.91 $m.s^{-1}$ and 69 km. On average an anti-cyclonic eddy interacting with the Agulhas Current increases the velocity by 0.16 ± 0.17 $m.s^{-1}$ and shifts the current to 100 ± 79 km from the coast[1]. At first our results appear to contradict a study by Leber and Beal (2014), which shows that although transport is maintained during a meander of the Agulhas Current, the current widens and its core velocity decreases by 0.70 $m.s^{-1}$. However, their case-study was much further south of the transect 30° S, 30.95° E to 32.4° S, 34.4° E, and was caused by an eddy that did not propagate within 50 km of the Agulhas Current core along this transect and therefore was not included in this study.

These results differ from the existing literature, which shows the dissipation of anti-cyclonic (cyclonic) eddies through the gradual equatorward (poleward) leakage of water resulting from eddy interactions with a boundary (Shi and Nof, 1993, 1994; Nof, 1999). It is also assumed that any leakage from the eddies in this study would be swept poleward, by the Agulhas Current. Associated with this entrainment and dissipation is a momentum transfer whereby velocities of the Current appear to increase. This is in agreement with the suggestion by Tsugawa and Hasumi (2010) that the Agulhas Current speed increases is due to the transfer of barotropic energy from the anti-cyclonic eddies. The equatorward flow component of the eddy can be seen east of the Agulhas Current, and remains visible for 2 weeks (Figure 3.6(a3)). The entire sequence took place over 7 weeks and is a typical example of anti-cyclonic eddy interaction with the Agulhas Current.

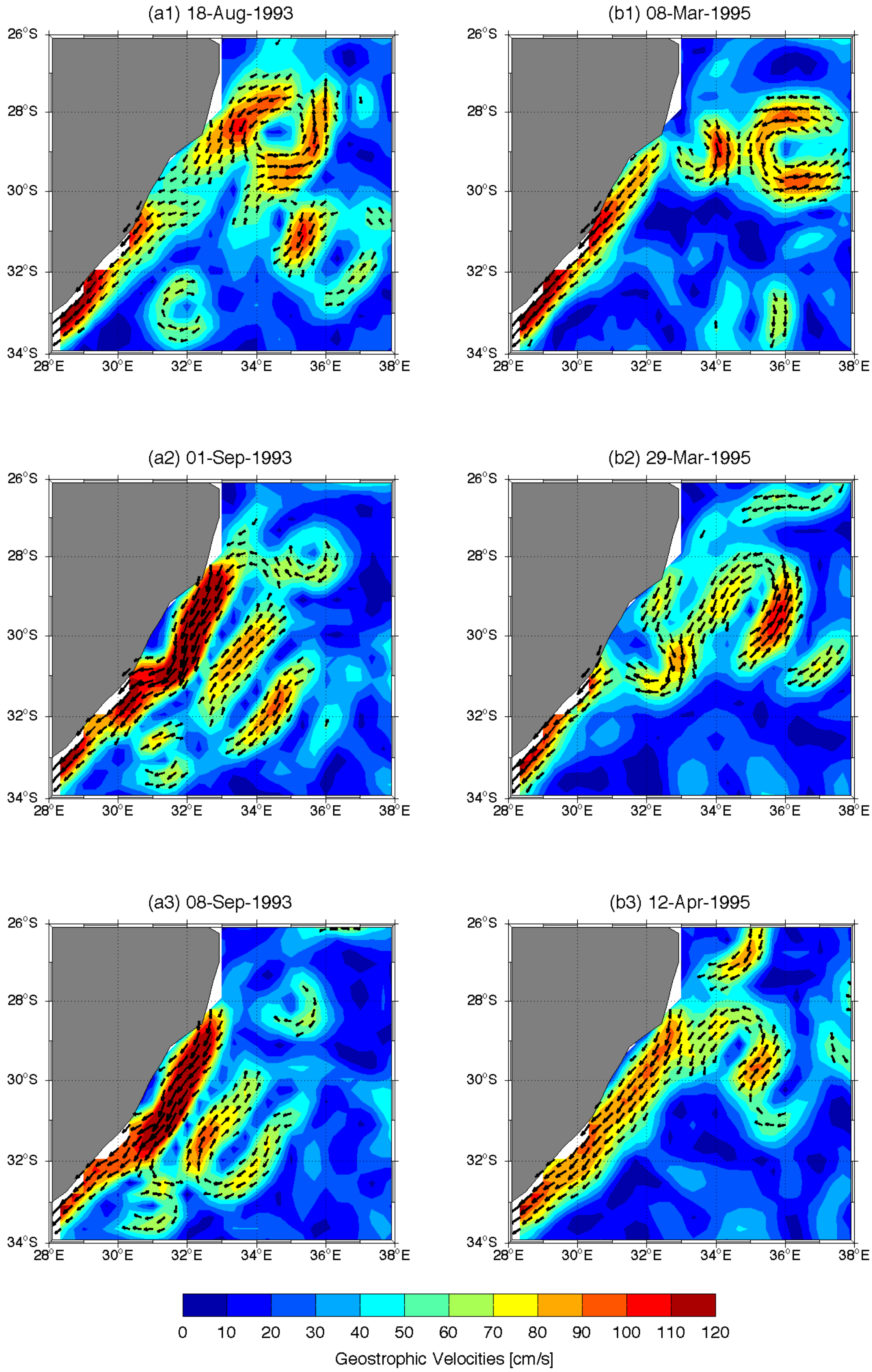

Figure 3.6: Stages of dissipation of a) an anti-cyclonic eddy and b) a cyclonic eddy shown by geostrophic velocities ($cm.s^{-1}$) derived from satellite altimetry SSH means. Arrows indicate the direction of flow in regions with velocities over 50 $cm.s^{-1}$.

In contrast, cyclonic eddies interacting with the Agulhas Current (blue vertical lines in Figure 3.7) are associated with a decrease of its velocity by 0.13 ± 0.16 $m.s^{-1}$ and an offshore shift to 145 ± 85 km from the coast. All of the mean changes associated with anti-cyclonic and cyclonic eddies observed here are significant at the 95% confidence interval using a student t-test. Similarly, examination of individual eddy-current interactions shows the leading equatorward flow of a cyclonic eddy to become weaker as it approaches the Agulhas Current. This is likely due to horizontal shear of the opposing flow. In Figure 3.6(b2), the interaction of a cyclonic eddy entering the Agulhas Current appears to result in a formation of a cyclonic meander at 30° S, which dissipates within 2 weeks. Overall the Agulhas Current velocity appears to have reduced by almost 30 $cm.s^{-1}$ following the entrainment of a cyclonic eddy. Observations of these interactions frequently showed the formation of cyclonic meanders in the Agulhas Current, or Natal Pulses. In contrast to existing literature which states that Natal Pulses are triggered by the interaction of an anti-cyclonic eddy with the Agulhas Current (de Ruijter et al., 1999; Schouten et al., 2002; Tsugawa & Hasumi, 2010), our results show that cyclonic eddy interaction result in an ever larger meander. Additionally, on 7 occasions the cyclonic eddies interacting with the Agulhas Current (Figure 3.7) have anti-cyclonic eddies located to their east-northeast suggesting the presence of dipole eddies similar to those documented in Ridderinkhof et al. (2013).

Results from Figure 3.8 show that there is no statistically significant seasonal cycle in the time series of Agulhas Current core velocities. Additionally, there did not appear to be any significant seasonality to the arrival of the tracked eddies at the Agulhas Current (from Figure 3.7). There is a peak at the annual cycle, however it is not statistically significant. The wavelet analysis shows that eddies cause a band of statistically significant variability in the Agulhas Current with a repeat period of 6 weeks to 6 months (2 − 8 times per year) in agreement with the documented Natal Pulse and source region eddy frequencies (Lutjeharms and Roberts, 1988; Rouault and Penven, 2011). These results are in accordance with a study on the South East Madagascar Current by Ponsoni et al., (2016) which also shows that westward-propagating, mesoscale eddies can have an important impact on the variability of an ocean current. This highlights the influence of eddies on Agulhas Current velocities and supports our results in Figure 3.6.

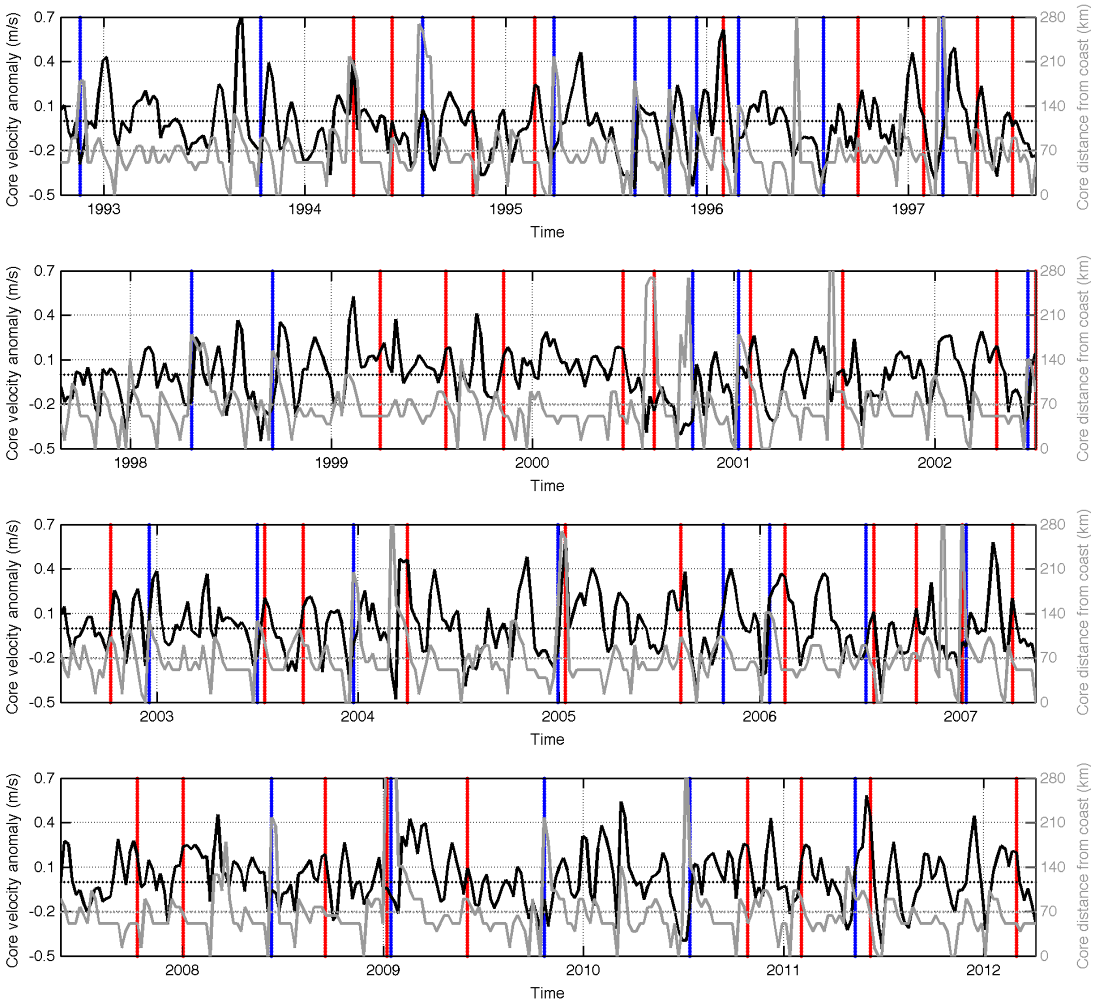

Figure 3.7: The time-averaged velocity anomaly of the Agulhas Current core (black), with the distance of the Agulhas Current core from the coast (grey) and cyclonic (blue) and anti-cyclonic (red) eddies interacting with the Agulhas Current core from a) 1992 – 1997, b) 1997 – 2002, c) 2002 – 2007 and d) 2007 – 2012. The position of 0 velocity anomaly is shown (black dotted line), as well as the mean distance of the Agulhas Current core from the coast (grey dotted line).

The composite analysis of eddy-current interaction events in Figure 3.9 shows the mean effect of anti-cyclonic and cyclonic eddies on the Agulhas Current (Figures 3.9(a1) and 3.9(b1) respectively). A consistent increase in the current velocity is noticeable when an anti-cyclonic eddy interacts with the Agulhas Current with the positive anomaly propagating downstream to about 26° E, 35° S at a rate of 44 km.day^{-1} (Figures 3.9(a2), 3.9(a3)), where after the signal is lost. For cyclonic eddy-current interaction events, the mean velocity core of the Agulhas Current consistently decreases close to the coast but has a strong positive velocity anomaly on the offshore edge of the current. The composite map (Figure 3.9(b1)) shows that a larger anti-cyclonic eddy lies to the northeast of the smaller cyclonic eddy indicating the consistent presence of dipole eddy pairs during cyclonic eddy-current interactions. The negative inshore and positive offshore velocity anomalies propagate downstream at 23 km.day^{-1} to 24° E, 36° S (Figures 3.9(b2, b3)) where the signal is lost. In both cases it is evident that a transfer of momentum occurs with the velocity anomalies propagating downstream at different speeds.

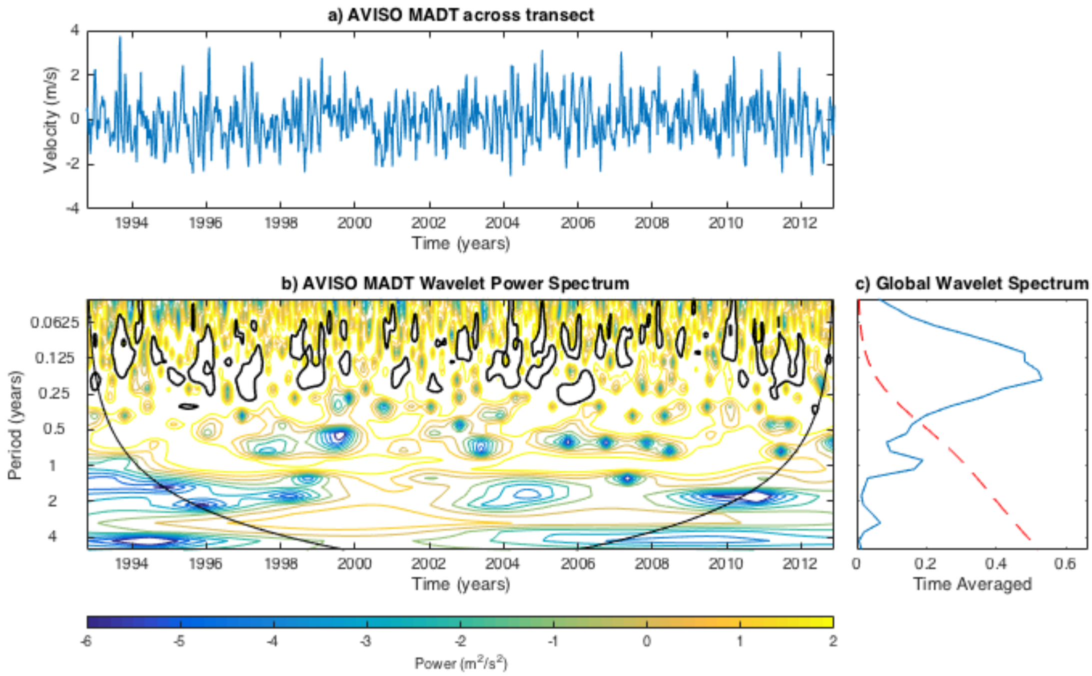

Figure 3.8: a) A time-series of Agulhas Current core velocities across the transect, 30° S, 30.95° E to 32.4° S, 34.4° E. b) A wavelet power spectrum with the 95% significance level shown by bold, black contours. A thin black line shows the cone-of-influence. c) A global wavelet spectrum (blue). The red dashed line indicates significance.

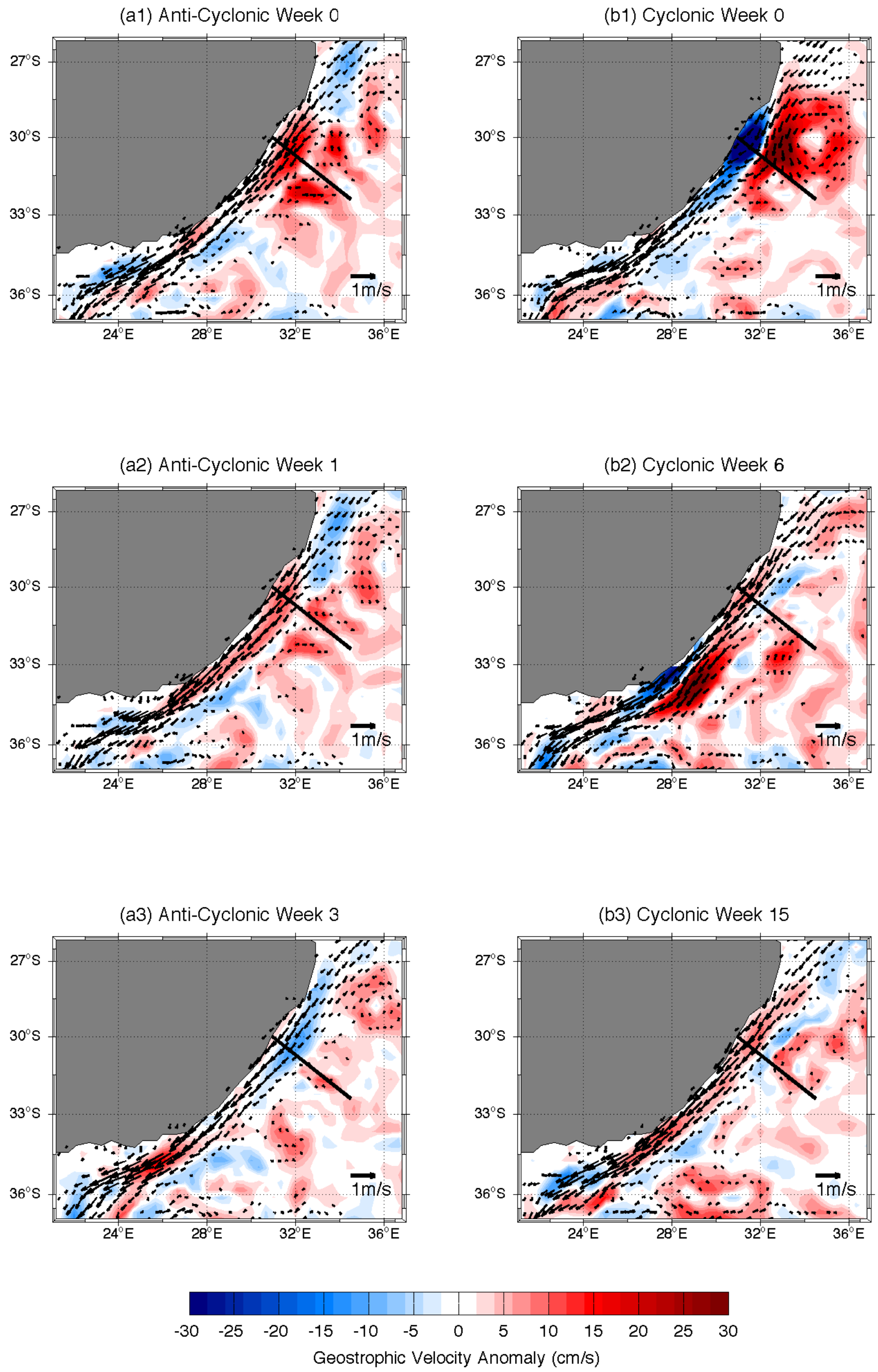

Figure 3.9: a1) The mean velocity anomaly of the Agulhas Current when an anti-cyclonic eddy is present based on 61 anti-cyclonic eddies detected from 1992 – 2012 and a2) the resulting effect on the Agulhas Current 1 week and a3) 3 weeks later. (b1) The mean velocity anomaly of the Agulhas Current when a cyclonic eddy is present based on 71 cyclonic eddies detected from 1992 – 2012 and b2) the resulting effect on the Agulhas Current 6 weeks and b3) 15 weeks later. The transect across which the Agulhas Current core properties were studied, 30° S, 30.95° E to 32.4° S, 34.4° E, is shown by a thin black line. The black vectors indicate absolute geostrophic velocity greater than 10 $cm.s^{-1}$ and show the direction of flow.

3.4 Conclusion

Using a combination of an eddy tracking dataset with *in-situ* surface drifter observations and altimetry-derived geostrophic currents, it has been shown that both cyclonic and anti-cyclonic source eddies dissipate upon approaching the Agulhas Current. On average the eddy dissipation process commences when eddies are within ± 100 km of the Agulhas Current. Their entrainment into the Agulhas Current affects its mean velocity and offshore position through a transfer of momentum, with anti-cyclonic eddies consistently increasing the Agulhas Current velocity by 0.16 ± 0.17 $m.s^{-1}$. In contrast, entrainment of cyclonic eddies results in a decrease in velocity by 0.13 ± 0.16 $m.s^{-1}$ and shifts the current up to 145 ± 85 km offshore. These velocity anomalies propagate downstream at rates of 44 $km.day^{-1}$ (anti-cyclonic) and 23 $km.day^{-1}$ (cyclonic).

Finally, the observed eddy interaction and dissipation process described in this study is poorly represented in many numerical models (e.g. Backeberg et al., 2014; Durgadoo et al., 2013; Loveday et al., 2014). In these models, eddies propagate from the source regions to the Agulhas retroflection as a train of successive eddies. This suggests that energy dissipation processes affecting the variability of the Agulhas Current are not adequately resolved in numerical models and may result in incorrect estimates of the transport associated with the Agulhas Leakage. Consequently, inaccurate parameterization of these models, through poor representation of eddy entrainment processes, may have further implications on the links between source region eddies and mesoscale variability within in the Agulhas Current, its retroflection and the exchange of heat and salt between the Indian and South Atlantic ocean basins, and thus on global climate.

CHAPTER 4.

THE IMPACT OF CHANGING WIND STRESS ON AGULHAS CURRENT SOURCE REGION EDDY CHARACTERISTICS IN HYCOM

4.1 Introduction

In Chapter 3, it was shown that both cyclonic and anti-cyclonic eddies from the Mozambique Channel and south of Madagascar dissipate as they approach the Agulhas Current and are able to significantly influence the velocity and position of the Agulhas Current core. Whilst existing numerical models are successfully able to capture many aspects of the Agulhas Current, they tend to overestimate or underestimate the frequency and size of the source region eddies and associated eddy kinetic energy (EKE) levels (Backeberg et al., 2014; Durgadoo et al., 2013; Loveday et al., 2014). Many numerical model configurations, at a range of horizontal resolutions, face problems in simulating the mesoscale dynamics accurately; including the Fine Resolution Antarctic Model (FRAM) (Lutjeharms and Webb, 1995); the Parallel Ocean Program (POP) model (Maltrud and McClean, 2005); the Ocean General Circulation Model (OGCM) for the Earth Simulator (OFES) (Sasaki et al., 2004); DRAKKAR, OCCAM and CLIPPER (Barnier et al., 2006); the Naval Research Laboratory (NRL) Layered Ocean Model (NLOM) (Wallcraft et al., 2002); the Hybrid Coordinate Ocean Model (HYCOM) (Backeberg et al., 2008, Backeberg et al., 2009, Backeberg et al., 2014; Thoppil et al., 2011); The Regional Ocean Modelling System (ROMS) (Loveday et al., 2014) and the Nucleus for European Modelling of the Ocean (NEMO) model (Durgadoo et al., 2013). The observed eddy dissipation process of source region eddies as they approach the Agulhas Current, described in the previous chapter, is also poorly represented in numerical models (Backeberg et al., 2008; Backeberg et al., 2014; Durgadoo et al., 2013; Loveday et al., 2014). In these models, eddies tend not to dissipate but rather they propagate along the offshore edge of the current towards the Agulhas retroflection, an example of which is given in Figure 4.1.

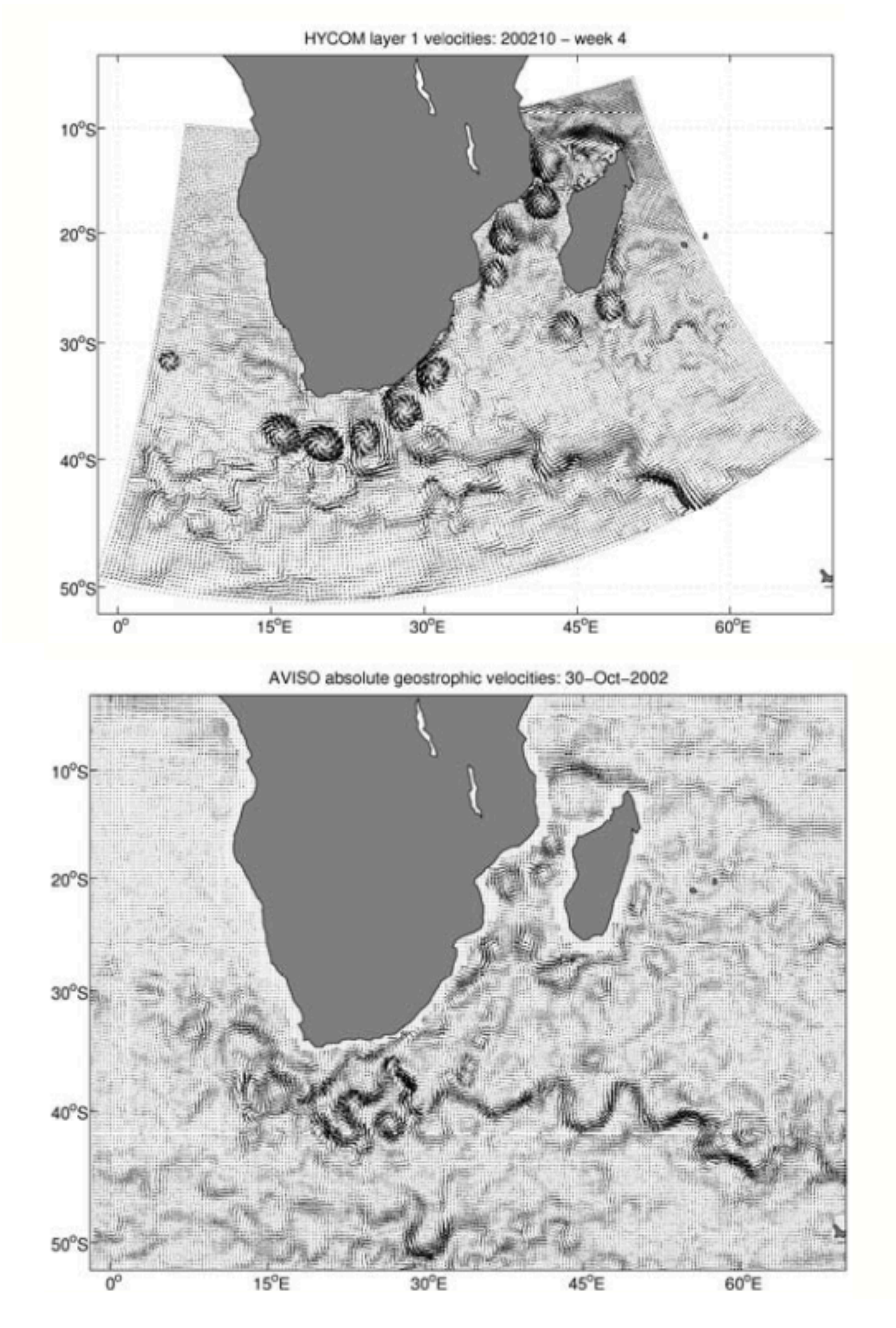

Figure 4.1: Weekly surface velocities from a) a numerical model and b) AVISO satellite altimetry (Source: Backeberg et al., 2008).

Studies have shown that coupled ocean-atmosphere models are better able to simulate mesoscale variability than uncoupled models (McClean et al., 2011; Putrashan et al., 2015; Chen et al., 2016; Renault et al., 2016a; Renault et al., 2016b; Renault et al., 2017). This is because coupled models are able to incorporate important air-sea interactions through the inclusion of small-scale processes in the ocean which enable the atmosphere to be more realistically forced (Renault et al., 2017). Two of the most commonly studied ocean-atmosphere feedbacks are thermal and current feedbacks, whereby the influences of sea surface temperature (SST) and sea surface velocity on the atmosphere are investigated.

4.1.2 Thermal Feedback

Although thermal feedback is not the focus of this investigation, most studies on ocean-atmosphere feedback tend to focus on the effects of SST gradients on gradients in the surface wind and stress (Cornillion and Park 2001; Chelton et al., 2004; Park et al., 2006; Chelton et al., 2007; Minobe et al., 2008). SST feedback has been shown to have an effect on wind stress which results in an increase in Ekman pumping velocities, causing the dampening of mesoscale eddies, however it primarily influences the propagation of the eddies (Seo et al., 2015). SST gradients of Agulhas Rings are known to be weaker in a coupled model than an uncoupled model and may explain improvements in the simulation of Agulhas ring pathways (Renault et al., 2017). However, it was also shown that thermal feedback does not induce an ocean-atmosphere transfer of energy that affects the EKE over the Agulhas retroflection region (Renault et al., 2017). The impact of SST on wind stress was however found to be significant in *in-situ* observations (Rouault et al., 2000; Rouault et al., 2003). A recent study by Krug et al. (2018) also revealed that SST has an influence on observed winds, as well as the wind stress. For the purposes of this study, a coupled model is not used and therefore the importance of thermal feedback cannot be investigated.

4.1.3 The Impact of Current Feedback on Coupled Models

Even though sea surface velocities are usually much weaker than wind velocities, surface ocean currents can affect the atmosphere; this is known as current feedback (Renault et al., 2017). A study by Dewar and Flierl (1987) showed that including the effect of sea surface velocity in wind stress calculations caused model Gulf Stream rings to weaken. Since then, several studies (Duhaut and Straub, 2006; Dawe and Thompson, 2006; Eden and Dietze, 2009; Renault et al., 2016a; Renault et al., 2016b; Abel et al., 2017; Renault et al., 2017) have shown that the inclusion of surface currents in wind stress calculation caused a significant reduction in the energy of coupled ocean-atmosphere models though "mechanical dampening". This effect of currents on winds in western boundary currents has also been shown in satellite data (Kelly et al., 2001; Chelton et al., 2004). More recently, current feedback to the atmosphere, in coupled models, has been shown to reduce the work done by the wind on the ocean (wind work) and hence the EKE in the ocean (Hughes and Wilson 2008; Scott and Xu 2009; Renault et al., 2016a; Renault et al., 2016b; Renault et al., 2017). Wind work can be calculated using the following equation:

$$FK = \frac{1}{\rho_0}(\overline{\tau_x u_o} + \overline{\tau_y v_0}) \tag{4.1}$$

where F is the buoyancy and wind forcing term at the surface and K is the Mean Kinetic Energy, ρ_0 is the mean seawater density, τ_x, τ_y are the time mean wind stress, over the whole period, in the zonal and meridional directions respectively, u_o and v_o are the time mean surface ocean currents in the x and y directions.

Consequently, current feedback is often referred to as an "eddy killer" (Renault et al., 2016a; Renault et al., 2016b; Renault et al., 2017). Abel et al. (2017) found including current feedback in an ocean-only model to be more accurate than a coupled ocean-atmosphere model.

A recent study in the Gulf Stream has shown that current feedback has two different effects (Renault et al., 2016a). Firstly, the reduction in wind work caused the model North Atlantic gyre to slow down, resulting in a weakening of the Gulf Stream.

Secondly, the current feedback caused a wind stress curl contrary to the current vorticity that resulted in a loss of energy from the geostrophic current to the atmosphere. The relationship between the vorticity and the curl was calculated using a similar method to Chelton et al. (2017), by averaging a 1 month running means of the wind stress curl as a function of the current vorticity running means for 1 month, for the full time period. The consequent effect is a 27% reduction in EKE (Renault et al., 2016a).

In a similar study by Renault et al. (2016b), the current feedback to the atmosphere in the California Upwelling System was assessed using a coupled ocean-atmosphere model and an uncoupled model. It was concluded that the current feedback, through mechanical dampening, reduced surface EKE by 50%. It was also shown that a decrease in surface stress could lead to an increase in the wind. As in Renault et al. (2016a) the geostrophic current feedback caused a surface stress curl that was opposed to the current vorticity. This caused energy to be transferred from the current to the atmosphere and a decay of eddies in the region. It was also shown that current feedback could lead to an increase in the wind, which partially re-energises the ocean. The results from the study by Renault et al. (2016b) shows that by reducing eddy amplitudes, rotational speeds and eddy lifespans, current feedback improves eddy simulation in the California Upwelling System.

4.1.4 The Effects of Current Feedback on the Agulhas Current System

A modelling study of the Agulhas Current System by Renault et al. (2017) showed two mechanisms for EKE reduction. Firstly, the surface ocean current feedback to the atmosphere reduced the wind work and caused a mean energy decrease over the domain of 25%. Baroclinic and barotropic energy conversion terms, which show where EKE is generated or lost (Kundu, 1990; Halo et al., 2014b) were calculated for the region. The reduction in wind work resulted in an 8% reduction in the barotropic conversion from mean kinetic energy to EKE and a 5% reduction of the baroclinic conversion from eddy potential energy to EKE over the Mozambique Channel. Secondly, the current feedback caused a surface stress curl opposite to the vorticity of the current that was shown to weaken eddies by decreasing the energy transfer from the geostrophic currents (the eddies) to the atmosphere. The uncoupled model showed an over estimation of EKE over the whole domain by 75% with respect to AVISO satellite data. The decrease of eddy geostrophic wind work is a major contributor to the reduction of EKE of the Agulhas System (Renault et al., 2017). Eddy wind work is calculated using the method described by Marchesiello et al. (2003) as

$$F_e K_e = \frac{1}{\rho_0}(\overline{\tau'_x u'_o} + \overline{\tau'_y v'_o}) \tag{4.2}$$

where u'_o and v'_o are the horizontal fluctuations in mean ocean surface current velocities in the x and y directions and τ'_x and τ'_y are fluctuations in wind stress in the zonal and meridional directions respectively. Eddy wind work can be further divided into its geostrophic and ageostrophic components. Eddy geostrophic wind work can therefore be defined by the equation:

$$F_e K_{eg} = \frac{1}{\rho_0}(\overline{\tau'_x u'_{og}} + \overline{\tau'_y v'_{og}}) \tag{4.3}$$

whereby u'_{og} and v'_{og} are the horizontal fluctuations in mean ocean surface geostrophic velocities in the x and y directions.

It was noted by Renault et al. (2017) that the inclusion of the entire Indian Ocean Gyre into their domain would have further reduced the wind work on the ocean, the mean circulation speed and the EKE in the Agulhas Current region. Renault et al. (2017) showed a strong correlation between eddy wind work and the EKE whereby regions with the largest EKE lost the most energy. The reduction of EKE, through the inclusion of current feedback in the numerical simulation, enabled a more realistic simulation of the Agulhas Current, the Agulhas Current retroflection and Agulhas Current leakage (Renault et al., 2017).

Renault et al. (2016b, 2017) have shown that current feedback prompts supplementary Ekman pumping, which enables dampening of eddies in the region. Interestingly, these results are comparable to the effect of thermal feedback on Ekman pumping velocities with values of approximately 10 $cm.day^{-1}$ (Gaube et al., 2015; Seo et al., 2015). The Ekman pumping from thermal feedback does not, however, have an effect on eddy amplitude but rather on eddy propagation (Renault et al., 2016b). This further highlights the value of incorporating ocean-atmosphere feedbacks in numerical simulations.

In this chapter, we compare two simulation experiments in a regional Hybrid Coordinate Ocean Model (HYCOM), in which we change the local wind forcing, and using an eddy tracking algorithm we quantify the local effect of the current feedback on mesoscale eddies forming in the Mozambique Channel and South of Madagascar and their interaction with the northern Agulhas Current. Building on the work done by done by Renault et al. (2017), this study investigates whether or not there is consistency in the processes across different modelling frameworks. Although neither of the HYCOM simulations models are coupled ocean-atmosphere models, the effect of the surface current on the wind is accounted for in the forcing (described in detail in Chapter 2 of this thesis). The first simulation experiment is forced by absolute winds; the second is forced by relative winds (the wind speed relative to the surface current speed). It is anticipated that through the process of "mechanical dampening", a reduced EKE would enable a more accurate representation of cyclonic and anti-cyclonic eddy dynamics in the source region of the Agulhas Current and that the eddy-current dissipation processes shown in the previous chapter would be better simulated in the regional HYCOM. In addition to this, a detailed investigation of the eddy field in the source region of the Agulhas Current is undertaken. Going beyond the work of Renault et al. (2017), we explore the impact of current feedback on eddy properties in the regional HYCOM. Previous studies have investigated the relative contributions of eddies and meanders to the overall EKE in the Agulhas region to investigate the impact of assimilating along track Sea Level Anomaly data (de Vos et al., 2018). The impact of mechanical dampening on mesoscale variability has not yet been separated into these components, hence we use an eddy-tracking algorithm to explore separately the contribution of eddies and meandering currents to the total change in mesoscale variability.

4.2 Data

4.2.1 The Hybrid Coordinate Ocean Model

The Hybrid Coordinate Ocean Model (HYCOM) used in this study is described extensively in Chapter 2 of this thesis. The regional model uses a combination of isopycnic vertical co-ordinates in the stratified open ocean, fixed-grid co-ordinates in the upper ocean mixed layer and sigma coordinates in shallow coastal regions at each time step of the simulation (Bleck, 2002). The domain of the regional HYCOM spans the entire Agulhas Current system at a resolution of approximately 10 km. This model is nested within a larger model (INDIA), which covers the Indian and Southern Oceans at a lower resolution of 14 km – 45 km.

INDIA provides boundary conditions to the nested model every 6 hours. INDIA is initialized from Levitus climatology and spun up for 10 years using ERA40 and ERA-interim forcing (Dee et al., 2011). The nested model is then initialized from the balanced field of the INDIA model interpolated onto a higher resolution grid (Backeberg et al., 2014). Both models are run using ERA40 and ERA-interim forcing.

4.2.2 Absolute and Relative Wind Forcing Experiments

Two experiments are examined in order to determine the local effects of absolute versus relative wind forcing in the regional HYCOM. In the model forced by absolute winds (ABS), the forcing speed in the wind stress calculation is determined from wind velocity only. The model forced by relative winds (REL) takes into account the effect of the surface ocean currents on wind velocities. In this way, we can observe the influence of surface currents on the wind work on the ocean.

4.2.3 Satellite altimetry data

AVISO Satellite altimetry data produced by Ssalto/Duacs and distributed through CMEMS (available at http://marine.copernicus.eu/services-portfolio/access-to-products/?option=com_csw&view=details&product_id=SEALEVEL_GLO_PHY_L4_REP_OBSERVATIONS_008_047) were used extensively in this study. The delayed time data are merged from several different satellites including Topex/Poseidon, Topex/Poseidon on its new orbit, ERS-1, ERS-2, Jason-1, Jason-2, Jason-1 on its new orbit, Jason-1 geodetic orbit, Envisat, Envisat on its new orbit, GFO, Cryosat-2 and Saral/AltiKa.

In order to compare the two simulation experiments to a reference data set, which is more representative of the truth, data from the surface layer of both model experiments were compared to altimetry data. It is necessary to note that the satellite data does not include the ageostrophic components of the currents (de Vos et al., 2018). Therefore, strong ocean surface currents tend to be underestimated, whilst weak ocean surface currents tend to be overestimated, and consequently low (high) EKE levels are overestimated (underestimated) (Danielson et al., 2018; de Vos et al., 2018). Gridded maps of Absolute Dynamic Topography (MADT) at a 0.25° resolution were extracted over the Agulhas Current region for the period of January 1993 until December 2013. Weekly means of the AVISO data were constructed from the daily data, for a more accurate comparison with the model output. One known short-coming of this dataset is that the spatial smoothing of the merged altimetry product removes strong gradients resulting in a reduced EKE (Backeberg et al., 2014). This problem can be addressed by spatially low passing the higher resolution datasets before comparison, however this was not done in this study.

4.2.4 Eddy tracking algorithm

The eddy-tracking algorithm developed by Halo et al., (2014a) (hereafter referred to as H14) was used to study the effects of the change in forcing on the eddies. The eddy-tracking algorithm is described in detail in Chapter 2, where it is compared to the eddy-tracking dataset of Chelton et al., (2011) which was used in Chapter 3 to observe eddy dissipation in the Agulhas Current. Although the lifespan of the eddies tracked using the H14 algorithm was typically found to be shorter than that of the Chelton eddies, both algorithms were shown in Chapter 2 to successfully capture eddy dissipation in the Agulhas Current. To briefly recap: the H14 algorithm, which is applied to gridded maps of sea surface height (SSH) from AVISO and both HYCOM simulations, combines the regions where the Okubo-Weiss parameter is negative (and flow is thus dominated by vorticity) with closed SSH contours to detect both cyclonic and anti-cyclonic eddies (Halo et al., 2014a).

It is important to note, that the combined Okubo-Weiss / geometric method approach used in the algorithm has resulted in a more adaptable algorithm, with very few tuned parameters. This facilitates its use with multiple datasets and enables objective comparisons between eddies detected and tracked in gridded satellite altimetry data and numerical ocean models. The algorithm was applied to SSH data from both model simulations and to the satellite MADT data for the time period of 1993−2013. Once an eddy is identified, the H14 algorithm calculates its various properties at each time step, including the eddy's latitude, longitude, area, vorticity, radius, amplitude, eddy rotational speed and velocity of the eddy in the zonal and meridional directions. These properties are then compared against each other in order to quantify the impact that changing the wind forcing in HYCOM has on the eddy characteristics in the region.

4.3 Methods

4.3.1 Kinetic energy

In order to determine whether the change in wind forcing causes a reduction in energy over the Agulhas Current system, the eddy kinetic energy (EKE) and mean kinetic energy (MKE) are investigated. Eddy kinetic energy (EKE) which is used to measure the energy of mesoscale activity (eddies) (Colas et al., 2012), is calculated using the following equation

$$EKE = \frac{\overline{(u'^2+v'^2)}}{2}, \tag{4.4}$$

where u' and v' are the time fluctuations of the annual mean of horizontal components of geostrophic velocities derived from variations of SSH.

The mean kinetic energy, which reflects the kinetic energy of the mean flow is determined by

$$MKE = \frac{\bar{u}^2 + \bar{v}^2}{2}. \tag{4.5}$$

A comparison of the mean surface EKE and MKE for the model forced with absolute winds, the model forced with relative winds, and the AVISO satellite data is shown. A difference plot, which subtracts the relative wind data from the absolute wind data, further highlights the differences between the EKE and MKE in the models.

Similarly to de Vos et al. (2018), a 0.5° x 0.5° grid of the EKE data is calculated for each of the simulations and the AVISO data. Using the output from the eddy tracking algorithm, it is also possible to calculate the EKE of the eddies (hereafter refered to as; the energy within the eddies) by dividing each eddy's energy by the area which it covers. A 0.5° x 0.5° grid of the energy within the eddies over the Agulhas Current system was created. The number of eddies occurring in each grid cell at each time-step as well as the occasions where the cells were empty were taken into account. The fraction of each eddy contained by one grid cell was considered as most eddies were found to overlap multiple full grid cells and/ or parts of cells. By subtracting the Energy within the eddies from the overall EKE, it is possible to determine the residual EKE. This is the EKE resulting from meandering currents or other forms of mesoscale variability in the region, including eddies which were not tracked by the eddy tracking algorithm. To better illustrate the differences between the models, the differences in the energy within the eddies and the residual EKE between the two models are plotted.

In order to analyse how the change in EKE from ABS to REL influences eddy pathways, the EKE of both models with their corresponding eddy trajectories of all eddies passing through the region 32 − 50°E and 25 − 31° S from 1993 − 2013 are investigated. Eddy trajectory roses, which show the directional spread of eddies propagating through the subsetted region, further illustrate the different directions in which the eddies propagate in each model.

Eddy properties; including the frequency of eddy occurrences, eddy formation and eddy dissipation; were analysed within 1 degree cells. This same method was used to investigate other eddy properties including eddy amplitudes, radii and circum-averaged speeds. A subset of eddy properties was investigated for the region 32 − 50° E and 25 − 31° S, for which Q-Q plots were created for AVISO, ABS and REL eddies in order to observe whether the effects of a change in wind forcing are different for cyclonic and anti-cyclonic eddies.

4.3.2 Energy Conversion Terms

Baroclinic and Barotropic energy conversion terms are used to locate regions where EKE is formed and lost (Kundu, 1990; Cronin and Watts, 1996; Azevedo et al., 2008; Halo et al., 2014b; Renault et al., 2017). Regions of positive energy transfer indicate eddy formation, and region of negative energy transfer are indicative of eddy dissipation. The terms are derived from the depth-integrated evolution equation of the kinetic and potential energy budget as described by Marchesiello et al. (2003). To perform these calculations, the HYCOM data were interpolated from the raw grid to a Mercator grid. One limitation of re-gridding the data is a potential loss of information or smoothing of the data. The terms were depth integrated throughout the water column.

The Barotropic Energy Conversion from mean kinetic energy to eddy kinetic energy (KmKe) is determined by

$$K_mK_e = \int_z^0 \ -(\overline{u'u'}\frac{\partial\bar{u}}{\partial x} + \overline{u'v'}\frac{\partial\bar{u}}{\partial y} + \overline{u'w'}\frac{\partial\bar{v}}{\partial z} + \overline{v'u'}\frac{\partial\bar{v}}{\partial x} + \overline{v'v'}\frac{\partial\bar{v}}{\partial y} + \overline{v'w'}\frac{\partial\bar{v}}{\partial z}), \tag{4.6}$$

where u', v' and w' are the fluctuations in time of the zonal, meridional and vertical components of the flow field. $\bar{u}$ and $\bar{v}$ are the time-mean velocities. x, y and z are the zonal, meridional and vertical directions, respectively.

The baroclinic energy conversion from eddy potential energy to eddy kinetic energy (PeKe) is calculated using the following equation

$$P_eK_e = \int_z^0 \ -\overline{\rho'w'}\frac{g}{\rho_0}, \tag{4.7}$$

where ρ' is the fluctuation of seawater density, computed using the equation described by Jackett and McDougall (1995). g is the acceleration due to gravity and ρ_0 is the reference density of seawater density.

The batoropic and baroclinic energy conversion terms for each of the models is calculated, and are used to further explain why there are differences in EKE between the models, and the differences in regions of eddy formation and dissipation.

4.3 Results

4.3.1 Winds and wind stress

Firstly, a seasonal plot of the mean ERA-interim winds at 10 m is shown in Figure 4.2; whereby data from December, January and February were used to produce the Summer mean; data from March, April and May were used to create the Autumn mean; data from June, July and August for the Winter mean and data from September, October and November were used to create the Spring mean. Whilst the dominant wind is in a similar direction over the whole Agulhas Current domain, it should be noted that the seasonality of winds varies in different locations of the

Agulhas Current region. Over the Agulhas Current, and in the region south of Madagascar, winds are strongest in Summer and tend to come from the East. However, winds are strongest in the Mozambique Channel during Winter and to come from the South East. These seasonal differences in wind velocities are important as they could have significant influences on the wind stress as well as the EKE in the regional HYCOM.

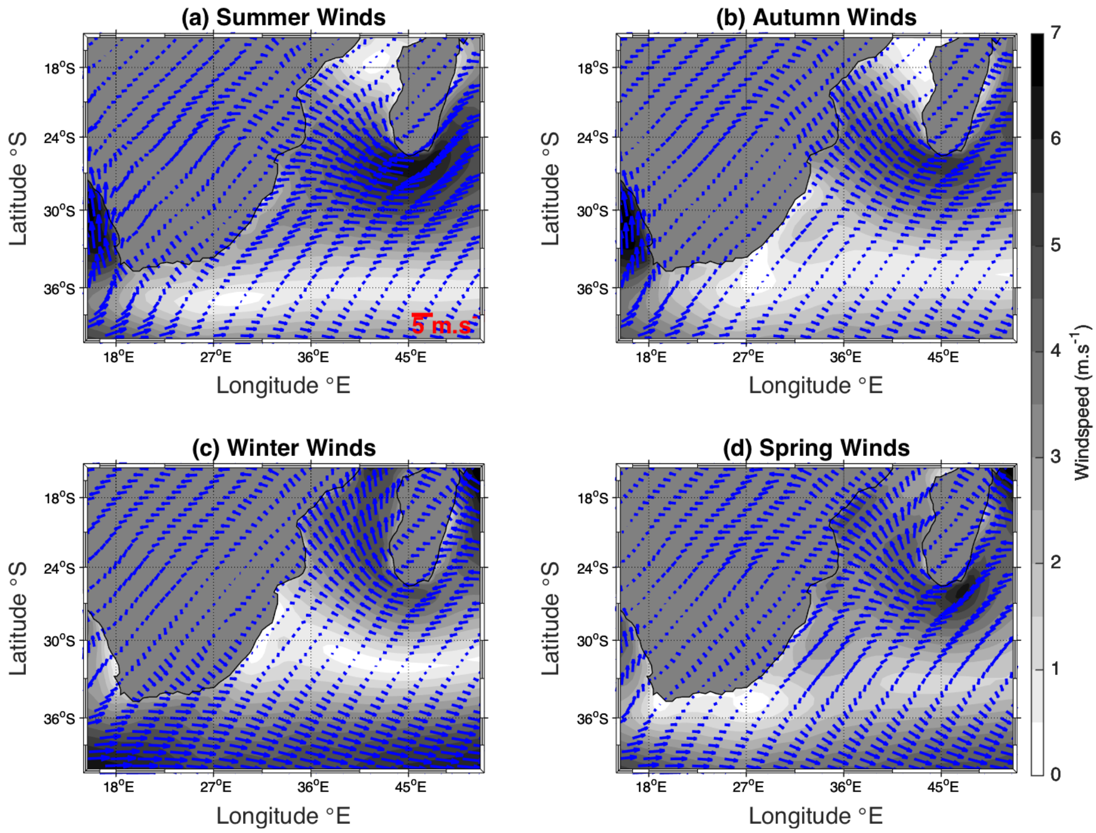

Figure 4.2: Mean ERA-interim winds at 10 m for a) Summer, b) Autumn, c) Winter and d) Spring from 1993– 2013. Shading denotes the speed of the wind, whilst the blue arrows indicate the direction of flow. The scale for the vectors is given in red.

The mean wind stress from 1993 until 2013 of each model simulation is shown for each season below in Figures 4.3 and 4.4. Subtracting the surface current velocities from the wind speed at 10 m before calculating the surface wind stress has resulted in an overall reduction in the mean wind stress in the relative winds experiment (REL) compared to the absolute winds experiment (ABS). As expected, the most noticeable differences of up to 0.01 $N.m^{-2}$ occur in regions where mean surface current velocities are high and the direction of the winds are opposite to the direction of the current. In the South East Madagascar Current (SEMC), the western boundary of the Mozambique Channel, and in the region south of Madagascar towards the African coast, the wind stress in ABS (Figure 4.3) is stronger than in REL (Figure 4.4). The weakened wind stress in REL is more spread out, particularly in the Mozambique Channel and south of Madagascar.

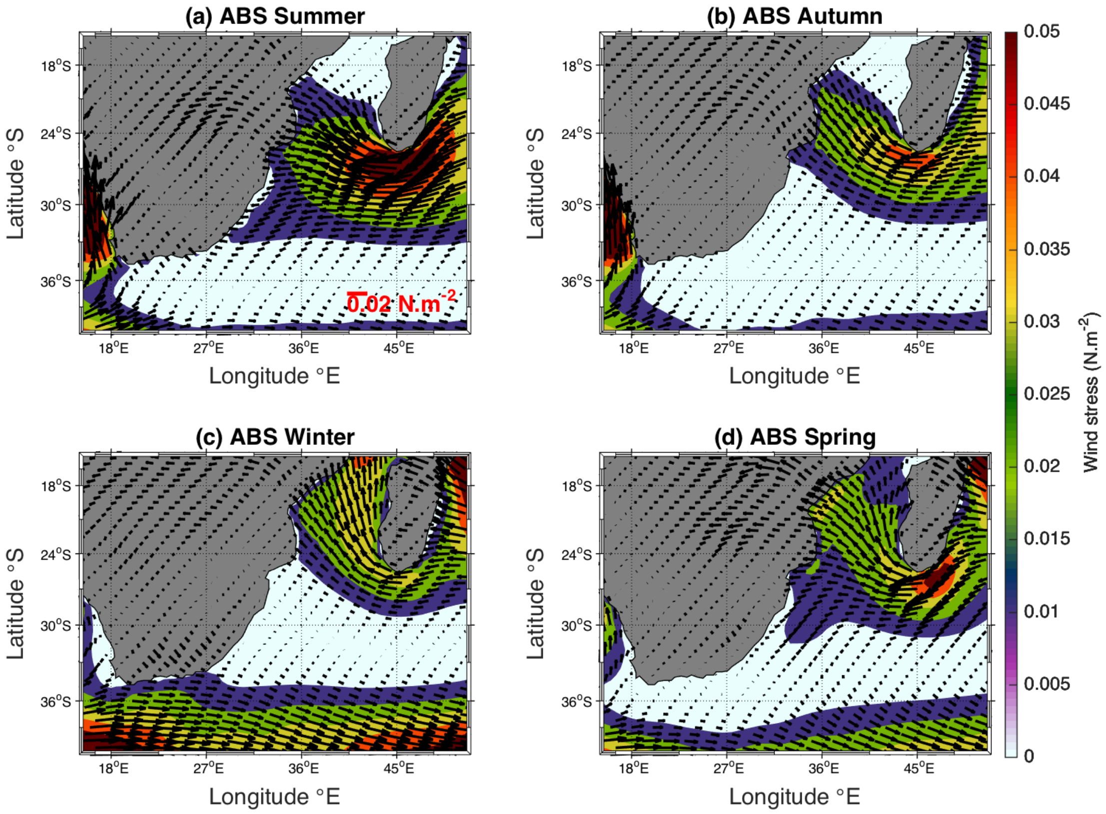

Figure 4.3: Mean wind stress (N.m^{-2}) for the simulation with absolute wind forcing in a) Summer, b) Winter, c) Autumn and d) Spring from 1993 – 2013. Arrows indicate the direction of the stress, with the scale of the arrows shown in red.

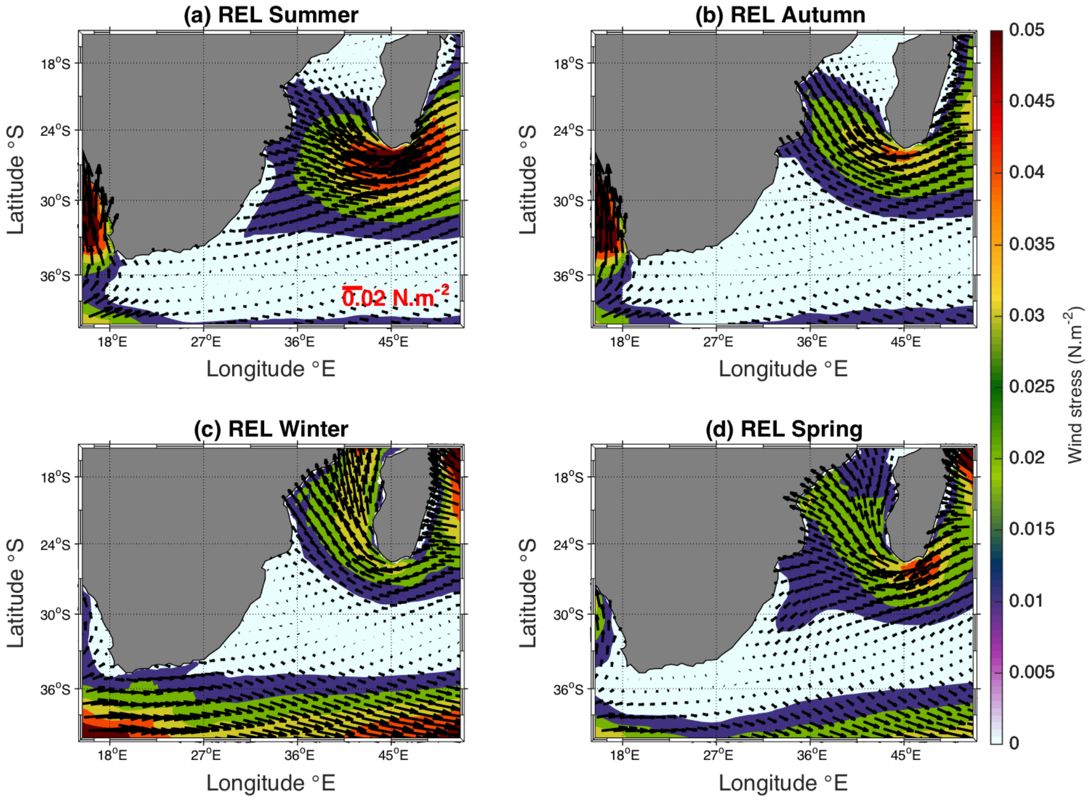

Figure 4.4: Mean wind stress (N.m^{-2}) for the simulation with relative wind forcing from 1993– 2013. Arrows indicate the direction of the stress, with the scale for the arrows shown in red.

The seasonal differences in wind stress between the 2 simulations is most easily observed in Figure 4.5, where the wind stress in the REL simulation has been subtracted from the wind stress in the ABS simulation. For the region south of Madagascar, the largest differences between the 2 simulations occurs in Summer, with changes of up to 0.01 N.m^{-2} (Figure 4.5a). Similarly, the differences in wind stress over the northern Agulhas Current are also largest in Summer, with changes of up to 0.005 N.m^{-2} occurring between ABS and REL. Whist changes in the southern parts of the Agulhas Current are evident in Summer, the largest difference in wind stress for this region occurs in Winter, where changes of 0.005 N.m^{-2} to 0.01 N.m^{-2} are observed. Differences in wind stress occur all year around for the Mozambique Channel, with the largest differences occurring in Winter and Spring (Figures 4.5c, d). Perhaps the most notable change that occurs in Autumn, is that which occurs in the central Agulhas Current (Figure 4.5b). This is the only region, where the wind stress in ABS is smaller than that of REL.

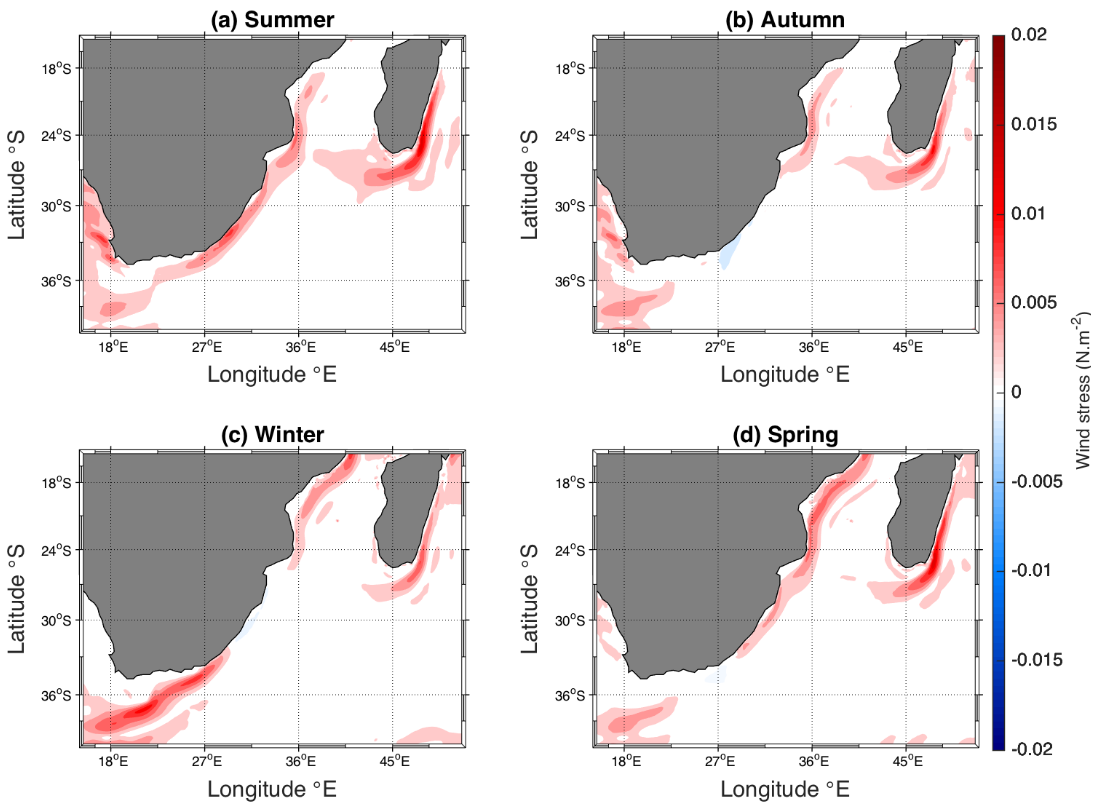

Figure 4.5: The difference in mean wind stress (N.m^{-2}) between the model forced by absolute winds and the model forced by relative winds for a) Summer, b) Autumn, c) Winter and d) Spring.

4.3.2 Kinetic energy

In order to investigate the effect of the relative wind forcing in the regional HYCOM, the mean surface EKE and MKE from ABS, REL and AVISO satellite data are calculated from the weekly surface currents (for HYCOM) and geostrophic currents for AVISO from 1993 − 2013 and are shown in Figure 4.6.

All three sets of data similarly show regions of elevated EKE in the Mozambique Channel, the Agulhas Current and south of Madagascar; indicating the presence of eddies, meanders and mesoscale variability in the region. The mean EKE in the northern Mozambique Channel is significantly higher in the ABS experiment with maximum values ranging from approximately 2500 cm^2.s^{-2} to 3200 cm^2.s^{-2} (Figure 4.6a) compared to REL and the satellite data which have maximum EKE values of approximately 1000 $cm^2.s^{-2}$ to 2000 $cm^2.s^{-2}$ (Figure 4.6b) and 700 $cm^2.s^{-2}$ to 1500 $cm^2.s^{-2}$, respectively (Figure 4.6c). The large difference in EKE between the regional HYCOM simulation forced with absolute winds and the AVISO data over the Agulhas Current System is also shown by Backeberg et al. (2014). At the southern end of the SEMC, the mean surface EKE in ABS has a maximum of 2200−2800 $cm^2.s^{-2}$. In this region, the EKE in REL is very significantly reduced, showing a maximum of 1000 − 2000 $cm^2.s^{-2}$ which is more similar to the relatively low EKE values of 400 − 800 $cm^2.s^{-2}$ estimated from the satellite product. This suggests that EKE is over-estimated in ABS and has been significantly reduced by the change in wind forcing. Elevated regions of EKE at the southern extent of the SEMC extend across the Mozambique Channel towards the African coast with values of 1000 − 2000 $cm^2.s^{-2}$ in ABS, and very similar values 500 − 1000 $cm^2.s^{-2}$ in REL and 500 − 900 $cm^2.s^{-2}$ in the AVISO data. One further region where the EKE of the models are different to AVISO is in the Agulhas Current. In ABS, an elevated EKE is shown offshore of the Agulhas Current core, ranging from 1000 − 2000 $cm^2.s^{-2}$ in the northern Agulhas Current and reaching a maximum of approximately 3500 $cm^2.s^{-2}$ south of the African Continent at the Agulhas retroflection (Figure 4.6a). The EKE in the Agulhas Current in REL is very similar to that captured by the satellite data in that the EKE in the Agulhas Current is reduced, with maxima of approximately 2300 $cm^2.s^{-2}$ (Figures 4.6b,c). There is however still and exaggeration of EKE offshore of the Agulhas Current around 33° − 36° S, 27° − 30° E. Whist there is some seasonality to the EKE observed in both simulations of the regional HYCOM, there is not much change to the differences between ABS and REL (figures not included). The differences between the two HYCOM simulations are further evident in Figure 4.7.

The MKE in the core of the Agulhas Current captured by the model experiments closely resembles that of the AVISO data. There is a higher MKE in the ABS experiment in the western Mozambique Channel of approximately 1000 − 2000 $cm^2.s^{-2}$ (Figure 4.6d), relative to an MKE which ranges from 500 − 1500 $cm^2.s^{-2}$ (Figure 4.6e) in REL and 600 − 1400 $cm^2.s^{-2}$ over the same region in the AVISO data (Figure 4.6f). The MKE over the South East Madagascar Current has a similar maximum of 3000 − 3500 $cm^2.s^{-2}$ in both of the model simulations and in the AVISO data. The region of elevated MKE does however extend further across the Mozambique Channel in the ABS simulation or the AVISO data, relative to the ABS simulation which shows and MKE of 0 − 500 $cm^2.s^{-2}$. The MKE reaches a maximum of 3000 − 3500 $cm^2.s^{-2}$ in the Agulhas Current in the ABS model, REL model and the AVISO data.

The differences in EKE and MKE between the models are more easily observed in Figure 4.7. Regions in red indicate where the EKE and MKE in ABS > REL, and regions in blue denote where ABS < REL. In Figure 4.7a, it is clearly visible that the mean surface EKE has reduced from ABS to REL with differences of up to 1500 $cm^2.s^{-2}$ in the Mozambique Channel, in the eddy pathway between Madagascar and the African coast and on the offshore edge of the Agulhas Current. An overall reducion in EKE of 33% occurred over the Agulhas Current domain. In Figure 4.7b, it is clear that the MKE reduces from ABS to REL by values of up to 1000 $cm^2.s^{-2}$ in the Mozambique Channel, up to 500 $cm^2.s^{-2}$ on the offshore edge of the SEMC and up to 600 $cm^2.s^{-2}$ on the offshore edge of the Agulhas Current. It is very interesting to note the increase in MKE in the core of the SEMC of approximately 400 $cm^2.s^{-2}$ as well as an increase in the Agulhas Current core of up to 1000 $cm^2.s^{-2}$.

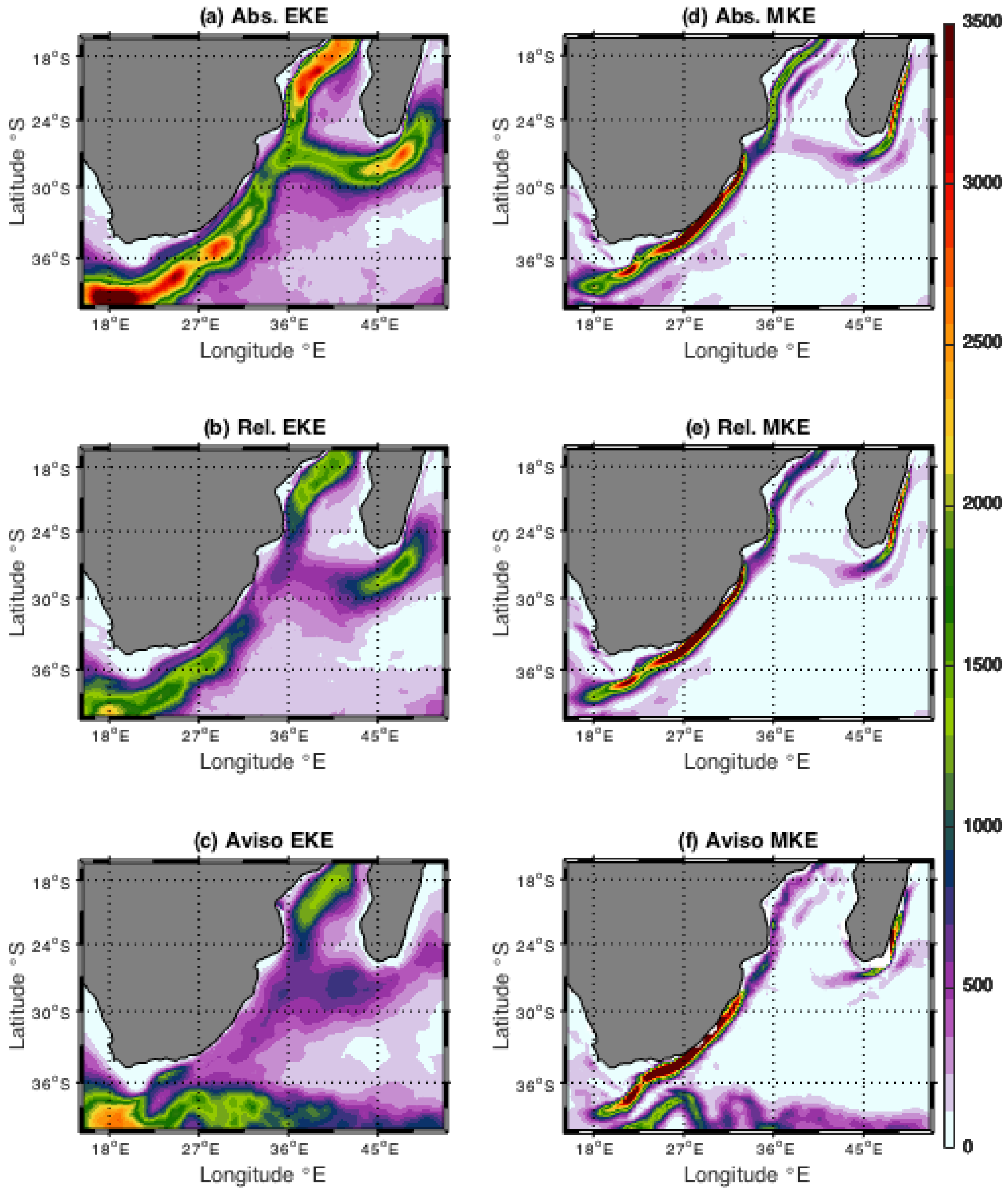

Figure 4.6: The mean surface EKE for a) the model forced by absolute winds b) the model forced by relative winds and c) AVISO data; the mean surface MKE for d) the model with a absolute wind forcing, e) the model with relative wind forcing and f) AVISO data from 1993 – 2013.

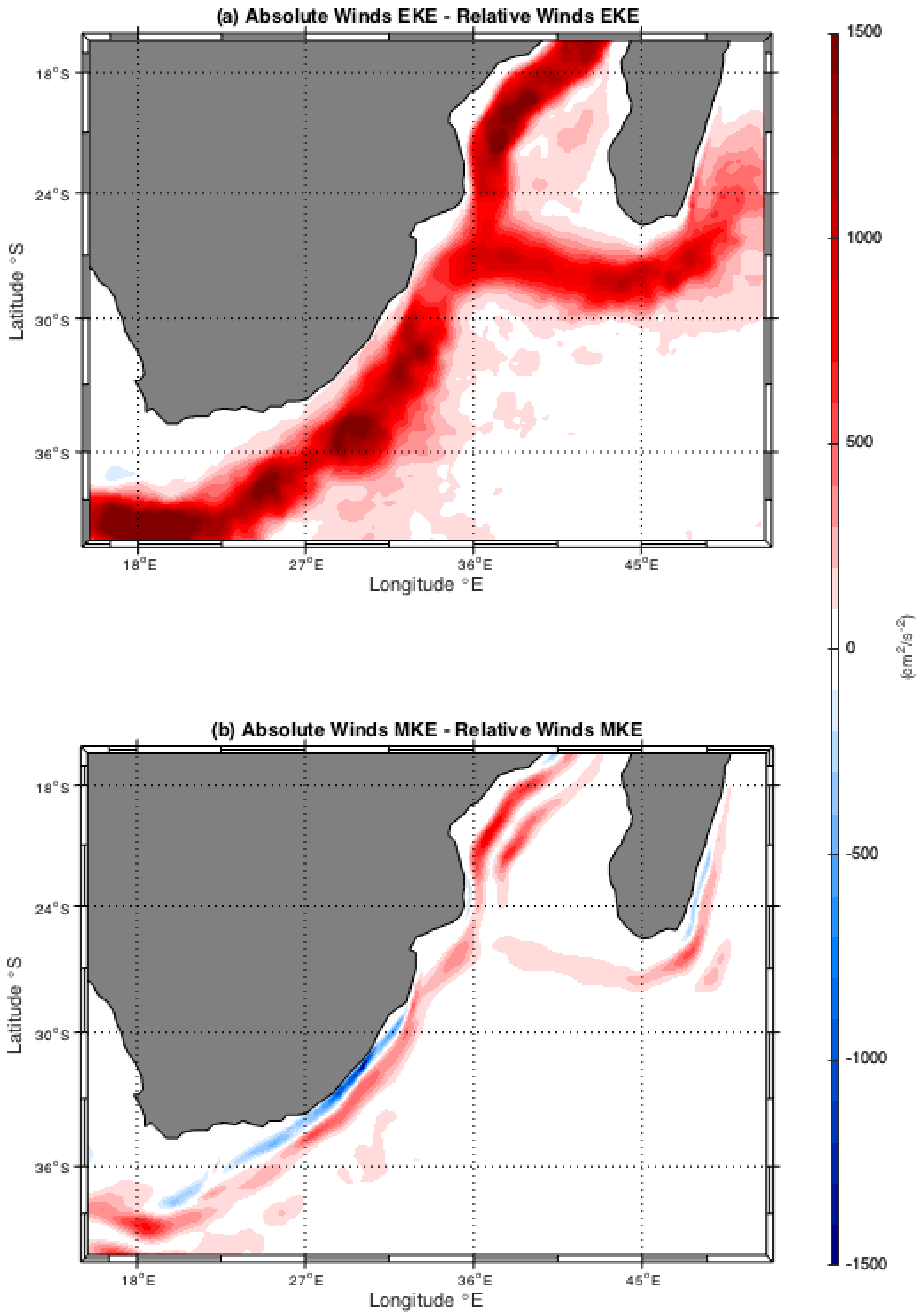

Figure 4.7: Differences in the mean surface a) EKE and b) MKE between the experiment forced by absolute winds and the experiment forced by relative winds from 1993 – 2013.

By tracking the eddies, calculating their EKE, mapping it to a 0.5° x 0.5° grid and subtracting it from the total EKE (Figure 4.6), the residual EKE is calculated. Figures

4.8 and 4.9 show the contribution the mesoscale eddies that are tracked by the eddy-tracking algorithm, to the overall EKE of the Agulhas Current system. The energy within the eddies calculated from AVISO data (Figure 4.8a) is much lower than the energy within the eddies of the ABS experiment (Figure 4.9b) with maximum values of approximately 300 − 600 $cm^2.s^{-2}$ in the Mozambique Channel relative to a maximum of approximately 600 − 1000 $cm^2.s^{-2}$ in the ABS experiment. The energy within the eddies in REL is much more similar to the AVISO energy within the eddies with maximum values of 300 − 700 $cm^2.s^{-2}$ in the Mozambique Channel (Figure 4.9c). In the region south of Madagascar, the AVISO energy within the eddies reaches a maximum of appoximately 200 − 300 $cm^2.s^{-2}$ with a very small region of elevated energy within the eddies of 300 − 400 $cm^2.s^{-2}$ at the south western tip of Madagascar. Comparatively, in this region ABS has a similar maximum energy within the eddies of 200 − 300 $cm^2.s^{-2}$ whilst the maximum in REL is between 0 and 100 $cm^2.s^{-2}$. The region of elevated energy within the eddies in ABS and REL is much narrower than the AVISO energy within the eddies, which is more spread out in the region between south of Madagascar and the African coast. The energy within the eddies reaches a maximum of 200 $cm^2.s^{-2}$ in AVISO, 500 – 620 $cm^2.s^{-2}$ in ABS and 500 $cm^2.s^{-2}$ in REL occurs in the Agulhas Current.

Figure 4.9 shows the residual EKE, which is the difference between the overall EKE gridded to a 0.5° x 0.5° grid, and the energy within the eddies; this gives an indication of the contribution of meandering currents and other sources of variability to the overall EKE. The mean values of residual EKE are far greater than the mean values of energy within the eddies. In AVISO, a mean residual EKE of approximately 1000 − 1500 $cm^2.s^{-2}$ occurs in the Mozambique Channel, whilst values of 500 − 650 $cm^2.s^{-2}$ occur in the region south of Madagascar and a maximum residual EKE of approximately 500 $cm^2.s^{-2}$ occurs in the northern Agulhas Current (Figure 4.9a). Residual EKEs of approximately 1500 − 2200 $cm^2.s^{-2}$ in the Mozambique Channnel, 1500 − 2500 $cm^2.s^{-2}$ in the region south of Madagascar and a maximum of 2200 $cm^2.s^{-2}$ in the northern Agulhas Current are found in ABS (Figure 4.9b). The residual EKE values in REL are lower than ABS, with values of 800 − 1500 $cm^2.s^{-2}$ in the

Mozambique Channel, 800 – 1600 $cm^2.s^{-2}$ in the region south of Madagascar and a maximum of 1000 $cm^2.s^{-2}$ in the northern Agulhas Current (Figure 4.9c).

Figure 4.10 shows the difference in energy within the eddies and residual EKE between the models. Regions which are red (blue) in colour denote a decrease (increase) in energy within the eddies or residual EKE from ABS to REL. The difference in energy within the eddies from ABS to REL is between 100 – 400 $cm^2.s^{-2}$ in the Mozambique Chanel, south of Madagascar and in the Agulhas Current (Figure 4.10a). For these same regions, the changes in residual EKE from ABS to REL is between 400 and 1000 $cm^2.s^{-2}$ (Figure 4.10b). The difference in energy within the eddies between the model experiments is approximately 2.5 times smaller than the difference in residual EKE. Thus the difference in meanders and other forms of variability between the ABS and REL experiments is greater than the differences in mesoscale eddies between the two simulations.

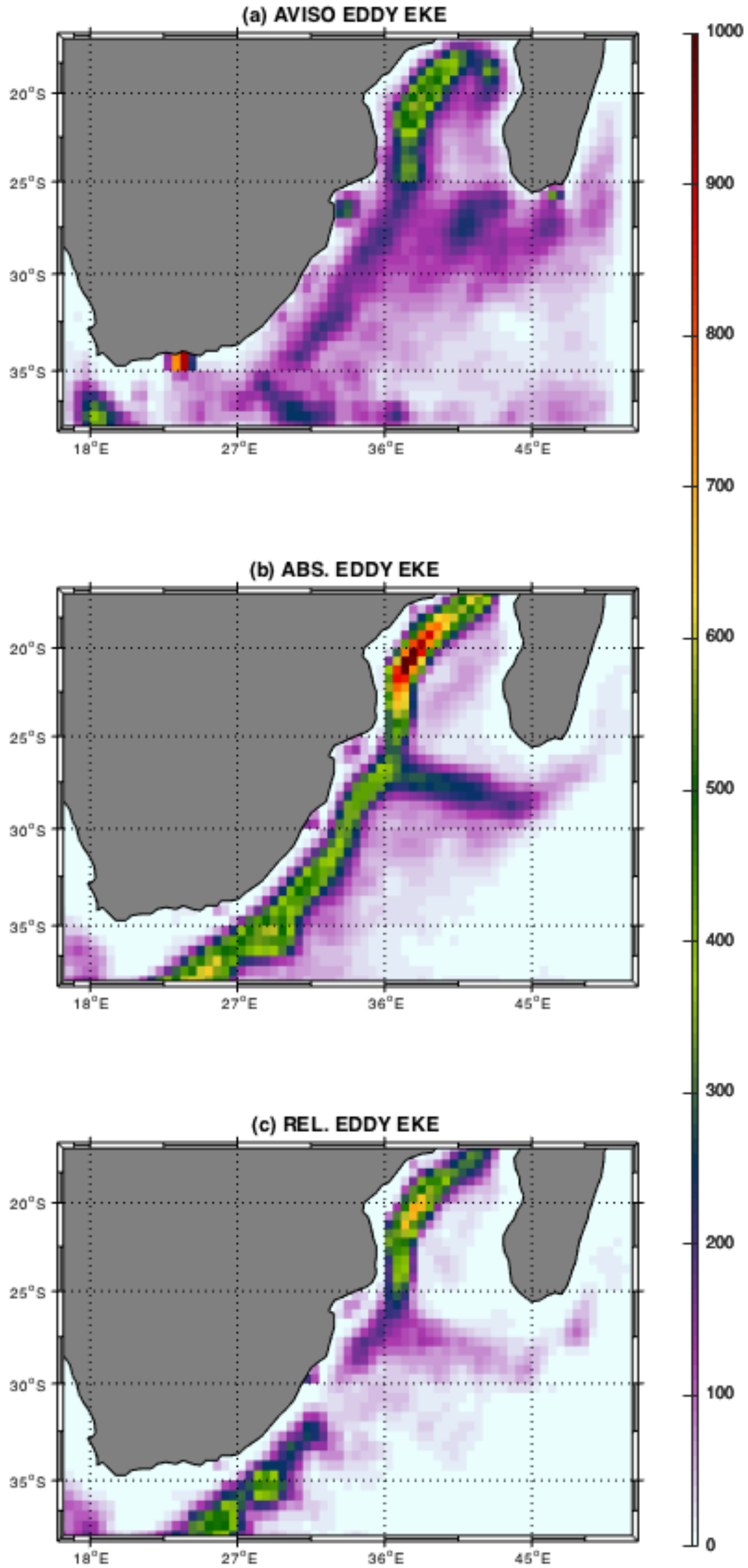

Figure 4.8: A 0.5° by 0.5° grid of the mean energy within the eddies ($cm^2.s^{-2}$) for a) AVISO, b) the model forced by absolute winds and c) the model forced by relative winds from 1993 – 2013.

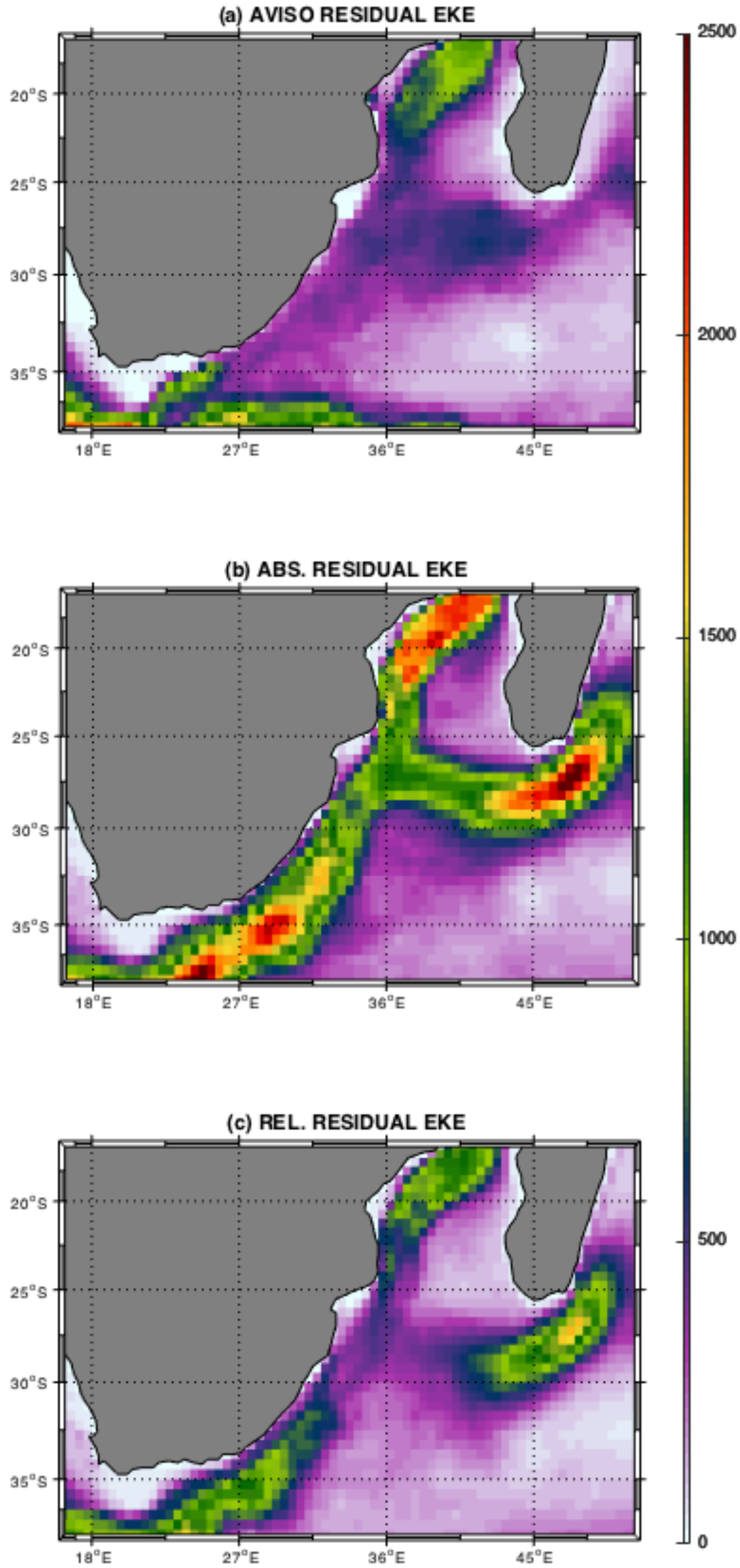

Figure 4.9: A 0.5° by 0.5° grid of the mean residual EKE ($cm^2.s^{-2}$) for a) AVISO, b) the model forced by absolute winds and c) the model forced by relative winds from 1993 – 2013.

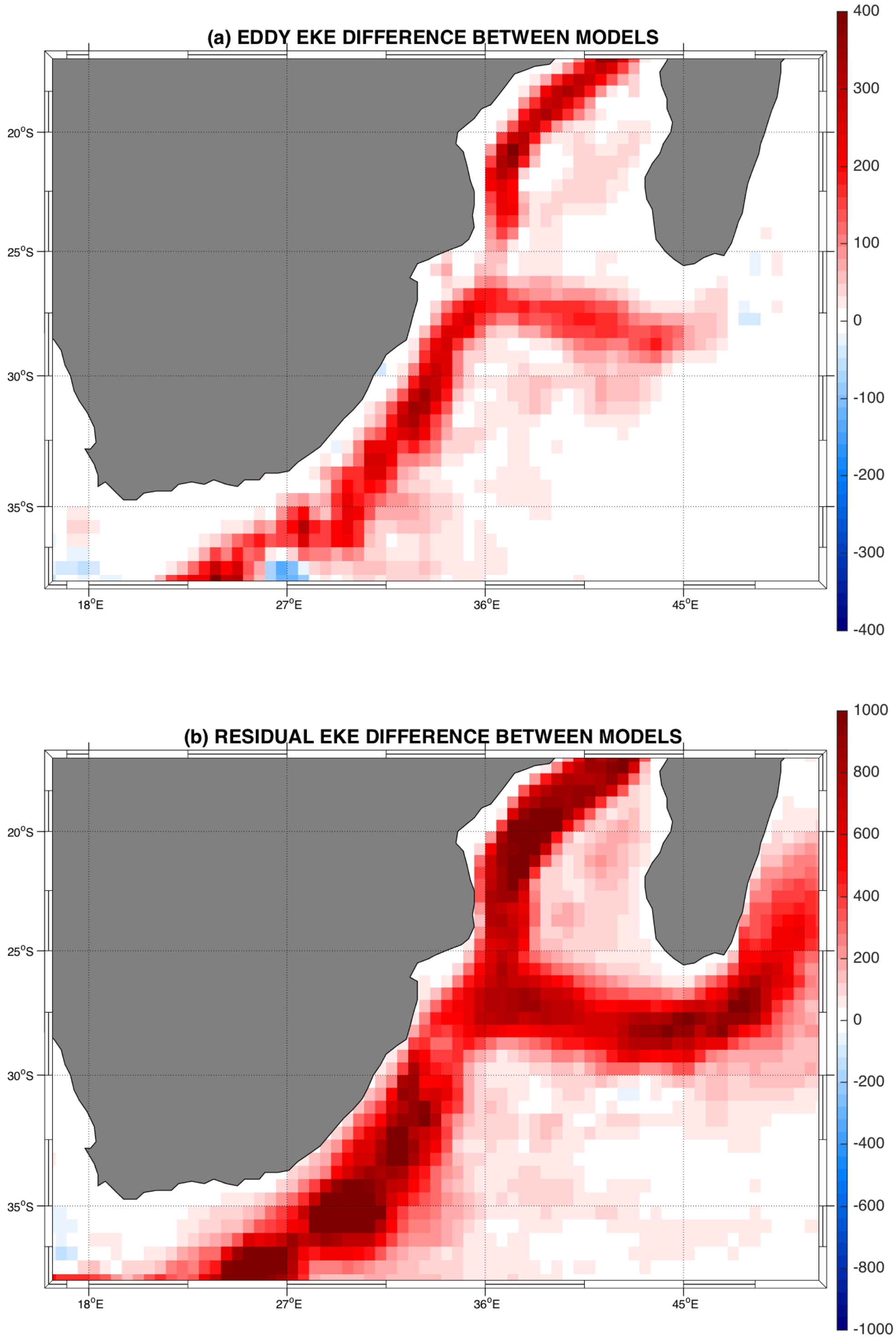

Figure 4.10: Differences in the mean surface a) energy within the eddies and b) residual EKE ($cm^2.s^{-2}$) between the absolute and relative winds models from 1993 – 2013.

4.3.3 Eddy pathways

Figure 4.11 compares the trajectories of all model eddies that pass through 32 − 50° E and 25 − 31° S (the region of elevated EKE that spans from south of Madagascar to the African coast, denoted by the black box) from 1993 − 2013; the comparison reveals that the eddy pathways between the south of Madagascar and the African coast are very similar for both absolute and relative wind forcing. Results from both ABS and REL show many anti-cyclonic eddies propagating down the western boundary of the Mozambique Channel. In REL there are fewer cyclonic and anti-cyclonic eddies forming in the region immediately south of Madagascar compared to ABS. This is mostly evident in the band of westward propagating anti-cyclonic eddies forming at the point where the SEMC breaks down (Figure 4.11).

This result is supplemented by Figure 4.12, which shows a directional rose of all eddy trajectories propagating through the subset region (the black box in Figure 4.11) between 1993 and 2013. The directions given in the rose are representative of the direction of eddy propagation for every time step of every eddy's trajectory. The directional roses in both forcings of the model similarly show a spread of directions and velocities in the eddy trajectories, with many eddies propagating in a south westerly direction. Results suggest that more eddies propagate in a southerly direction in REL (Figure 4.12b) compared ABS where more eddies propagate north westwards (Figure 4.12a).

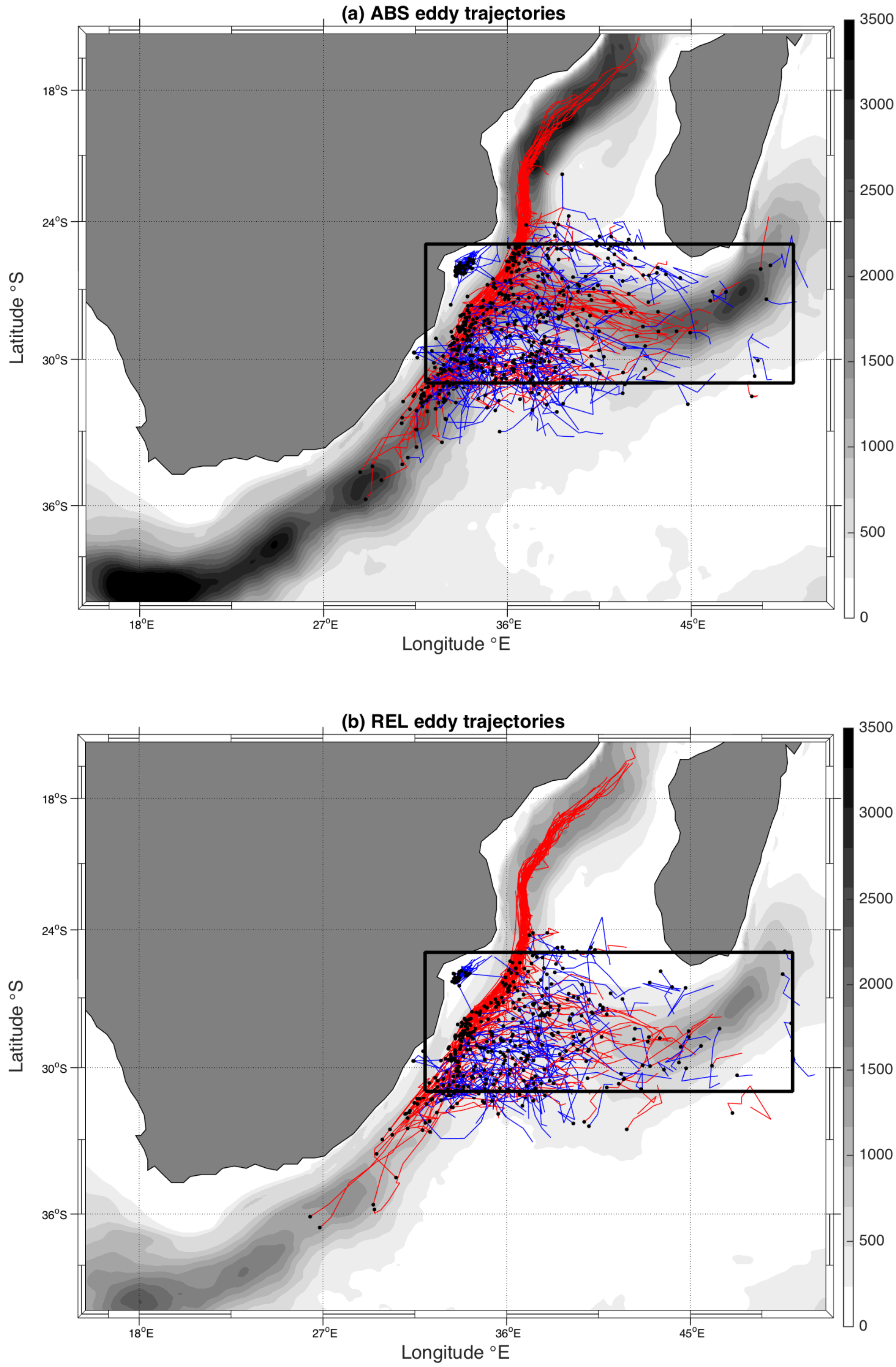

Figure 4.11: Trajectories of all eddies which pass through the black box (32 – 50° E and 25 – 31° S) from 1993–2013 overlaid on the mean EKE ($cm^2.s^{-2}$) for a) the model forced by absolute winds and b) the model forced by relative winds. Anti-cyclonic eddy trajectories are shown in red and cyclonic eddy trajectories are shown in blue. Black dots indicate locations of eddy dissipation.

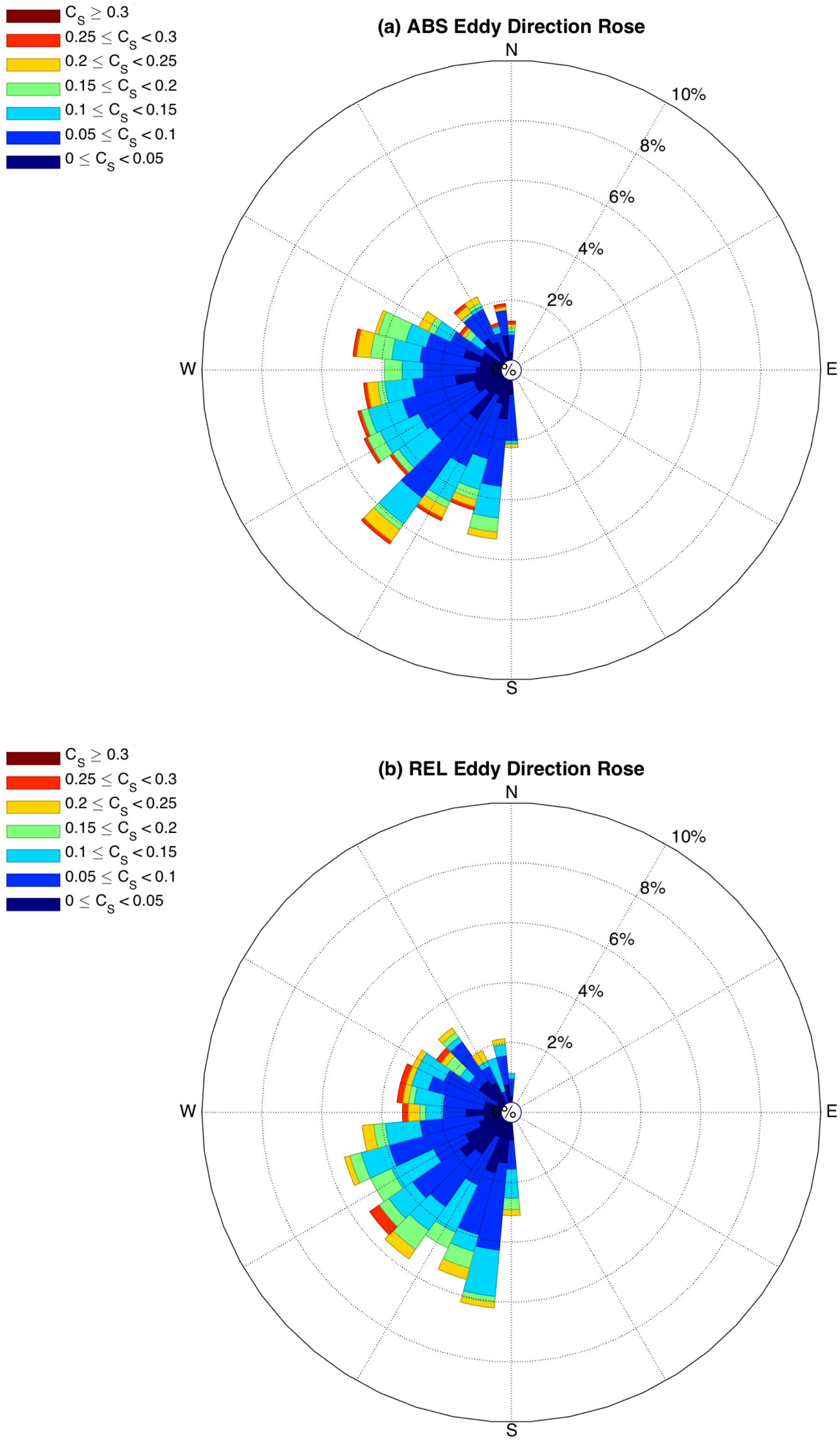

Figure 4.12: Eddy trajectory roses showing directions of all eddy trajectories, within 32 – 50° E and 25 – 31° S, from 1993 – 2013 for a) the model forced by absolute winds and b) the model forced by relative winds. C_s is the current speed in m.s^{-1}.

Figures 4.13a, b and c show a 1° x 1°grid of the number of eddy formations occurring in each grid cell per year; they reveal that regions of eddy formation between ABS and REL are very similar, with both cyclonic and anti-cyclonic eddies forming throughout the domain each year. Approximately 1 – 2 more eddies form in the north western Mozambique Channel each year in ABS compared to REL. There are also approximately 1 – 2 more eddies forming annually in ABS in the region just south and southwest of Madagascar. However, in a small region southeast of Madagascar, there is an increase of approximately 3 – 4 eddies per year from ABS to REL. In other regions of the Mozambique Channel and the domain, there are both positive and negative differences in the frequencies of eddies. There is no obvious pattern to these differences.

Regions of eddy dissipation between ABS and REL are very similar, with the highest frequency of approximately 5 eddies dissipating at 29 − 30° S, 31 − 32° E each year in both cases (Figures 4.13(d, e)). Figures 4.13c and f highlight the abundance of eddies forming, dissipating and occurring in the region south of Madagascar in the satellite data relative to the models with approximately 1 – 2 more eddies forming or dissipating at each grid point in this region of the AVISO data relative to either of the model experiments. Although this region of eddy dissipation is consistent with Chapter 3 of this study, the dissipation of eddies does not appear to improve in the REL case. Figures 4.13(g, h) indicate the similarity in frequencies of eddy occurrences in ABS and REL in the region south of Madagascar. Large numbers of eddies occur in the western Mozambique Channel in both model simulations. It is very interesting to note that there are 1 – 2 fewer eddies annually on the offshore edge of the Agulhas Current in REL compared to ABS. Figure 4.13i shows that there is a higher number of eddies occurring in the region south of Madagascar in the altimetry data relative to either of the model experiments. Eddy occurrences appear to be closer to the African coast in both model experiments, with approximately 1 - 2 too few eddies occurring at each grid point in the region surrounding southern Madagascar in both model experiments.

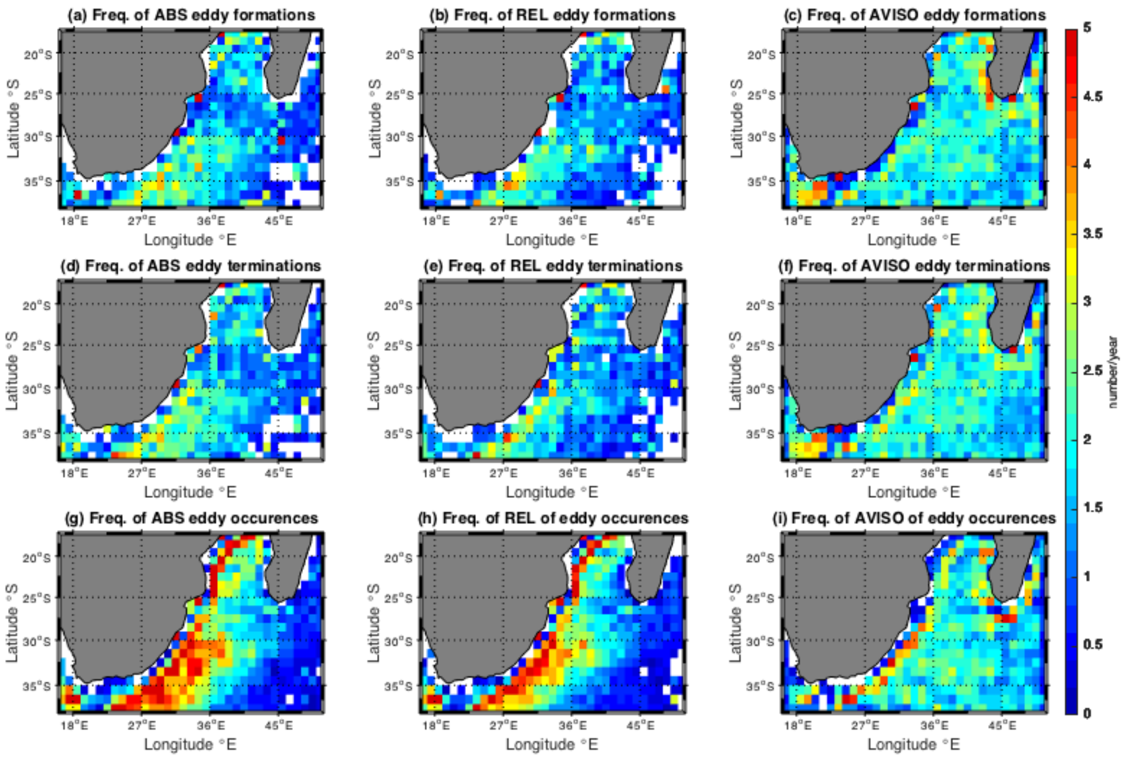

Figure 4.13: A 1° by 1° grid showing the frequency of a) ABS, b) REL and c) AVISO eddy formations, d) ABS, e) REL and f) AVISO eddy terminations and, the number of g) ABS, h) REL and i) AVISO eddy occurrences per year.

In addition to the frequencies and locations of eddy occurrences, the gridding method applied in Figure 4.13 was also used to study differences in eddy properties between ABS and REL. Results in Figure 4.14 show that both the ABS and REL simulation have similar regions of elevated eddy amplitudes and in general, a reduction in the mean eddy amplitudes from ABS (Figure 4.14a) to REL (Figure 4.14b). In the Mozambique Channel, eddy amplitudes decrease from a maximum of 15 – 30 cm in ABS to 10 – 25 cm in REL. The biggest change in eddy amplitudes occurs in the region south of Madagascar, where eddies with amplitudes of 30 – 40 cm frequently occur in ABS. In this same region, the REL simulation indicates maximum eddy amplitudes of 15 – 30 cm. On the offshore edge of the Agulhas Current eddy amplitudes also decreased from ABS to REL by 5 – 15 cm.

The eddy radii in Figure 4.15 show very little change from ABS to REL in the Mozambique Channel and offshore of the Agulhas Current where radii of maxima 90

– 100 km and 60 – 70 km occur, respectively. In the region south of Madagascar however, there is a reduction in radii of 70 – 100 km in ABS to 60 – 85 km in REL. The eddy rotational velocities shown in Figure 4.16 decrease from ABS to REL in the Mozambique Channel, south of Madagascar and along the offshore edge of the Agulhas Current. From ABS to REL, the circum-averaged velocities decrease from a maximum of 90 $cm.s^{-1}$ to 70 $cm.s^{-1}$ in the Mozambique Channel, from 95 $cm.s^{-1}$ to 70 $cm.s^{-1}$ in the region south of Madagascar and from 85 $cm.s^{-1}$ to 70 $cm.s^{-1}$ along the offshore edge of the Agulhas Current.

Significant changes in eddy properties occur in the regional HYCOM by changing the wind forcing with the largest changes in eddy properties occurring south of Madagascar where the amplitudes, radii and circum-averaged speeds of the eddies are all reduced.

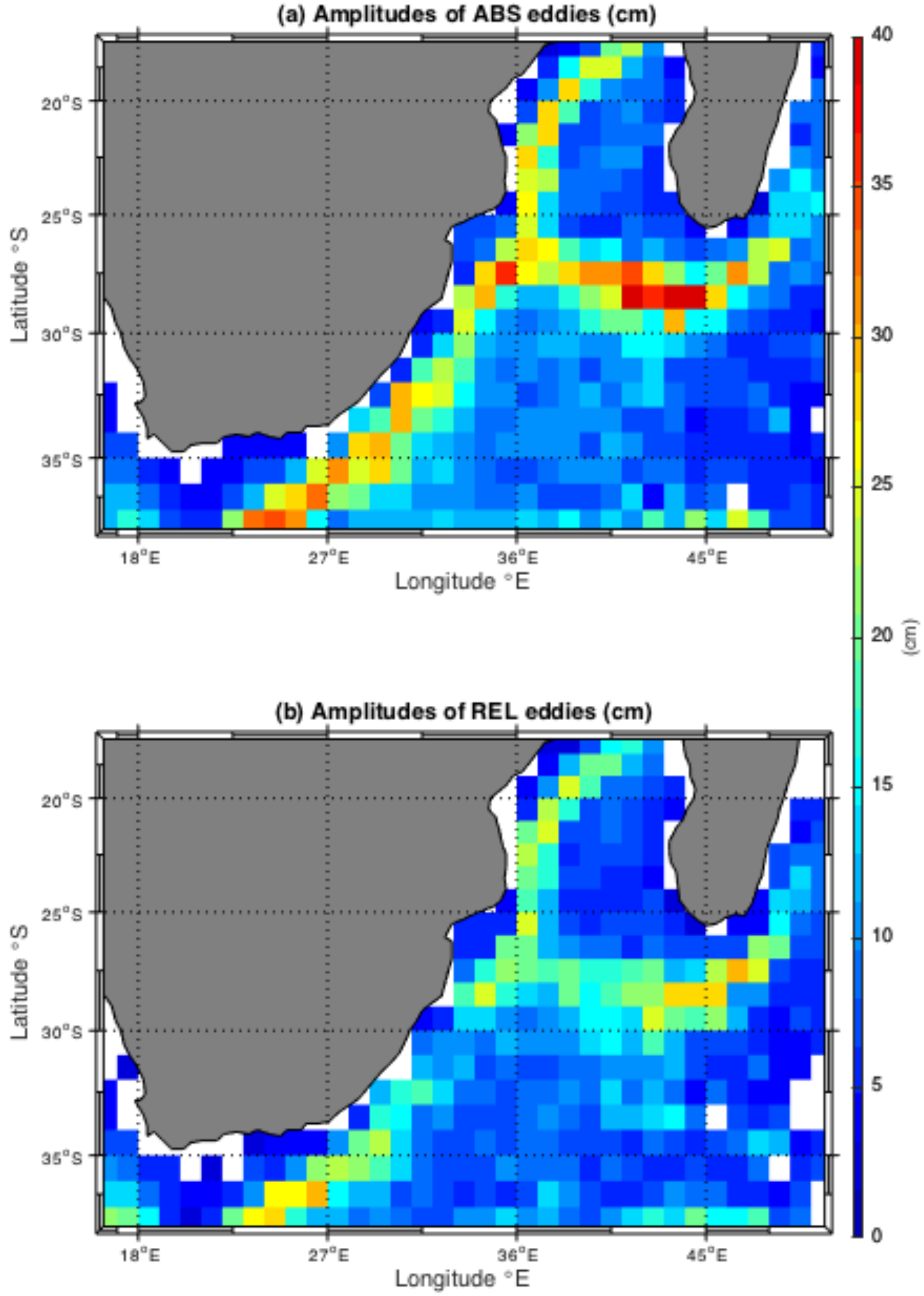

Figure 4.14: A 1° by 1° grid showing the means Amplitudes (cm) of a) ABS and b) REL eddies occurring in each grid cell.

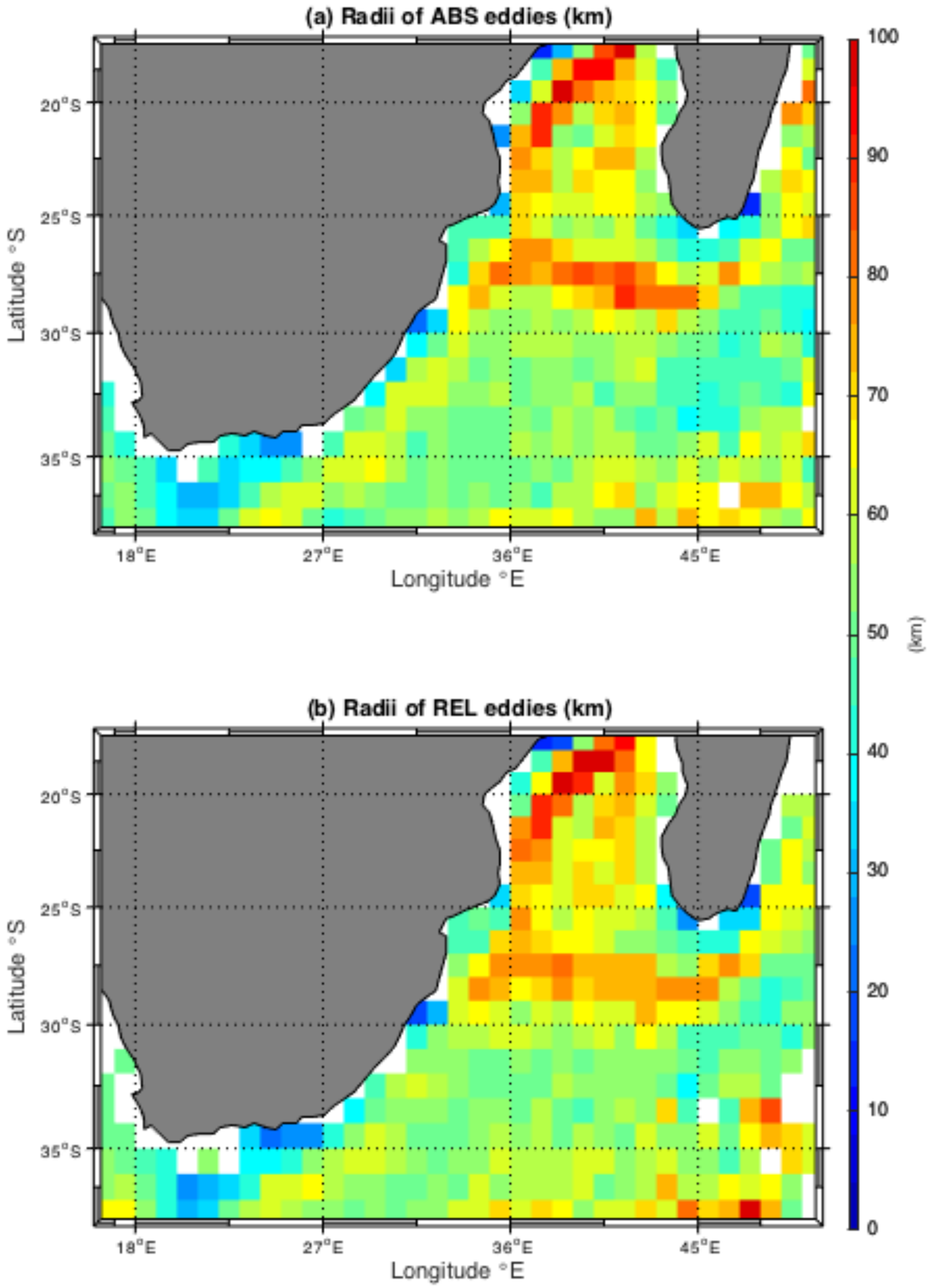

Figure 4.15: A 1° by 1° grid showing the mean radii (km) of a) ABS and b) REL eddies occurring in each grid cell.

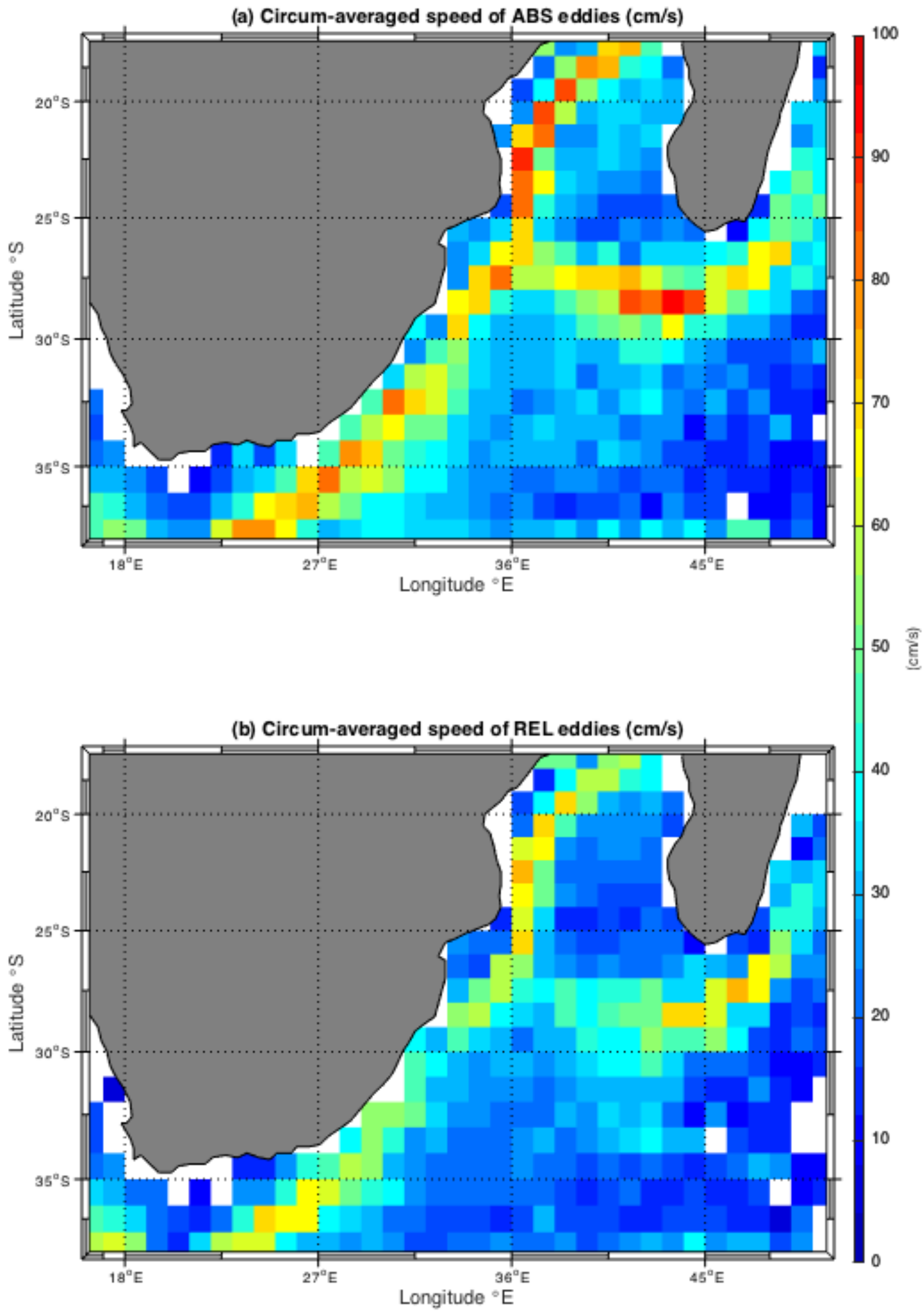

Figure 4.16: A 1° by 1° grid showing the mean circum-averaged speed (cm.s^{-1}) of a) ABS and b) REL eddies occurring in each grid cell.

Using the H14 eddy-tracking algorithm, results in Figure 4.17 reveal how eddy properties in the two experiments compare to the AVISO eddies. A subset of results is selected showing only the eddies which passed through the black box in Figure 4.11 from 1993 – 2013; the subset of eddy statistics is summarised below in Table 4.1.

	AVISO-AC	**AVISO-C**	**ABS-AC**	**ABS-C**	**REL-AC**	**REL-C**
No. eddies > 4weeks	524	740	182	191	166	140
Mean lifespan	6.31±2.76	7.07±3.59	6.32±2.88	5.33±1.90	5.97±2.38	5.39±2.16
Mean radius	63.64±17.57	60.80±14.58	80.83±19.88	52.50±12.03	81.64±16.05	53.18±12.36
Mean amplitude	11.87±8.90	12.67±7.83	31.22±18.37	8.38±4.11	23.95±11.04	7.36±2.66
Mean circum-averaged speed	39.72±20.88	41.91±21.39	74.59±34.06	28.27±13.82	58.97±21.71	24.00±10.13

Table 4.1: Eddies properties for eddies passing within 32 – 50° E and 25 – 31° S between 1993 – 2013 for both anti-cyclonic (AC) and cyclonic (C) eddies, including the number of eddies with lifespans greater than 4 weeks, mean lifespans of the eddies (weeks), mean eddy radii (km), mean eddy amplitudes (cm) and mean eddy circum-averaged speeds (cm.s^{-1}).

The number of eddies with lifespans of 4 or more weeks (tracked by the eddy tracking algorithm) are far more abundant in AVISO than either ABS or REL with 524 anti-cyclonic and 724 cyclonic eddies tracked between 1993 – 2013. In comparison, 182 anti-cyclonic and 191 cyclonic eddies were tracked by ABS relative to the 166 anti-cyclonic and 140 cyclonic eddies tracked by REL during the same period. Interestingly, cyclonic eddies, which are more abundant in AVISO and ABS, are less abundant in REL.

The maximum lifespan of a tracked anti-cyclonic eddy is 21 weeks for AVISO eddies, 17 weeks for ABS eddies and 21 weeks for REL eddies (Figure 4.17a). Although the maximum lifespan of an ABS eddy is shorter than that of a REL eddy, the REL eddies are generally very similar to those of the ABS experiment and AVISO eddies (Figure 4.17a). The mean lifespan of an anti-cyclonic eddy is 6.31 ± 2.76 weeks for AVISO, 6.32 ± 2.88 weeks for ABS and 5.97 ± 2.38 weeks for REL. The mean lifespan of a cyclonic eddies is slightly longer for AVISO at 7.07 ± 3.59 weeks with a maximum lifespan of 31 weeks. The maximum lifespan of cyclonic eddies tracked by the regional HYCOM is much shorter, with approximately 15 weeks for ABS and 17 weeks for REL (Figure 4.17b). The mean cyclonic eddy lifespan is very similar for ABS and REL, with a mean of 5.33 ± 1.90 weeks for ABS and 5.39 ± 2.16 weeks for REL. Unlike AVISO, both HYCOM experiments suggest that the mean lifespan of a cyclonic eddy is shorter than an anti-cyclonic cyclonic eddy, whilst AVISO data indicates that cyclonic eddies are longer lived.

An investigation of the subsets of eddy radii, amplitudes and circum-averaged speeds reveals that on average, anti-cyclonic eddies tracked in both the ABS and REL experiments are stronger than the AVISO eddies whilst the cyclonic eddies are weaker. The radii of eddies in the ABS and REL experiments are very similar to each other (Figures 4.17c,d). The maximum radius of an anti-cyclonic eddy for ABS and REL is approximately 132 km for ABS and 125 km for REL, whilst the largest anti-cyclonic AVISO eddy is 118 km in radius. The maximum radius of a cyclonic eddy is 119 km for an AVISO eddy, 1034 km for an ABS eddy, and 90 km for REL. The eddies tracked in AVISO reveal that anti-cyclonic and cyclonic eddies are very similar in size with a mean radius for anti-cyclonic (cyclonic) eddies of 64 ± 18 km (61 ± 15 km). Both ABS and REL however, suggest that anti-cyclonic eddies are larger with a mean radius of 81 ± 20 km for ABS anti-cyclonic eddies and 82 ± 16 km for REL anti-cyclonic eddies. The mean radius of a cyclonic eddy is 53 ± 12 km for ABS and 53 ± 12 km for REL. The radii of eddies does not appear to be significantly affected by the change in wind forcing in the regional HYCOM.

In Figures 4.17(e, f) the anti-cyclonic eddies tracked in the regional HYCOM experiments are larger in amplitude than those recorded in the AVISO data, whilst the cyclonic eddies in both experiments are smaller. The maximum amplitude of an anti-cyclonic AVISO eddy is 60 cm, with a mean of 12 ± 9 cm. In comparison an anti-cyclonic ABS eddy has a maximum amplitude of 82 cm with a mean of 31 ± 18 cm whilst an anti-cyclonic REL eddy tends to be more similar to the AVISO eddies with a maximum amplitude of 53 cm and a mean of 24 ± 11 cm. Similarly to Figures 4.17(c, d), results of the AVISO data indicate that cyclonic and anti-cyclonic eddies are very similar in size, with the mean amplitude of a cyclonic eddy being similar to that of an anti-cyclonic eddy at 13 ± 8 cm. The maximum amplitude of a cyclonic eddy is 47 cm for AVISO eddies, 32 cm for ABS eddies and 16 cm for REL eddies. The mean amplitudes of both ABS and REL cyclonic eddies are lower than that of the AVISO eddies (Figure 4.17f), with a mean ABS amplitude of 8 ± 4 cm and a smaller mean REL amplitude of 7 ± 3 cm.

The trend of the eddy circum-averaged speeds (Figures 4.17 (g, h)) is similar to that of the eddy amplitudes. Results indicate a similar mean circum-averaged speed for both anti-cyclonic and cyclonic AVISO eddies with a mean circum-averaged speed for anti-cyclonic eddies of 40 ± 21 $cm.s^{-1}$ compared to a cyclonic mean of 42 ± 21 $cm.s^{-1}$. ABS eddies have a mean circum-averaged speed of 75 ± 34 $cm.s^{-1}$ for anti-cyclonic eddies and 28 ± 14 $cm.s^{-1}$ for cyclonic eddies. In comparison, REL eddies have a smaller mean circum-averaged speed of 59 ± 22 $cm.s^{-1}$ for anti-cyclonic eddies and 24 ± 10 $cm.s^{-1}$ for cyclonic eddies. The maximum circum-averaged speed of an anti-cyclonic eddy is 146 $cm.s^{-1}$ for AVISO, 152 $cm.s^{-1}$ for ABS and 114 $cm.s^{-1}$ for REL where as the maximum for a cyclonic eddy is 110 $cm.s^{-1}$ for AVISO eddies, 99 $cm.s^{-1}$ for ABS and 66 $cm.s^{-1}$ for REL. The change in wind forcing in the regional HYCOM causes the circum-averaged speed of anti-cyclonic eddies to become similar that of AVISO eddies, but also causes cyclonic eddies to become even slower (Figures 4.17 (g, h)).

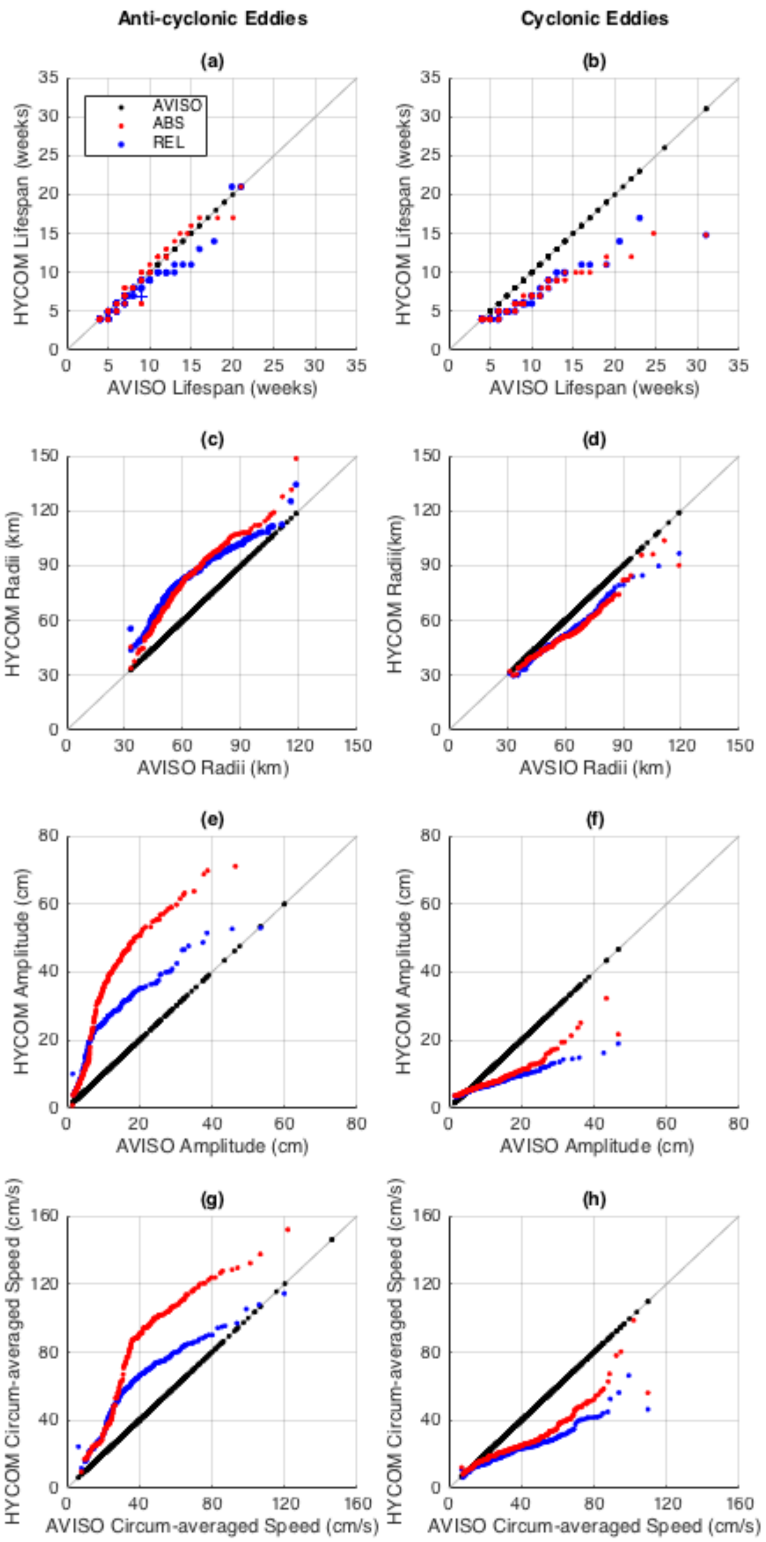

Figure 4.17: Q-Q plots of eddies occurring within 32 – 50° E and 25 – 31° S, from 1992 – 2013, showing a) anti-cyclonic eddy lifespans, b) cyclonic eddy lifespans, c) anti-cyclonic eddy radii, d) cyclonic eddy radii, e) anti-cyclonic eddy radii, f) cyclonic eddy radii, g) anti-cyclonic eddy radii and h) cyclonic eddy radii. AVISO-AVISO plots are indicated in black (along with a thin grey line along the diagonal to show the reference position), AVISO-ABS in red, and AVISO-REL are indicated in blue.

4.3.4 Energy Conversion terms

In an attempt to explain the EKE differences between ABS and REL, and the differences in regions of eddy formation and termination between the simulations, two pathways of energy were examined. Figures 4.18 and 4.19 show the depth integrated barotropic and baroclinic energy conversion terms, respectively. In Figure 4.18, regions of positive (negative) energy transfer from mean kinetic to eddy kinetic energy indicates eddy formation (dissipation) through barotropic instabilities of the mean flow (Kundu, 1990; Biastoch and Krauss, 1999, Halo et al., 2014b). In both models, a strong positive barotropic transfer of energy occurs south of Madagascar, on the offshore edge of the SEMC where the current begins to separate from the coast. In both models there is also a small region of positive barotropic energy transfer south of Madagascar on the inshore edge of the SEMC. There is a strong negative KmKe in the Agulhas Current in both ABS and REL. A strong positive transfer of energy exists offshore of the Agulhas Current in both of the models. In both models, there is a negative barotropic energy conversion on the western boundary of the Mozambique Channel. A negative transfer of energy also occurs in the SEMC and extends westward, from south of Madagascar towards the Agulhas Current. The negative energy transfer in southern SEMC is reduced by between 30 and 60% from ABS (Figure 4.18a) to REL (Figure 4.18b). Similarly, the negative energy transfer in the Agulhas Current is also reduced. There are positive and negative differences in barotropic energy conversion in the southern extent of the Agulhas Current. There is also a decrease in the barotropic energy conversion on the offshore edge of the Agulhas Current, suggesting that fewer eddies are forming here. There is an overall reduction of 34.10% in the barotropic conversion from mean kinetic to eddy kinetic energy from ABS to REL.

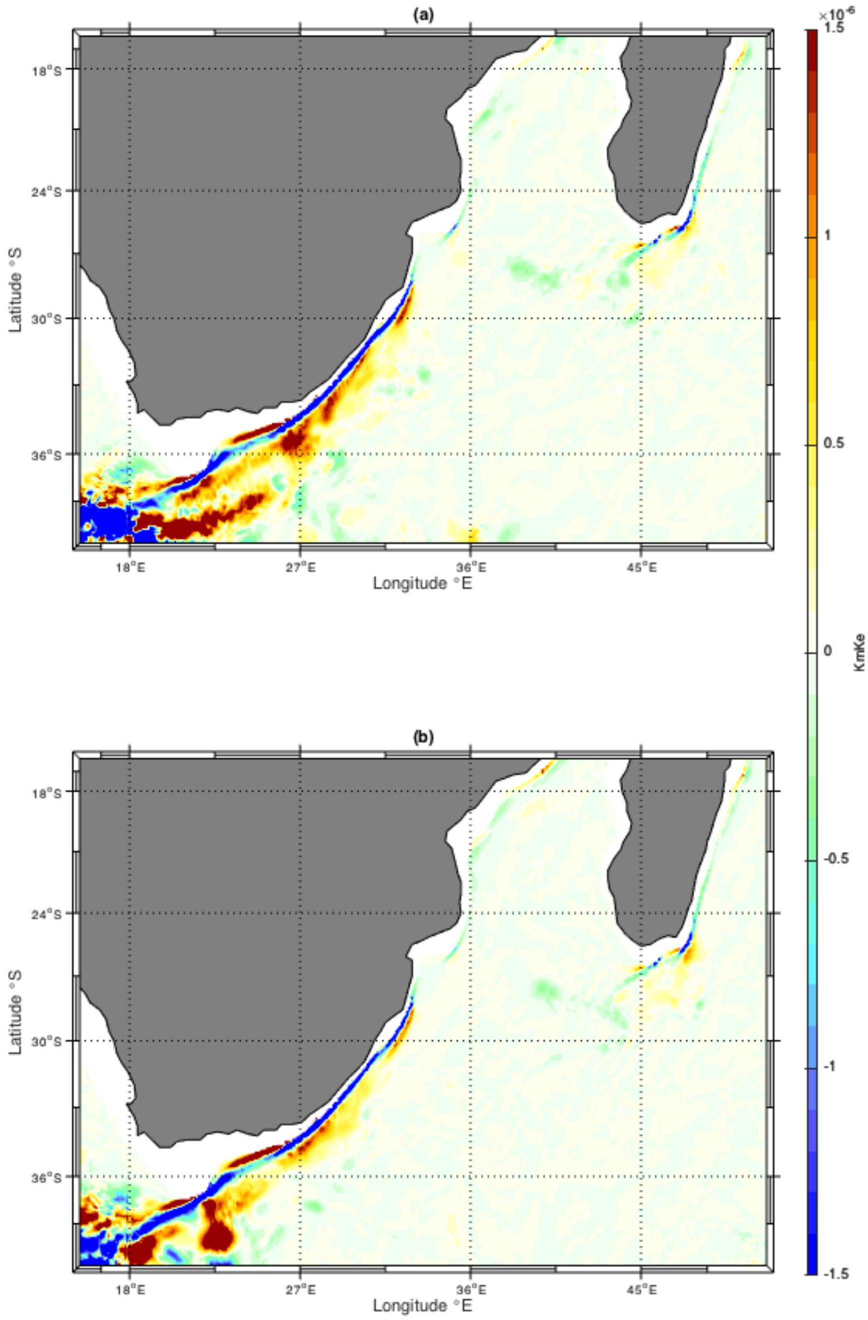

Figure 4.18: The depth integrated barotropic energy conversion for a) the model forced with absolute winds and b) the model forced with relative winds.

Regions of positive baroclinic energy transfer in Figure 4.19, indicate eddy formation due to baroclinic instabilities, otherwise it indicates dissipation toward the mean eddy potential energy. A strong positive transfer of baroclinic energy occurs in the northwestern Mozambique Channel in both ABS (Figure 4.19a) and REL (Figure 4.19b). In both ABS and REL turbulent regions of positive and negative baroclinic energy conversion occur offshore of the SEMC as well as the Agulhas Current. It is however evident that the energy is significantly reduced from ABS to REL in both these regions. In the regional HYCOM, there is an overall reduction of 43.52%.

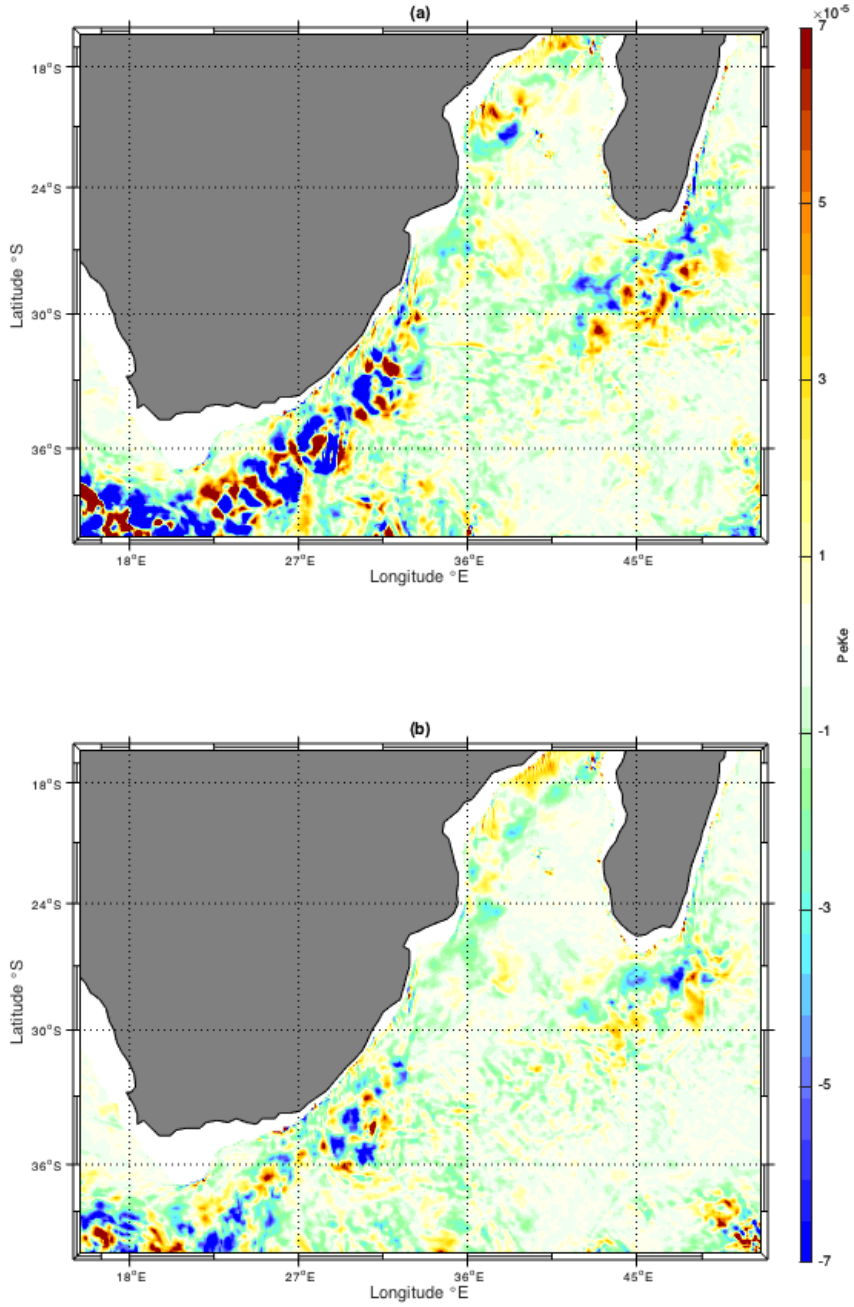

Figure 4.19: The depth integrated baroclinic energy conversion for a) the model forced by absolute winds and b) the model forced by relative winds.

4.4 Discussion

The response of the EKE to current feedback in HYCOM is similar to that demonstrated in a previous study using a coupled-ocean atmosphere model of the Agulhas Current system (Renault et al., 2017). The results of this study suggest that the "mechanical dampening" process observed by Duhaut and Straub, 2006; Dawe and Thompson, 2006; Eden and Dietze, 2009; Renault et al., 2016a; Renault et al., 2016b and Renault et al., 2017 can also be caused by changing the wind forcing in the regional HYCOM model from absolute to relative winds.

From Figures 4.3, 4.4 and 4.5 it was evident that change in wind forcing in the regional HYCOM has resulted in a reduction in wind stress from ABS to REL, particularly in the Mozambique Channel, south of Madagascar and the Agulhas Current. Previous studies (Duhaut and Straub, 2006; Dawe and Thompson, 2006; Eden and Dietze, 2009; Renault et al., 2016a; Renault et al., 2016b; Renault et al., 2017) have shown a significant reduction in the energy of the ocean with the inclusion of surface currents in the wind stress. In particular Renault et al. (2017), demonstrated an overall reduction in energy over the Agulhas Current system of 25%. The difference in EKE betweeen ABS and REL is approximately 33% (Figures 4.6, 4.7a). In the regional HYCOM, it is evident that results from REL are more representative of the EKE observed in the satellite product, AVISO compared to ABS. Whist the altimetry product is more representitive of actual EKE values, it is important to note that the altimetry likely underestimates EKE. A study by Backeberg et al. (2014) showed the EKE of the altimetry product to be much lower than the EKE derived from drifters. This is because satellite data does not include the ageostrophic component of the currents and cannot capture small and short-lived eddies (de Vos et al., 2018).

The MKE from ABS to REL is also significantly reduced, with the exception of an increase in MKE in the core of the Agulhas Current as well as the SEMC (Figure 4.7b). Backeberg et al., 2008 shows that the velocities of the Agulhas Current in the HYCOM simulation are weaker than observed in the satellite product. An increase in the MKE from ABS to REL, indicates that the change in wind forcing has improved the representation of the Agulhas Current. The pattern of the EKE and MKE reductions from ABS to REL is strongly reflective of those seen in the wind stress, thus implying that the wind stress is directly influencing the energy of the Agulhas Current system.

Figures 4.8, 4.9, 4.10 show the contribution of kinetic energy from eddies tracked by the eddy tracking algorithm to the overall EKE. There is a reduction in energy within the eddies from ABS to REL in the Mozambique Channel, south of Madagascar and in the Agulhas Current of approximately 100 − 400 $cm^2.s^{-2}$. The residual EKE, which is the difference between the total EKE and the energy within the eddies is also observed. The difference in residual EKE between ABS and REL is approximately 2.5 times greater than that of the difference in energy within the eddies. This suggests that the contribution of meandering currents, smaller eddies and other forms of variability to the overall EKE is more signifcant than the contribution from the tracked eddies. This implies that the contribution of mesoscale eddies to the overall EKE is not as important as other forms of variability in the Agulhas Current system. However, it is important to note that from Chapter 2 of this study that this could be partially due to limitations of the eddy tracking algorithm. For example, there may be some mesoscale eddies which were not tracked by the algorithm. Given the effect of relative winds on mesoscale eddies, it is possible that the effect of relative winds on smaller eddies or submesoscale features could be destroyed completely. It is important to note that at $1/10^{\circ}$ the regional model is not able to simulate submesoscale processes. It is also possible that the strengthening of the Agulhas Current, or that the weakening of the MKE on the offshore edge of the Agulhas Current has resulted in fewer meanders. The representation of meanders in the Agulhas Current is investigated further in the following chapter of this study; Chapter 5.

Results suggest that the change in wind forcing in the regional HYCOM has resulted in fewer eddies forming in the south of Madagascar, due to a reduction in EKE in this region. Results in Figure 4.11 show fewer westward propagating eddies in the region south of Madagascar in REL compared to ABS. This is further supported by the eddy trajectory roses in Figure 4.12, which show that more eddies appear to propagate in a south westward direction in REL compared to ABS as a result of the paucity of eddies in the region south of Madagascar. One possible reason for this is the reduction in MKE south of Madagascar, and thus a weaker SEMC which is responsible for the formation of anti-cyclonic eddies in the region (de Ruijter et al., 2004; Halo, 2008; Siedler et al., 2009; Ridderinkhof et al., 2013; Halo et al., 2014b).

Figures 4.13 (g,h) show fewer eddies propagating along the offshore edge of the Agulhas Current in REL compared to ABS, suggesting that the accuracy of the regional HYCOM model in representing mesoscale variability has been improved with the change in wind forcing. Previously, Backeberg et al., (2008) highlighted the overestimation of large anti-cyclonic eddies occurring on the offshore edge of the Agulhas Current in the model relative to the altimetry product. The observed eddy dissipation process of source region eddies as they approach the Agulhas Current, described in the previous chapter, is also poorly represented in many numerical simulations (Backeberg et al., 2014; Durgadoo et al., 2013; Loveday et al., 2014). In these models, eddies tend not to dissipate but rather they propagate along the offshore edge of the current towards the Agulhas retroflection. Results of Figures 4.13(g, h) suggest that this result improved by changing the wind forcing in the regional HYCOM. In ABS the representation of the Agulhas Current was wider and weaker. It is likely that the this decrease in the number of eddies propagating along the offshore edge of the Agulhas Current is responsible for the narrower, stronger Agulhas Current observed in REL.

In addition to this, an investigation into the eddy properties indicates that a change in wind forcing in the regional HYCOM has a significant dampening effect on the eddies themselves. Figures 4.14, 4.15 and 4.16 show a reduction in eddy amplitudes, radii and circum-averaged speeds from ABS to REL, with the largest changes evident in the region south of Madagascar. These results are further supported by Figure 4.17 which shows a reduction in anti-cyclonic eddy life-spans, as well as in both anti-cyclonic and cyclonic eddy amplitudes and circum-averaged speeds. These results are consistent with a study of the California upwelling system which showed that current feedback to the atmosphere resulted in a more accurate representation of eddies in the region (Renault et al., 2016b). Additionaly, there are significantly more eddies tracked in ABS than REL, which could suggest that eddy formation is linked with increased energy imparted on the ocean currents in HYCOM in the absolute winds simulation. It is evident from Figure 4.17 that the impact of mechanical dampening is larger on larger eddies. At smaller scales, eddies are more similar in ABS and REL. Renault et al. (2017) show that the correlation between eddy windwork and EKE is very high, where by the greater the EKE, the greater the loss of energy in that region. This could explain why the mechanical dampening effect is stronger for larger eddies and weaker for smaller eddies. To fully understand and quantify this would require further idealised experiments.

In both ABS and REL, there is a small region of positive barotropic energy transfer south of Madagascar on the inshore edge of the SEMC. This result is similar to that of Halo et al. (2014b) who also found a strong positive barotropic transfer of energy near to the continental shelf, indicating a strong shear formation of cyclonic eddies on the inshore edge of the SEMC. Consistent with Renault et al. (2017), a strong positive transfer of energy exists in the Agulhas Current in both of the models. The barotropic and baroclinic energy conversion terms reveal a large reduction in energy over the Agulhas Current domain from ABS to REL of 34.10% for the barotopic energy conversion term (Figure 4.18) and 43.52% for the baroclinic energy conversion term (Figure 4.19). Renault et al. (2017), found a reduction the barotropic transfer of energy of 15%, over the Agulhas Current domain but only a 5% reduction in the baroclinic transfer of energy in the Mozambique Channel. The effect here of the change in wind forcing in the regional HYCOM is much larger. One reason for the large difference between the two models, is because HYCOM has too many eddies propagating along the offshore edge of the Agulhas Current, compared to the model used by Renault et al. (2017). This is where the biggest reduction is seen in HYCOM, whilst there is very little change in the study by Renault et al. (2017) for the same region.

Because of the improvement in the representation of EKE in the regional HYCOM, the dampening coefficient (of approximately 0.7) used by Renault et al. (2017) was not applied to the change in wind forcing in the regional HYCOM. This coefficient allows for the influence of the surface ocean currents velocities to be reduced in the relative wind stress equation by only taking into account 70% of the ocean currents for the Agulhas Current region (Renault et al., 2017). Had the dampening coefficient been applied, it is very likely that the resulting difference in EKE, eddy properties and the energy conversion terms between the two experiments would have been smaller. As the lifespans of eddies are reduced from ABS to REL, future studies could include tuning the relative winds more carefully based on these results. However, for the purposes of this study, we wanted to see the direct impact of the relative winds, and not a scaled version thereof. In addition to this, the EKE in HYCOM was much larger than that of the study by Renault et al. (2017). The results of the change in wind forcing in the regional HYCOM, without the dampening coefficient, were found to reduce EKE and be more agreeable to that of the AVISO EKE. It can also be noted that in the new version of HYCOM (Version 2.2.98), relative winds has been included as an option when calculating forcing and fluxes, and the formulation implemented does not include the dampening coefficient used by Renault et al. (2017). It is also important to note that the EKE results observed here could be different if the HYCOM data were averaged to 1/4° applying the method used in the AVISO satellite product.

4.5 Summary and Conclusion

Analysing two simulation experiments in HYCOM, one forced with absolute winds and the other forced with relative winds, the response of the model to current feedback was investigated. The response in the ocean only HYCOM model was found to be stronger than that of the coupled ocean-atmosphere ROMS model of the Agulhas Current System used by Renault et al. (2017). Changing the wind forcing from absolute to relative winds decreases the overall wind stress of the domain by up to 0.01 Pa in regions with strong surface currents (Figures 4.3, 4.4, 4.5). In REL, the weaker wind stress is also more spread out through the Mozambique Channel.

There is a reduction in EKE from ABS to REL, particularly in the Mozambique Channel, south of Madagascar and in the Agulhas Current (Figures 4.6a). There is a reduction in the overall EKE from ABS to REL of 33% and the resulting EKE from the change in wind forcing is similar to that observed in the AVISO satellite product. The pattern of reduction in the EKE is very similar to that observed in the changes in wind stress from ABS to REL. Results from this study suggest that the "mechanical dampening" of EKE described by previous studies (Duhaut and Straub, 2006; Dawe and Thompson, 2006; Eden and Dietze, 2009; Renault et al., 2016a; Renault et al., 2016b; Renault et al., 2017) occurs in the regional HYCOM.

It is important to note that the residual EKE of the simulations is a factor of 2.5 times larger than the energy within the eddies, indicating that meanders and other forms of variability (including smaller scale eddies or short-lived eddies) have a much larger influence on the overall EKE than the eddies tracked by the eddy tracking algorithm (Figures 4.9). Figure 4.10 shows that the difference in eddy energy between ABS and REL is relatively small, but the change that occurs in meandering currents and other forms of mesoscale variability, is approximately 2.5 times greater. Beyond the large mesoscale eddies, other processes such as meanders, small eddies and short lived eddies contribute extensively to the overall eddy kinetic energy budget. Whilst some of the difference can likely be attributed to limitations of the eddy tracking algorithm, the influence of the change in wind forcing on meanders in the Agulhas Current will be investigated in Chapter 5 of this study.

The eddies forming at the SEMC tend to propagate in a focused, narrow, westward trajectory in ABS, while in REL the eddy trajectories appear to be slightly more spread out, with fewer eddies forming south of Madagascar and propagating westward (Figures 4.11 and 4.12). However, from Figure 4.8, it is apparent that this is due to fewer westward propagating anti-cyclonic eddies occurring in the region of elevated EKE south of Madagascar. The eddy pathways in both ABS and REL are very similar, with very few differences in regions of eddy formation and dissipation (Figure 4.13a, b, c, d). Figures 4.13(e, f), which show the annual frequency of eddy occurrences, indicate that there are fewer eddies propagating along the offshore edge of the Agulhas Current in both ABS and REL and suggest that current feedback in the regional HYCOM reduces the bias of eddies propagating all the way through the Agulhas Current.

Figures 4.14, 4.15, 4.16 and 4.17 show a reduction in eddy lifespans, radii, amplitudes and circum-averaged speeds from ABS to REL. The change in wind forcing has resulted in a more accurate simulation of anti-cyclonic eddies in the regional HYCOM, but it has made cyclonic eddies which were already under-sized even smaller.

Although the barotropic and baroclinic energy transfer patterns in the regional HYCOM experiments are consistent with previous research (Halo et al., 2014b; Renault et al., 2017), the reduction in energy observed from ABS to REL of the Agulhas Current is larger in the regional HYCOM than in previous studies due to the over representation of mesoscale eddies propagating along the offshore edge of the Agulhas Current in ABS (Figures 4.18 and 4.19).

Previous studies have shown that current feedback to the atmosphere significantly reduces the energy of the ocean and acts as an “eddy killer” (Duhaut and Straub, 2006; Dawe and Thompson, 2006; Eden and Dietze, 2009; Renault et al., 2016a; Renault et al., 2016b; Renault et al., 2017). In particular, Renault et al. (2017) showed that current feedback caused a 25% reduction in EKE of the Agulhas Current. In the regional HYCOM the changes in EKE, eddy pathways, eddy properties and the energy conversion terms, resulting from the change in forcing from absolute to relative winds are consistent with, but often even larger than observed in previous studies. The “mechanical dampening” observed in this study may be reduced by including a dampening coefficient as used by Renault et al. (2017).

Renault et al. (2017) noted that the mean wind work of their coupled ocean-atmosphere model could be further reduced by including the entire Indian Ocean Gyre in the domain. This is also in agreement with another HYCOM study by Zamudio et al. (2011). It is possible that local response to current feedback would be greater if the changes in wind forcing were applied to both the regional HYCOM model as well the outer INDIA model. As the EKE is significantly reduced from ABS to REL, the representation of cyclonic and anti-cyclonic eddy dynamics in the source region of the Agulhas Current was also significantly influenced. In the regional HYCOM the influence of the change in wind forcing on meanders and variability in the Agulhas Current is still unknown, and will be investigated in the following chapter.

CHAPTER 5.

THE EVOLUTION OF MEANDERS IN THE AGULHAS CURRENT FROM HYCOM AND SATELLITE OBSERVATIONS

5.1 Introduction

The arrival of deep sea eddies which are formed in the Mozambique Channel and south of Madagascar at the offshore edge of the Agulhas Current can lead to the formation of a large cyclonic meander in the Agulhas Current (de Ruijter et al., 1999; van Leeuwen et al., 2000; de Ruijter et al., 2002; Schouten et al., 2002; Backeberg et al., 2008; Tsugawa and Hasumi, 2010). Previous research has shown that when large, anti-cyclonic, source region eddies interact with the Agulhas Current near to the Natal Bight (at approximately 29° S), instabilities, caused by the barotropic transfer of energy from the eddy to the Agulhas Current, can trigger a meander known as a Natal Pulse, which propagates down the coast (de Ruijter et al., 1999; Schouten et al., 2002; Tsugawa and Hasumi, 2010). Natal Pulses tend to occur irregularly every 50 to 150 days (de Ruijter et al., 1999).

Natal Pulses range in size from approximately 30 km in size to 200 km and propagate at a speed of 0.1 to 0.2 $m.s^{-1}$ (8.64 to 17.28 $km.day^{-1}$)(Van der Vaart and de Ruijter, 2001; Bryden et al., 2005; Tsugawa and Hasumi, 2010; Rouault and Penven, 2011; Krug et al., 2014). Results from Chapter 3 of this study showed that the formation of meanders can be triggered by both cyclonic and anti-cyclonic eddies when they reach the eastern boundary of the Agulhas Current. Anti-cyclonic eddies arriving at a transect of the northern Agulhas Current (30° S, 30.95° E to 32.4° S, 34° E) caused the current to meander from its mean position of 69 km offshore to an average distance of 100 ± 79 km offshore. Cyclonic eddies arriving at the same transect had a greater impact and caused the Agulhas Current to move to an average distance of 145 ± 85 km from the coast). After passing the Agulhas Bank (approximately 38° S) Natal Pulses generally become much slower with a speed of approximately 0.05 $m.s^{-1}$ (Lutjeharms and Roberts, 1988).

5.1.1 The interaction of Natal Pulses with shelf topography

The presence of a cold-core cyclonic eddy on the inshore edge of the Agulhas Current is often associated with a Natal Pulse (Lutjeharms, 2006; Leber and Beal, 2014). Natal Pulses have a known impact on the coastal and shelf circulation in the region. They can also cause water to upwell along the continental shelf at a rate of 50 – 100 $m.day^{-1}$ (Bryden et al., 2005). Malan et al. (2018) show that the leading edge of large meanders can cause upwelling and downwelling inshore of the Agulhas Current promoting shelf-slope exchange. Warm plumes and filaments of water associated with the meanders drive Agulhas Current water onto the shelf and influence the cross-shelf exchange in the region (Bryden et al., 2005; Jackson et al., 2012; Krug et al., 2014; Malan et al., 2018). A study by Pivan et al. (2016) demonstrated a contribution of Eastern Agulhas Bank water, Indian Equatorial Water and Antarctic Intermediate Water to the cross-shelf exchange associated with a Natal Pulse. Pivan et al. (2016) also demonstrate using observations that Natal Pulses extend to a depth of 1000m.

5.1.2 The downstream impacts of Agulhas Current meanders

Between one and two Natal Pulses propagate as far as the southern Agulhas Current region each year (Rouault and Penven, 2011, Krug et al., 2014). A study by Leber and Beal (2014) demonstrates that the southwestward transport of the Agulhas Current (at approximately 34° S) remains very consistent during a meander. Nevertheless, some early retroflections of the Agulhas Current, south of the African continent, have been associated with Natal Pulses (Lutjeharms and van Ballegooyen, 1988; van Leeuwen et al., 2000; Rouault et al., 2010; Elipot and Beal, 2015). Natal Pulses are considered to play a significant role in the variability of the southern Agulhas Current and sometimes in the number of large Agulhas Rings that are shed into the South Atlantic Ocean (de Ruijter et al., 1999, Schouten et al., 2002). Biastoch et al. (2008), however, show using a numerical model that Natal Pulses do not significantly influence Agulhas leakage. Further studies have also shown that the connection between Natal Pulses and the number of rings shed is neither systematic nor that strong (Rouault and Penven, 2011; Elipot and Beal, 2015).

5.1.3 Improving the simulation of Natal Pulses in numerical models

The complex variability of the southern Agulhas Current, the Agulhas Current retroflection and associated Agulhas leakage are very difficult to model accurately. In Chapter 4 of this study, two simulation experiments were used to investigate the effects of the change in wind forcing from absolute winds (ABS) to relative winds (REL) on Agulhas Current source region eddies in the regional Hybrid Coordinate Ocean Model. Results revealed a very large reduction in eddy kinetic energy (EKE) over the Agulhas Current and its source regions. The response of mesoscale eddies to this change in wind forcing can be summarized by a typical example for the week of 15/02/1993 given in Figure 5.1 below. As in the study by Backeberg et al. (2008), many strong eddies in ABS (Figure 5.1a) propagate towards the Agulhas Current and along the offshore edge of the Agulhas Current. In Figure 5.1b, it is clear that the intensity of eddies forming in the Mozambique Channel and south of Madagascar has been significantly reduced in REL. In addition to this the number of eddies propagating down the offshore edge of the Agulhas Current has notably decreased. Eddies in REL tend to be more similar to those captured in AVISO data (it is important to note that neither of the model simulations are assimilated) (Figure 5.1c), indicating that the representation of mesoscale eddies in the Agulhas Current has significantly improved by changing the wind forcing from absolute to relative winds in the regional HYCOM.

In addition to these changes, a sizable reduction in the barotropic energy transfer on the offshore edge of the Agulhas Current from ABS to REL was also observed in

Chapter 4 of this study. The barotropic conversion of energy has been shown to be the main driver of EKE in the source regions of the Agulhas Current (Halo et al., 2014; Renault et al., 2017) and it triggers the formation of Natal Pulses.

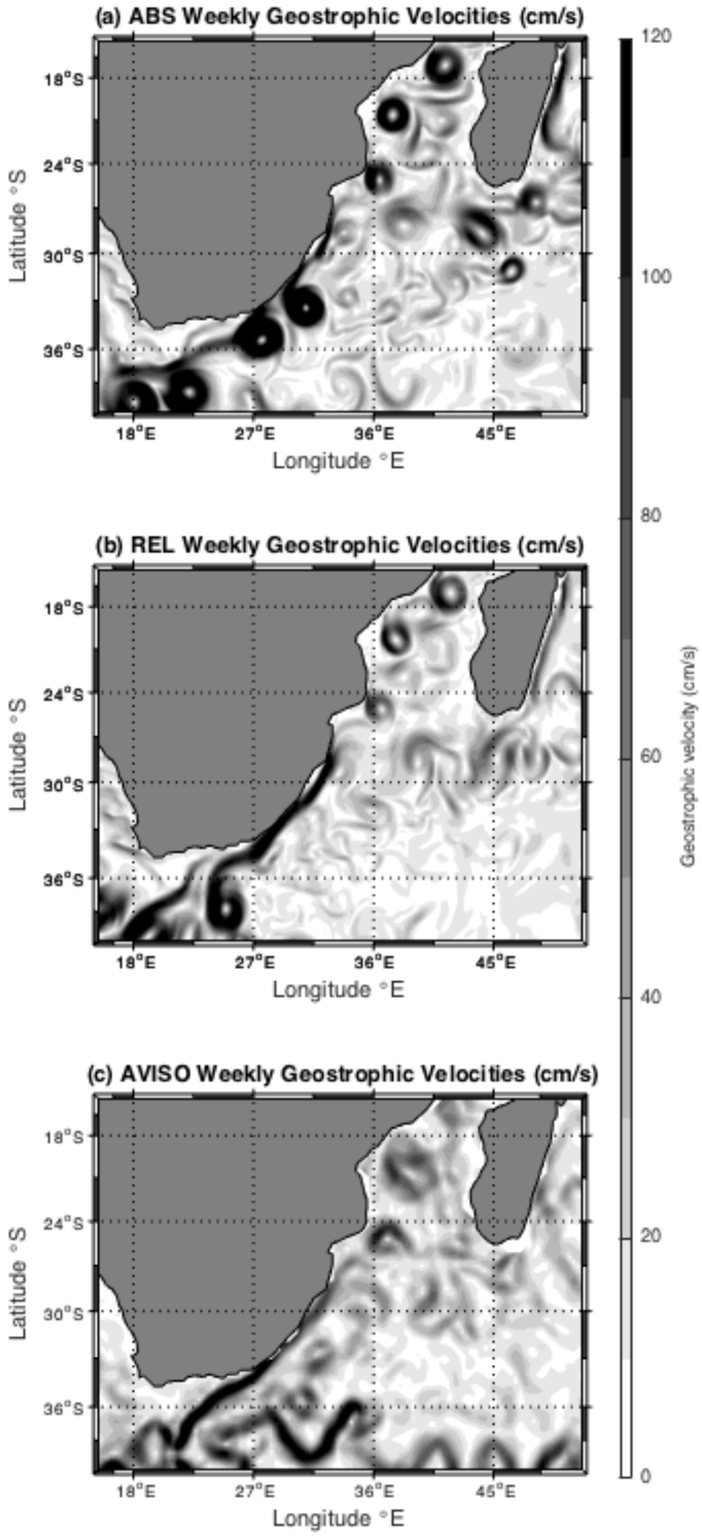

Figure 5.1: Weekly geostrophic velocities (cm.s^{-1}) for a) the model forced by absolute winds, b) the model forced by relative winds and c) AVISO for the week of 15/02/1993.

Using a coupled ocean-atmosphere model which included feedback from the Agulhas Current to the overlying winds, Renault et al. (2017) revealed a reduction in EKE, in the number of Natal Pulses and their influence on variability of the Agulhas Basin. Additionally, an improvement in the location of the mean Agulhas Current retroflection was observed; however, the variability in the region was still too large (Renault et al., 2017). This study, and the improvements observed in the simulation of mesoscale eddies regional HYCOM in Chapter 4 of this thesis, together with the large decrease in the barotropic transfer of energy, suggest that the change in wind forcing from absolute to relative winds could also significantly impact the formation of mesoscale meanders in the regional HYCOM.

Using the same two simulation experiments from Chapter 4 of this thesis, the objective of this chapter is to evaluate the overall changes in Agulhas Current meanders from the experiment forced by absolute winds to the experiment forced by relative winds in the regional HYCOM. The variability of the strength and direction of the Agulhas Current is investigated. The evolution of meanders as they propagate down the Agulhas Current will be also be explored using the regional HYCOM model, with particular focus on the influence of current feedback on the formation and dissipation of Natal Pulses, the properties thereof, and the role that Agulhas Current source region eddies play in these complex meandering events.

5.2 Data

5.2.1 The Hybrid Coordinate Ocean Model

The Hybrid Coordinate Ocean Model (HYCOM) used here is explained in detail in Chapter 2 of this thesis. The regional model, which spans the entire Agulhas Current system at a resolution of approximately 10 km, uses a combination of isopycnic vertical co-ordinates in the stratified open ocean, fixed-grid co-ordinates in the upper ocean mixed layer and sigma coordinates in shallow coastal regions at each time step of the simulation (Bleck et al., 2002).

In Chapter 4, two simulation experiments are used to investigate the local effects of absolute versus relative wind forcing in the regional HYCOM. In the model forced by absolute winds (ABS), the forcing speed in the wind stress calculation is determined from wind velocity only. The model forced by relative winds (REL) takes into account the effect of the surface ocean currents on wind velocities. These experiments are described in full in Chapter 2. Here, the effects of the change in wind forcing in the regional HYCOM on meanders in the Agulhas Current are investigated.

5.2.2 Observations (in-situ and satellite data)

5.2.2.1 ACT data

An array of moorings across the Agulhas Current, known as the Agulhas Climate Time-Series (ACT) experiment (Beal et al., 2015) provides a very valuable time-series of *in-situ* measurements of Agulhas Current velocities, in a region where *in-situ* data are very scarce and the complex variability in the region is difficult to capture in numerical model simulations. The array extends across the Agulhas Current at approximately 33.35° S at an angle of approximately 75° to the continental shelf and consists of 7 current meter moorings (full-depth) and 4 current pressure inverted echo sounders (CPIES), the positions of which can be observed in Figure 5.2 (Beal et al., 2015). The data has a 12 hour temporal resolution, and was interpolated into a vertical grid with 20 m intervals for the full depth of the water column, and a horizontal grid of 500 m intervals to a distance of 300 km from the coast(Beal et al., 2015). The *in-situ* data captured across the ACT array, and used in this thesis, spans from April 2010 up until February 2013. In a previous study, the ACT array was found to capture the full Agulhas Current Jet, even during meandering events (Beal et al., 2015). In this thesis, the data from the ACT array will be used as a reference to compare the regional HYCOM simulations, described below.

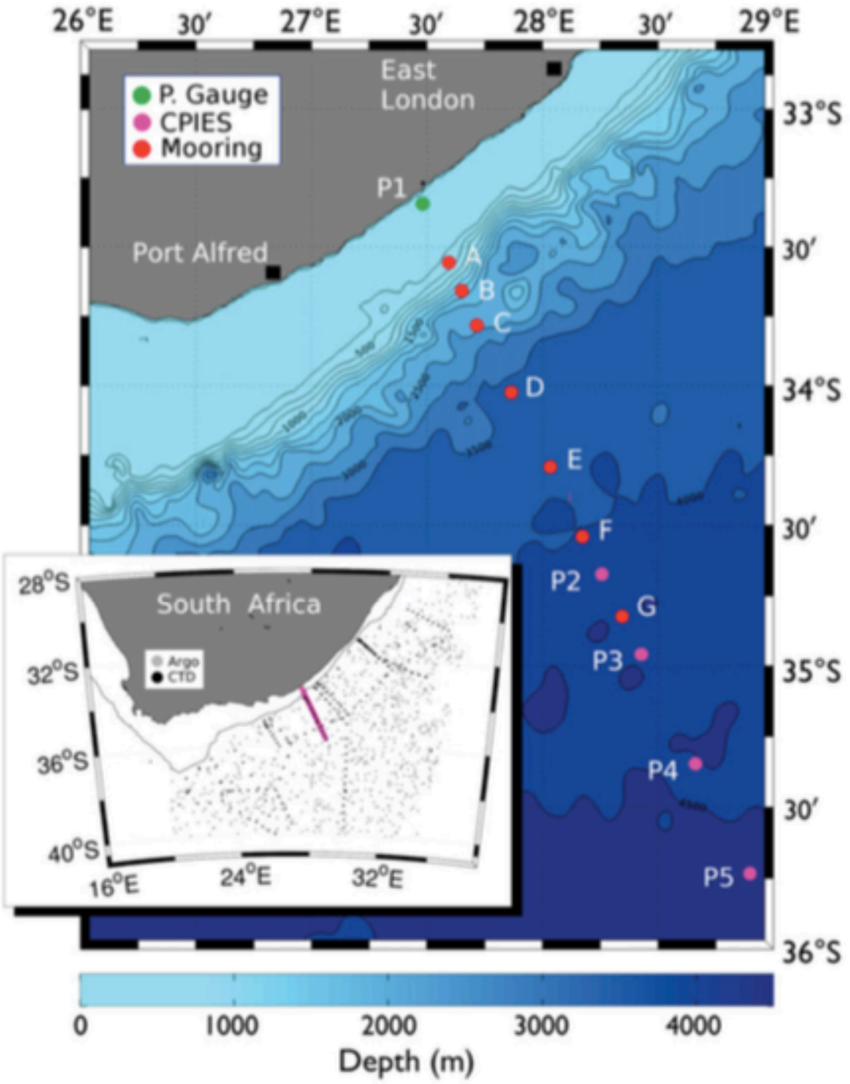

Figure 5.2: The location of the Agulhas Current Time-Series mooring array. Current meter moorings are indicated by red dots, whereas C-Pies are indicated by magenta dots. The shading indicates the depth of the ocean. The smaller map insert gives reference to the position of the ACT array along the South African coastline. (Source: Beal et al., 2015)

5.2.2.2 ADCP data

Acoustic Doppler Current Profilers (ADCPs) were used by Eskom (South Africa's power utility) to measure Agulhas Current velocities at selected sites along the continental shelf of South Africa. In all cases, the RDI 300 ADCPs were used at water depths ranging from 60 m to 96 m. All of the ADCPs sampled current velocities for the full depth of the water column in 2 m high vertical bins, at 1 hour time intervals. Data from the 2 Cape Morgan sites were concatenated, as were the data from the 2

East London sites and the data from the 2 Fish River sites, by joining the data at the nearest bin (the locations of which are shown in Figure 5.3). A summary of the ADCP data locations and the time period over which the data were collected is also provided below in Table 5.1. For the purposes of this study, the hourly ADCP data were averaged to weekly data to match the temporal resolution of the model output.

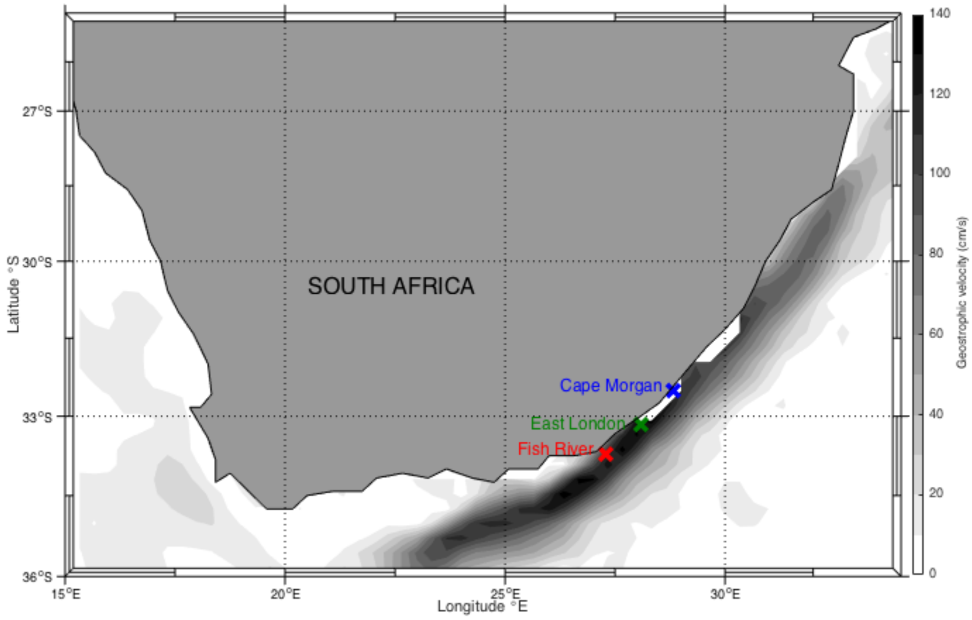

Figure 5.3: The position of the ADCP sites (x's) overlaid on the mean AVISO geostrophic velocity ($cm.s^{-1}$) from 1993 – 2013.

ADCP Location	**Longitude (°E)**	**Latitude (°S)**	**Depth of ADCP (m)**	**Time period**
Cape Morgan	28.83183	32.50733	89	05/12/2009-03/03/2010
Cape Morgan	28.83179	32.50725	87	03/03/2010-13/09/2010
East London	28.00866	32.15145	82	04/12/2009-03/03/2010
East London	28.08651	33.15140	85	03/03/2010-13/09/2010
Fish River	27.29750	33.70335	88	04/12/2009- 03/03/2010
Fish River	27.29745	33.71332	91	03/03/2010-13/09/2010

Table 5.1: The locations and times at which the RDI 300 ADCP measurements of Agulhas Current velocities were collected.

5.2.2.3 Aviso Data

AVISO Satellite altimetry data produced by Ssalto/Duacs and distributed through CMEMS (http://marine.copernicus.eu/services-portfolio/access-to-products/?option=com_csw&view=details&product_id=SEALEVEL_GLO_PHY_L4_REP_OBSERVATIONS_008_047) were used extensively in this study. Gridded maps of Absolute Dynamic Topography (MADT), including the zonal and meridional velocities were extracted at a 0.25° resolution over the Agulhas Current region for the period from January 1993 until December 2013. Daily data were averaged to a weekly resolution so as to be more representative of the weekly averaged HYCOM data.

5.2.2.4 GlobCurrent Data

In addition to the AVISO satellite data, the 15-m depth Version 2 GlobCurrent data, available from http://www.globcurrent.org were used. In the GlobCurrent dataset the combined current is calculated by adding the geostrophic component to the Ekman component of the current. The GlobCurrent geostrophic currents are derived from AVISO gridded fields of Sea Surface Height (SSH) (Rio et al., 2014). The Ekman currents, which are driven by the local wind forcing, are calculated with Lagrangian ocean current measurements from Argo floats and surface drifters (Rio et al., 2014). The data set is comprised of 13 years of global gridded current fields, at 3 hour time intervals and a 0.12° resolution. Data were weekly averaged to the same temporal resolution as the HYCOM data. The GlobCurrent data were compared with *in-situ* ADCP data and to the two regional HYCOM simulations (ABS and REL) to investigate the variability within the Agulhas Current.

Note that the GlobCurrent product should be more representative of the total currents output of the model than the AVISO data, since it includes the Ekman flow (Rio et al., 2014; Krug et al., 2018).

5.3 Methods

5.3.1. Principal Component Analysis

Principal component analysis (PCA) was used to explore the mean properties of the flow within the Agulhas Current. It is used at a single point to determine the principle axis of the flow and its orientation. A 95% confidence interval error ellipse was used to explain the mean velocity and the variability around the mean at 3 different locations within the Agulhas Current; offshore of Cape Morgan, East London and Fish River. This ellipse defines the region in which 95% of all the data that can be extracted from the underlying Gaussian distribution is contained. It gives us the main axes (principal components) of the flow. In PCA, the first two principal components should explain most of the variance in the data. An eigenvector with the highest eigenvalue is the first principal component; the second eigenvector is perpendicular to the first and is the second principal component. An eigenvector indicates the direction of the most variance; the eigenvalue denotes how much variance there is in that direction. In this way, it is possible to observe how well the GlobCurrent data and the HYCOM simulations are able to capture the different forms of variability, including meanders and Natal Pulses, in the Agulhas Current. It will also be possible to observe whether or not the change in wind forcing from absolute to relative winds influences the variability of the Agulhas Current in the regional HYCOM. The *in-situ* ADCP measurements were compared to the GlobCurrent data and then to both HYCOM experiments (ABS and REL). All data were weekly averaged for the same time period as the ADCP data for comparison purposes.

5.3.2 Transects

In Chapter 4 of this thesis an increase in Mean Kinetic Energy was observed from ABS to REL over the Agulhas Current core. In this chapter, the mean properties of the Agulhas Current at two transects (the locations of which are shown in Figure 5.4) are investigated in order to understand how well the regional HYCOM is able to simulate the Agulhas Current at depth relative to *in-situ* data and the influence of the change in wind forcing from ABS to REL has on the mean properties of the Agulhas Current. HYCOM data were extracted along the ACT transect for both the ABS and REL HYCOM simulations for April 2010 to February 2013 when ACT data are available.

5.3.3 Identifying the position of the Agulhas Current core to characterize meanders

A method developed by Krug (pers. comm, Dr Marjolaine Krug) was used to identify the position of the Agulhas Current core in AVISO, ABS and REL data from January 1993 to December 2013. As SSH data is required, it was not possible to use GlobCurrent for this section of the study. In this method, the maximum velocity at each latitude is determined over a specified domain where the Agulhas Current is well established and strong (in this instance between 25° E - 30° E and 30° S - 34° S). The SSH associated with the speed maximum at that latitude is identified, after which the mean value of the SSH maxima over the domain is calculated. The longest SSH contour corresponding to the SSH maxima value is extracted as the location of the Agulhas Current core. The distances of the Agulhas Current core from two different locations along the South African coastline (namely, Port Edward at 30.2224° E, 31.0509° S and south at the start of the ACT transect at 27.4777° E, 33.3450° S) were used to measure the sizes and frequencies of Agulhas Current meanders at both of these locations in the current (Figure 5.4). A zero crossing method was used to determine the duration of the meanders (as in Krug et al., 2014) whereby the length of a meander is determined by the time period between two zero crossing points of the Agulhas Current position at each site. In this way, the evolution of meanders from the northern location to the southern one can be compared.

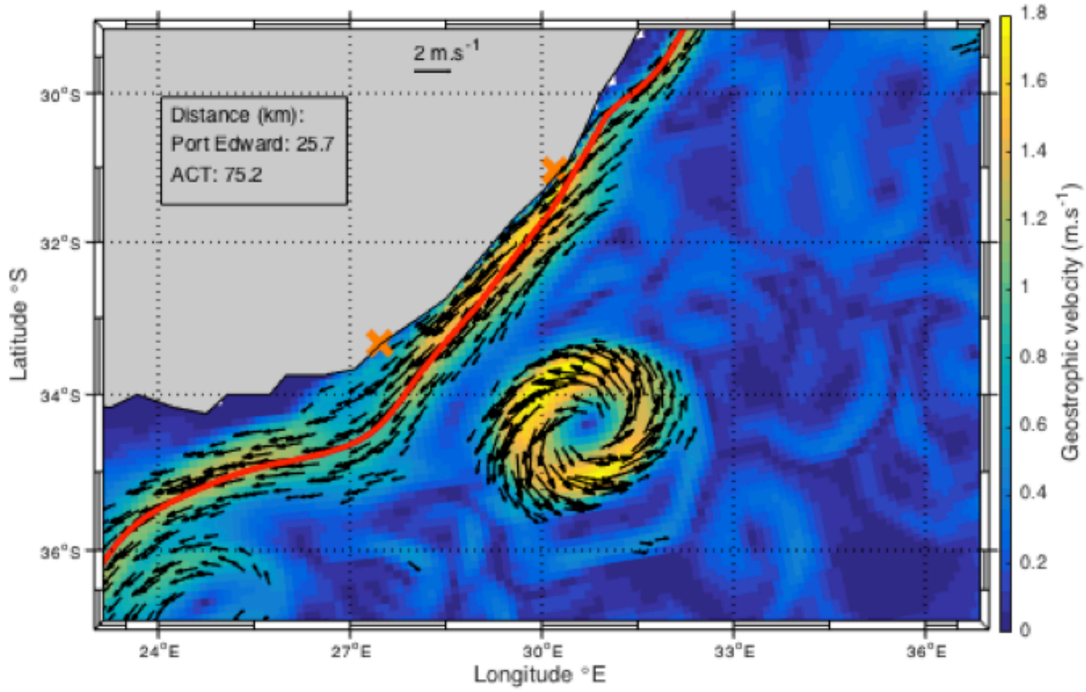

Figure 5.4: An example of Agulhas Current core detection applied to the ABS model output. The map shows weekly velocities (m.s^{-1}) of the Agulhas Current (colour) with the SSH contour representative of the Agulhas Current core overlaid in red. Black vectors indicate the direction of flow for velocities greater than 0.5m.s^{-1}. Orange crosses indicate the positions of the Port Edward (north) and ACT (south) transects.

In an attempt to separate the large mesoscale meanders (similar to Natal Pulses) from smaller meanders in the Agulhas Current, the meanders were separated into two different categories. These were meanders which were less than 50 km in size and those meanders which were equal to or greater than 50 km in size. In Krug et al. (2014), only meanders of the Agulhas Current which are greater than 1 standard deviation from the mean position of the Agulhas Current are considered to be Natal Pulses. The standard deviation of the Agulhas Current in AVISO, ABS and REL at both the ACT and Port Edward locations was found to be less than or equal to 42 km. Large mesoscale meanders are those that are greater than 42 km in size. Considering the resolution of the AVISO altimetry data, the 42 km was rounded up to 50 km. For these reasons, the 50 km threshold was selected. Note however, that the results were found to not be sensitive to this 50 km criterion, and in fact, the results shown below display the same behaviour if either a 40 km or a 60 km criterion were used.

5.3.4 Composite plots

A composite analysis of the synoptic circulation of the Agulhas Current region during meandering events was performed in AVISO, ABS and REL data for the time period of January 1993 to December 2013 for meanders occurring offshore of the start of the ACT transect. The method used to create the composites is similar to that described in Krug et al. (2014) where time-averaged velocity fields during meanders which were greater than or equal to 50km in size were used to create a composite average. Velocity anomalies of the Agulhas Current during a large Agulhas Current meander or Natal Pulse in the three different data sets.

5.4 Results

5.4.1 Variability within the Agulhas Current

Principal component analysis was used to highlight the variance in the Agulhas Current (Figure 5.5). From Figure 5.5(a) it is evident that the ADCP data contains the most variance. Whilst the GlobCurrent, ABS and REL data correctly capture the directions of maximum variance, they are unable to accurately represent all of the variance in the Agulhas Current at the Cape Morgan location. Figure 5.5(a) indicates that the GlobCurrent data better represents the variability at this location than either of the unassimilated HYCOM simulations for the period of 05/12/2009-13/09/2010. From Table 5.2 we can compare the exact eigenvalues at this location. At Cape Morgan, the ADCP data indicates a major axis of 1.39 $m.s^{-1}$ (the mean flow speed along-shelf), and a minor axis of 0.59 $m.s^{-1}$ (the mean cross-shelf flow). In the GlobCurrent data the major component is 0.70 $m.s^{-1}$ whereas the minor component is 0.27 $m.s^{-1}$. The results from the ABS and REL data are very similar at Cape Morgan with eigenvalues of 0.39 and 0.23 $m.s^{-1}$ for ABS and 0.45 and 0.20 $m.s^{-1}$ for REL (Table 5.2). Both HYCOM simulations underestimate along-shelf variations more than GlobCurrent.

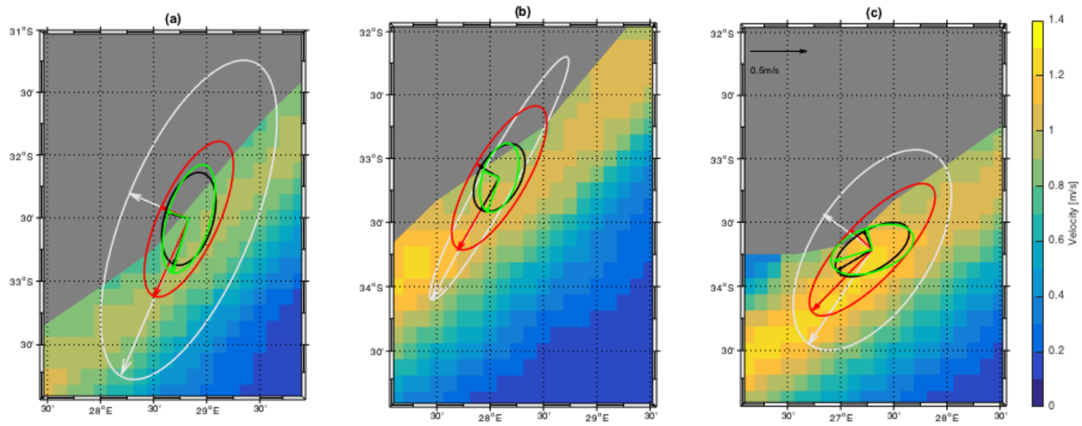

Figure 5.5: Time averaged GlobCurrent velocities (colour) overlaid with current ellipses from ADCP data (white), GlobCurrent (red), the HYCOM experiment forced by absolute winds (black) and HYCOM data from the experiment forced by relative winds (green) for a) Cape Morgan b) East London and c) Fish River.

The across-shore variability captured in all datasets is most similar at the East London location (Figure 5.5(b)). ADCP data shows eigenvalues of 1.14 and 0.15 $m.s^{-1}$, while GlobCurrent data shows eigenvalues of 0.68 and 0.24 $m.s^{-1}$ indicating higher levels of lateral variability than what is captured by the ADCP data (Table 5.2). The variability in the poleward direction is however more accurate than that of the HYCOM simulations which indicate similar variances of 0.31 (ABS) and 0.29 $m.s^{-1}$ (REL). The lateral variability captured by the HYCOM simulations is very similar to that of the ADCP data, with ABS data indicating a variance of 0.19 $m.s^{-1}$ and REL data being the most accurate with a variance of 0.16 $m.s^{-1}$.

At the Fish River location, the PCA reveals that the GlobCurrent and HYCOM data have slightly different eigenvectors to those of the ADCP data. The largest eigenvectors follow the direction of the coast more in the GlobCurrent and HYCOM data than the *in-situ* data suggests (Figure 5.5(c)). The eigenvalues of the ADCP data are 0.95 and 0.51 $m.s^{-1}$. The GlobCurrent data is once again most representative of the variance in the ADCP data with eigenvalues of 0.75 and 0.25 $m.s^{-1}$. At this location, the REL data is slightly more similar to that of the ADCP data with eigenvalues of 0.40 and 0.17 $m.s^{-1}$ compared to ABS eigenvalues of 0.37 and 0.16 $m.s^{-1}$ (Table 5.2).

Location	Cape Morgan		East London		Fish River	
Principal Component Number	**1**	**2**	**1**	**2**	**1**	**2**
ADCP eigenvalues ($m.s^{-1}$)	1.39	0.59	1.14	0.15	0.95	0.51
GlobCurrent eigenvalues ($m.s^{-1}$)	0.70	0.27	0.68	0.24	0.75	0.25
ABS eigenvalues ($m.s^{-1}$)	0.39	0.23	0.31	0.19	0.37	0.16
REL eigenvalues ($m.s^{-1}$)	0.45	0.20	0.29	0.16	0.40	0.17

Table 5.2: Table showing the smallest and largest eigenvalues ($m.s^{-1}$) of ADCP, GlobCurrent, ABS and REL data at the Cape Morgan, Fish River, and East London locations.

Figure 5.6 indicates that the mean Agulhas Current velocities of the mooring data are higher than either the ABS or REL velocities across the ACT transect. Mean velocities of the mooring data from April 2010 to February 2013 indicate maximum velocities of up to 1.64 $m.s^{-1}$. The maximum velocities in ABS and REL are very similar (up to 1.18 $m.s^{-1}$ and 1.21 $m.s^{-1}$ respectively). In addition to this, the mean depth of the Agulhas Current is shallower in the ACT data than in either ABS or REL. In the ACT data, the maximum depth of the mean current is approximately 1460 m, whereas the mean depth of the Agulhas Current is 1730 m in ABS and up to 1830 m in REL. In the ACT data, the width of the Agulhas Current is clear, with poleward velocities only evident up to a maximum of 176 km offshore. However, in both ABS and REL, whilst poleward flow becomes much shallower at approximately 170 km offshore, there is still a mean poleward flow of approximately 0.5 $m.s^{-1}$ in ABS and approximately 0.4 $m.s^{-1}$ in REL up to 280 km offshore. Figure 5.6(d) shows that the poleward flow in the core of the Agulhas Current is about 0.06 $m.s^{-1}$ stronger in ABS than in REL. Further offshore, a decrease in poleward velocities of up to 0.16 $m.s^{-1}$ is observed from ABS to REL. Thus, in REL the mean velocities in the core of the Agulhas Current, as well as offshore of the ACT transect, are more representative of the *in-situ* data than those in ABS.

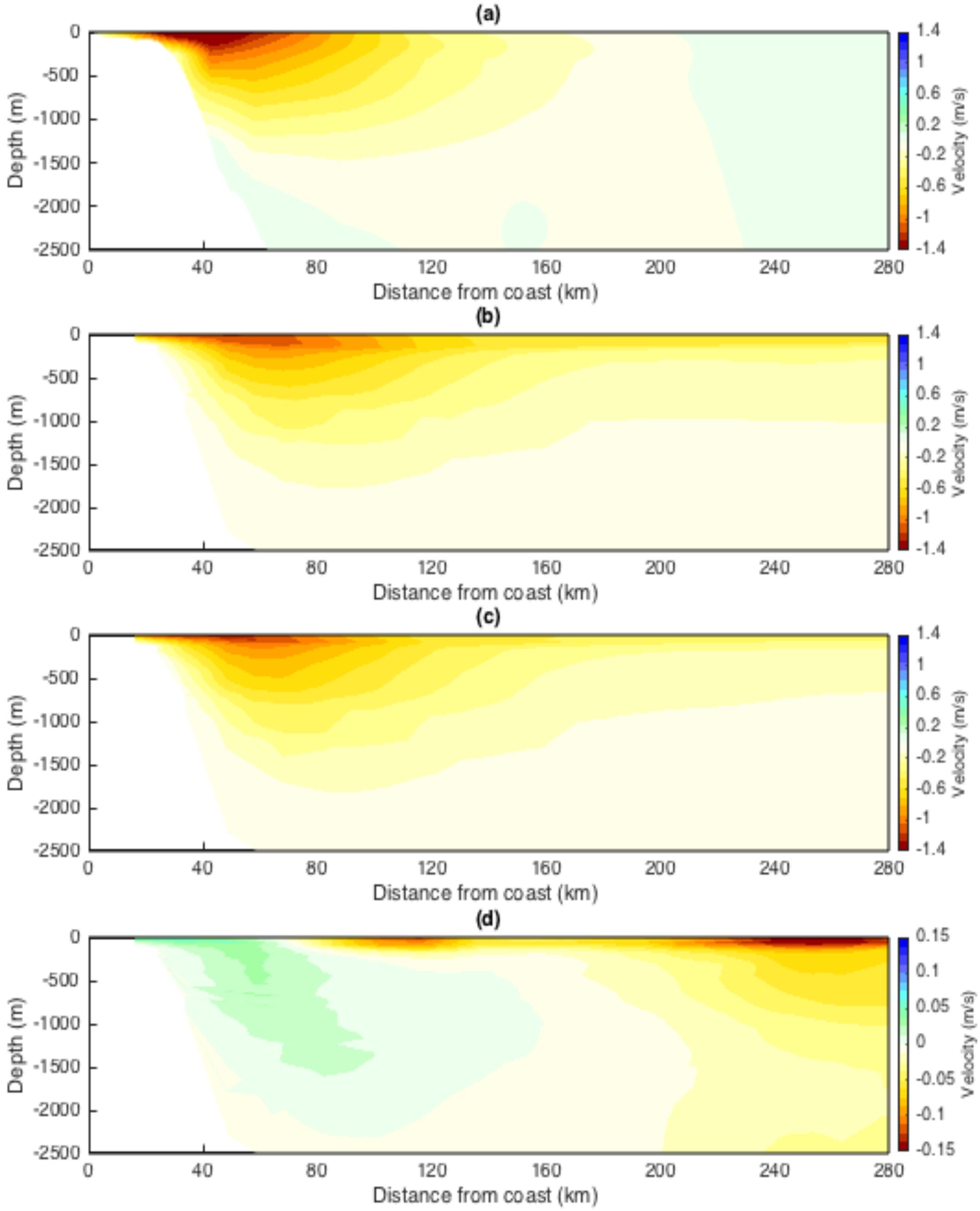

Figure 5.6: Mean Current velocities from April 2010 to February 2013 across the ACT transect ($m.s^{-1}$) of a) the *in-situ* mooring data b) the regional HYCOM simulation forced by absolute winds and c) the regional HYCOM simulation forced by relative winds. d) The differences in mean velocities between ABS and REL.

5.4.2 The evolution of meanders in the Agulhas Current

Tables 5.3 and 5.4 list the properties of meanders at two different locations in the Agulhas Current, one off the coast of Port Edward and another further south in the current at approximately 33.345° S (the position of the ACT array). In all 3 datasets, it is observed that the position of the Agulhas Current core is closer to the coast at the Port Edward location than it is at the ACT location. During the period January 1993 to December 2013, the mean distance of the core from the coast at Port Edward is very similar in AVISO, ABS and REL at Port Edward with mean distances of 52 ± 28 km, 52 ± 42 km and 52 ± 41 km respectively. At the ACT array position, for the same time period, the mean distance of the Agulhas Current core is slightly further offshore, in the model experiments than in AVISO.

As stated earlier, meanders were separated into those which were smaller than 50 km and those which were equal to or greater than 50 km. It was found that the number of meanders smaller than 50 km were far more frequent than those which were larger. Off the coast at Port Edward, the average number of smaller meanders occurring annually is 22% fewer in ABS and 20% fewer in REL compared to AVISO. The mean duration of smaller meanders at Port Edward is 15 ± 11 days in AVISO, and slightly shorter in the models with the duration of REL meanders being more similar to AVISO than ABS. The mean size of the smaller REL meanders is also more similar to AVISO than ABS.

For the larger meanders off the coast of Port Edward, approximately 26% more meanders per year occurred in ABS and 11% more meanders per year occurred in REL compared to the number of larger AVISO meanders. The frequency of large meander occurrences is on average more similar to AVISO in REL than in ABS here during January 1993 to December 2013. There is an improvement in the representation of the duration of meanders from ABS to REL. The lifespan of the larger meanders is almost 2 weeks longer than the smaller meanders in all cases at the Port Edward location. The mean size of these larger meanders is too large in both of the model experiments.

Meander Properties	**AVISO**		**ABS**		**REL**	
Mean distance of core from coast (km)	52±28		52±42		52±41	
Size of meanders (km)	**<50**	**≥50**	**<50**	**≥50**	**<50**	**≥50**
Number of meanders.year^{-1}	6.0	1.9	4.7	2.4	4.8	2.1
Mean meander duration (days)	15±11	29±17	11±7	25±17	13±8	26±21
Mean meander size (km)	22±14	69±13	18±13	110±56	19±13	124±65

Table 5.3: Mean meander properties off the coast of Port Edward for AVISO, ABS and REL data from January 1993 to December 2013.

Offshore of 33.345° S, an average of 6.3 smaller meanders occur annually in AVISO, with 21% fewer meanders occurring in ABS and 6% fewer meanders REL (Table 5.4). The biggest change from the Port Edward Location to 33. 345° S occurred in the REL data with an increase of 1.1 meanders per year at the southern location. The mean duration of these small meanders is 14 ± 11 days for AVISO, 12 ± 7 days in ABS and 15 ± 11 days in REL. These smaller meanders are very similar in size in all 3 data sets.

For the larger category, 1.6 meanders occur here on average each year in AVISO, while there are 13% more meanders in ABS relative to AVISO but 31% fewer meanders in REL (Table 5.4). Similarly to the smaller meanders, the biggest change in frequency of larger meanders occurred in REL with 1 larger meander fewer propagating past the southern location each year compared to the Port Edward location. These larger meanders have a mean duration of 36 ± 20 km in AVISO, 30 ± 25 days in ABS and 31 ± 19 days in REL. The lifespan of larger meanders in the southern location is longer than those at the northern location by 7 weeks in the AVISO data, 5 weeks in ABS and 5 weeks in REL. The mean size of larger meanders occurring in the region of the ACT array between January 1993 and December 2013 is longer in both of the model experiments than in AVISO. This equates to a 28% increase in larger meander size in AVISO, an increase in meander size of 6% in ABS and a decrease in size from Port Edward to the southern location of 6% in REL.

Meander Properties	**AVISO**		**ABS**		**REL**	
Mean distance of core from coast (km)	63±28		74±39		72±32	
Size of meanders (km)	**<50**	**≥50**	**<50**	**≥50**	**<50**	**≥50**
Number of meanders /year	6.3	1.6	5.0	1.8	5.9	1.1
Mean meander duration (days)	14±11	36±21	12±7	30±25	15±11	31±19
Mean meander size (km)	17±14	88±42	16±11	117±52	18±14	115±55

Table 5.4: Mean meander Properties in the region of the ACT array for AVISO, ABS and REL data from January 1993 to December 2013.

Composite averages of anomalies in the circulation during a meander of more than 50 km in size are shown in Figure 5.7. The AVISO data reveal an increase in the mean velocity of the Agulhas Current of up to 0.15 $m.s^{-1}$ during a meander near the ACT transect (Figure 5.7(a)). A similar decrease in velocity is observed immediately offshore of the Agulhas Current, followed by a strong increase in offshore circulation of up to 0.50 $m.s^{-1}$. In the southern part of the Agulhas Current, where the current begins to separate from the shelf, there is a decrease in mean velocity on the inshore edge of the current of approximately 0.10 $m.s^{-1}$.

The ABS composite (Figure 5.7(b)) reveals a broadly similar pattern but weaker magnitude than the AVISO data. There is a small increase in velocities from 0.05 to 0.15 $m.s^{-1}$ in the Agulhas Current. Another difference between the AVISO and ABS anomalies is a decrease of velocities up to 0.10 $m.s^{-1}$ on the inshore edge of the current. The area of decreased velocities in ABS is much larger than in AVISO but the magnitude of the velocity anomalies is similar. There are some regions near the offshore edge of the Agulhas Current where a negative velocity anomaly of 0.05 to 0.15 $m.s^{-1}$ occurs, however this feature does not extend the full length of the Agulhas Current as is the case in the AVISO data. A region of strong anti-cyclonic circulation occurs further offshore with positive velocity anomalies of up to 0.30 $m.s^{-1}$.

In the REL data, there is a positive velocity anomaly in the Agulhas Current of up to 0.10 $m.s^{-1}$ (Figure 5.7c). The region of negative velocity south of the south coast (up to 0.10 $m.s^{-1}$ in magnitude) is smaller in extent than in ABS and more comparable to that seen in the AVISO data. A negative velocity anomaly of up to 0.15 $m.s^{-1}$ is also observed offshore of the northern Agulhas Current. Positive velocity anomalies of up to 0.30$m.s^{-1}$ are observed further offshore in the 31 - 33° S region.

Figure 5.7d indicates the absolute difference in velocity anomalies between ABS and REL. There is a small region in the northern Agulhas Current where REL velocities are stronger than ABS, indicating that REL is more similar to AVISO here than ABS. South of the south coast, on the inshore edge of the Agulhas Current, velocity anomalies have decreased from ABS to REL by approximately 0.05 $m.s^{-1}$. Larger differences, which are both positive and negative, of up to 0.30 $m.s^{-1}$ are observed between ABS and REL in the region offshore of the Agulhas Current where all data sets show strong eddy activity.

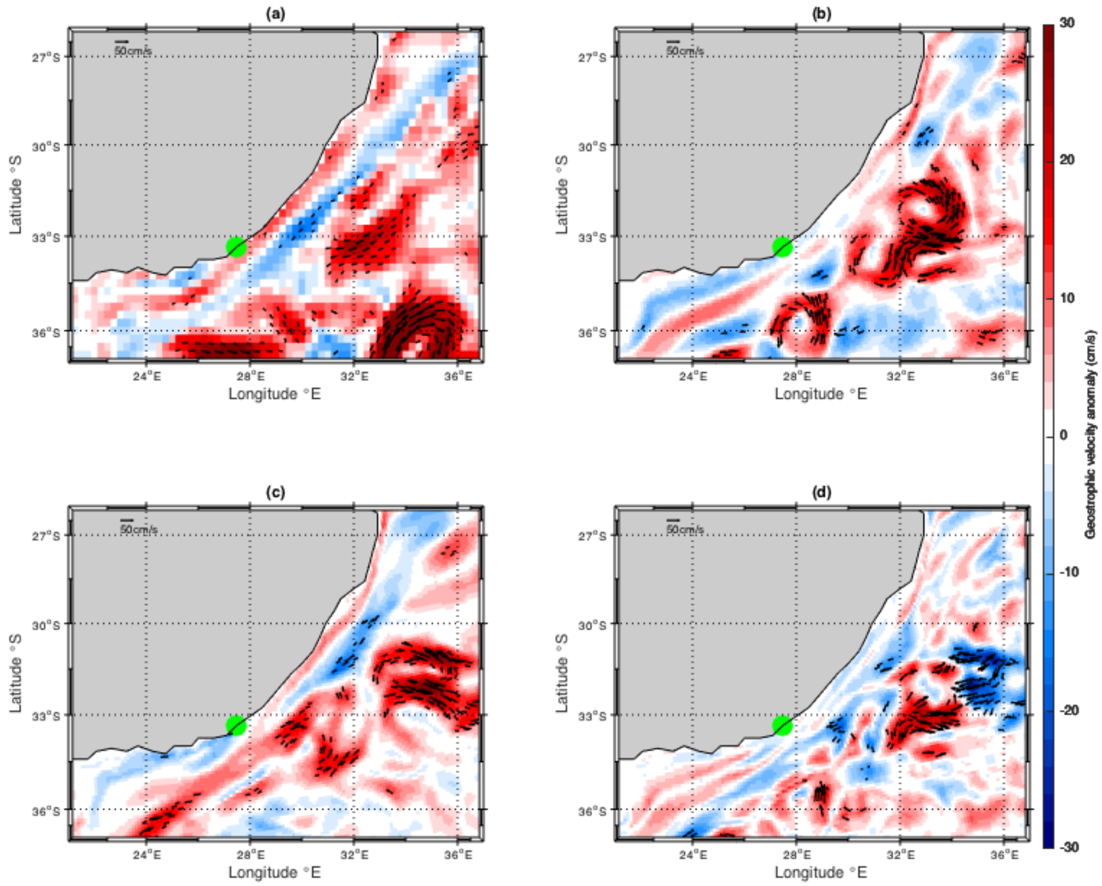

Figure 5.7: Composite plots of Agulhas Current velocity anomalies (cm.s^{-1}) during meanders greater than or equal to 50 km in size offshore of 33.345° S (the green circle) between January 1993 and December 2013 for a) AVISO, b) ABS, c) REL and d) the difference in velocity anomalies between ABS and REL. Vectors indicate regions where direction of flow for velocities greater than 10 cm.s^{-1}.

5.5 Discussion

Principal Component Analysis was used to investigate mean variance within the Agulhas Current at three different ADCP locations offshore of Cape Morgan, Fish River and East London (Figure 5.5). It was found that the GlobCurrent data best captured the variance within the Agulhas Current which is shown by the ADCP data. Although REL can be considered to perform slightly better than ABS at the Fish River location, neither of the unassimilated HYCOM simulations capture the variance at the three locations particularly well. It was expected that HYCOM, which has a higher spatial resolution, would have captured more of the variability and thus would have had a larger ellipse. Further investigation revealed that the locations of the ADCP sites appear to be inshore of the Agulhas Current in both HYCOM simulations (the position of the Agulhas Current is shown by the shading in Figure 5.5), explaining why the variance values are lower than one would expect.

Both ABS and REL do however adequately capture the lateral variability of the current at the East London ADCP location. Overall, the GlobCurrent data is more representative of the variability observed within the Agulhas Current than either of the HYCOM simulations (Figure 5.5). The GlobCurrent data however also fails to capture some of the variability within the current at these 3 locations. This is expected as the ADCP locations are within 50 km of the coast where altimetry data is sparse and is less accurate than at a greater depth. The change in wind forcing from absolute to relative winds does not appear to significantly impact the amount of variability in the Agulhas Current simulated by the regional HYCOM. This indicates that HYCOM does not capture processes in these shallower shelf regions well, with the ability of the model to simulate cross-self processes only improving very slightly from ABS to REL. The amplitude of the current is also too small in both HYCOM simulations. In Krug et al. (2014) the main impact caused by meanders is actually seen in deeper waters than those sampled by the ADCPs used here. This study, and other research in the Agulhas Current would benefit from more observations of the Agulhas Current.

The mean Agulhas Current velocities in ABS and REL are weaker than mean velocities from the ACT mooring array (Figure 5.6). Figure 5.6d indicates that when the forcing is changed from absolute to relative winds, the Agulhas Current is deeper and more intense. There is an increase in Agulhas Current core velocities of up to 0.06 $m.s^{-1}$ and a decrease in the mean velocity of the offshore flow of up to 0.16 $m.s^{-1}$. Whist values are still far from those given by the ACT array, there is an improvement in the vertical structure of the Agulhas Current, particularly offshore of the mean structure of the current. In Chapter 4, an increase in Mean Kinetic Energy was observed in the core of the Agulhas Current with the change in wind forcing from ABS to REL. The Agulhas Current is narrower and stronger due in REL to a decrease in the number of eddies occurring on the offshore edge of the Agulhas Current. The results presented in this chapter are consistent with this increase and suggest that the change in wind forcing from ABS to REL has improved the simulation of Agulhas Current velocities relative to the *in-situ* ACT data.

Furthermore, the REL case shows an improvement in the representation of meanders compared to ABS when their properties of meanders were evaluated at two different locations in the Agulhas Current, one off the coast Port Edward and another further south in the current at approximately 33.345° S (the position of the ACT array) (Tables 5.3 and 5.4). The meander properties were evaluated for two categories; those smaller than 50 km in size and those larger than this scale. However, changing this criterion to 40 km or to 60 km did not affect the results. In REL, the frequency of smaller meander occurrences as well as their duration is more similar to AVISO than the ABS data at both locations. However, it is important to note that in this instance the AVISO data is not necessarily produce the most accurate results as the effective spatial resolution of the altimetry product is not sufficient to image smaller meanders. Typically the lifespan of a small REL meander is longer than that of a small ABS meander. The size of the smaller meanders did not however vary much from ABS to REL. The change in wind forcing in the regional HYCOM from absolute to relative winds has improved the simulation of the duration of smaller meanders in the Agulhas Current.

It was found that smaller meanders were more numerous than those that were equal to or greater than 50 km. A small increase of 0.33 - 0.90 smaller meanders per annum occurred from the Port Edward location to the ACT array location whilst a decrease in larger meanders of 0.33 - 0.91 meanders occurred. Larger meanders, characteristic of Natal Pulses occurred at a frequency of 1.90 meanders per year in AVISO, 2.38 meanders per year in ABS and 2.05 meanders per year in REL off the coast of Port Edward. Further south slightly fewer meanders occur annually, with 1.57 meanders per year occurred in AVISO, 1.81 meanders per year occurred per year in ABS and 1.14 meanders per year occurring in REL. This result is consistent with Rouault and Penven (2011) which suggests that the number of meanders which occur off Port Edward is greater than the number of meanders which occur further downstream in the Agulhas Current at Port Elizabeth (with 11 meanders occurring off the coast of Port Edward and 9 occurring meanders off the coast of Port Elizabeth between June 2004 and December 2010). The results presented here indicate that some of the larger meanders have dissipated before they reach the ACT transect. The simulation of number of larger meanders significantly improves from ABS to REL at the northern location. This is coherent with results from Chapter 4 of this thesis which shows an improvement in the simulation of the EKE in the region. However, too much energy is lost southwards by the time the meanders reach the region of the ACT array as the REL experiment underestimates the number of larger meanders compared to the observations. There is a decrease of 16% in the number of larger meanders observed from the northern location to the southern location in AVISO, a 25% decrease in ABS and a very large decrease of 45% in the number of large meanders observed in REL. The decrease in REL is too large. Perhaps this is partially due to the 34% reduction in barotropic energy conversion over the domain which was observed in chapter 4 of this thesis. As discussed in Chapter 4, a dampening coefficient used by Renault et al. (2017) was not applied to the wind forcing in the REL simulation due to the improvement in the representation of EKE in the over the domain. Had it been applied, it is likely that the decrease in the frequency of large Agulhas Current meanders from ABS to REL would have been less and thus more similar to the frequency of meanders captured in AVISO and the study by Krug et al. (2014).

This study also suggests that the duration of meanders and their size increases from Port Edward to the ACT array location. The sizes of meanders observed in ABS and REL are consistent with previous studies where the maximum size of a meander is approximately 115 km (Krug et al., 2014).

The AVISO data reveal an increase in the mean velocity of the Agulhas Current of up to 0.15 $m.s^{-1}$ for those meanders at least 50 km in size (Figure 5.7). Whilst an increase of up to 0.15 $m.s^{-1}$ is also observed in ABS, the area of this increase is smaller than in AVISO. A positive velocity anomaly of up to 0.10 $m.s^{-1}$ is also observed in REL. All 3 data sets indicate a negative velocity anomaly offshore of the northern Agulhas Current and a strong eddy presence, usually anti-cyclonic, offshore of the Agulhas Current during meandering events. There is a small region in the northern Agulhas Current where REL velocities are stronger than ABS, indicating that REL is more similar to AVISO in this region of the Agulhas Current than is ABS.

5.6 Conclusion

The change in wind forcing from absolute to relative winds in the regional HYCOM has not had a very large impact on the variability simulated within the Agulhas Current. The representation of mean velocities of the Agulhas Current across the ACT transect has however improved from the simulation forced with absolute winds to the simulation forced with relative winds, whereby the mean velocity of the Agulhas Current core has increased and offshore velocities have decreased. The representation of variability captured in both HYCOM simulations is very similar, indicating that changes in mesoscale meanders from ABS to REL is likely very small in the model.

The representation of small meanders (under 50 km in size) has improved from ABS to REL. The frequency of small meanders and their duration is more similar to AVISO in REL than in ABS. Whilst the change in wind forcing has resulted in a necessary decrease in the frequency of large meanders (greater than or equal to 50 km) from ABS to REL, the decrease is too large. It is possible that if the dampening coefficient described by Renault et al. (2017) had been applied, the change would have been smaller and that the frequency of large, Natal Pulse type meanders in the Agulhas Current would be more accurate. There is however a decrease in the frequency of meanders, over 50 km in size, observed from the location offshore of Port Edward to the region of the ACT array in all three datasets, indicating that some of the meanders have dissipated before reaching the ACT array.

CHAPTER 6.

SYNTHESIS

6.1 Key Findings

The main findings from the 3 results chapters (Chapter 3, Chapter 4, Chapter 5) of this thesis are summarized below.

6.1.1 Chapter 3

- Both cyclonic and anti-cyclonic source region eddies dissipate upon approaching the Agulhas Current.

- The entrainment of eddies into the Agulhas Current at 30° S affects the current's mean velocity, with anti-cyclonic eddies consistently increasing the Agulhas Current velocity and cyclonic eddies decreasing its velocity.

- Both anti-cyclonic and cyclonic eddies arriving at the Agulhas Current cause the current to meander, with anti-cyclonic eddies causing the current to meander from its mean position of 69 km to a mean 100 ± 79 km offshore and cyclonic eddies shifting the current to a mean of 145 ± 85 km offshore.

- The positive (negative) velocity anomaly associated with anti-cyclonic (cyclonic) eddies is visible for an average of 3 weeks (15 weeks) in the Agulhas Current.

6.1.2 Chapter 4

- Changing the wind forcing from absolute to relative winds in the regional HYCOM decreases the overall wind stress of the Agulhas Current domain by up to 0.01 $N.m^{-2}$ in regions with strong opposed surface currents.

- There is 33% reduction in EKE over the Agulhas Current domain from the simulation forced with absolute winds (ABS) to the simulation forced with relative winds (REL).

- Residual EKE of the simulations is a factor of 2.5 times larger than the energy within the eddies, suggesting that meanders and other forms of variability have a much larger influence on the overall EKE than the eddies tracked by the eddy tracking algorithm

- There are fewer westward propagating anti-cyclonic eddies occurring in the region of elevated EKE south of Madagascar in REL than in ABS. There are also fewer eddies propagating along the offshore edge of the Agulhas Current in REL and this suggests that current feedback in the regional HYCOM reduces the bias of eddies propagating all the way through the Agulhas Current.

- There is a mean reduction in eddy lifespans, radii, amplitudes and circum-averaged speeds from ABS to REL. The change in wind forcing has resulted in a more accurate simulation of anti-cyclonic eddies in the regional HYCOM, but it has made cyclonic eddies which were already under-sized even smaller.

- The reduction in barotropic and baroclinic energy conversion observed over the Agulhas Current domain from ABS to REL is larger in the regional HYCOM than in previous studies. This is likely due to the over representation of large mesoscale eddies propagating along the offshore edge of the Agulhas Current in the regional HYCOM, which has been significantly reduced with the change in wind forcing.

6.1.3 Chapter 5

- In the regional HYCOM, the change in wind forcing from absolute to relative winds has not had a very large impact on the variability simulated within the Agulhas Current. The representation of variability captured in both HYCOM simulations is very similar, indicating that changes in mesoscale meanders from ABS to REL is very small. The variability in both model experiments is underestimated compared to the observations.

- The representation of mean velocities of the Agulhas Current across the ACT transect has however improved from the simulation forced with absolute winds to the simulation forced with relative winds.

- The representation of small meanders (under 50 km in size) has improved from ABS to REL with their frequency, their duration and their size more similar to AVISO.

- Whilst the change in wind forcing has resulted in a necessary decrease in the frequency of large meanders (greater than or equal to 50 km) from ABS to REL, the decrease is too large.

- There is however a decrease in the frequency of meanders, over 50 km in size, observed from the location offshore of Port Edward to the region of the ACT array in all three datasets, indicating that some of the meanders have dissipated before reaching the ACT array.

6.2 Summary

Analysing eddy characteristics from a global data set of automatically tracked eddies for the Agulhas Current in combination with surface drifters as well as geostrophic currents from satellite altimeters, it is shown that eddies from the Mozambique

Channel and south of Madagascar dissipate as they approach the Agulhas Current. By tracking the offshore position of the current core and its velocity at 30° S in relation to eddies, it is demonstrated that eddy dissipation occurs through a transfer of momentum, where anti-cyclones consistently induce positive velocity anomalies in the Agulhas Current, and cyclones reduce the velocities and cause offshore meanders. Composite analyses of the anti-cyclonic (cyclonic) eddy-current interaction events demonstrate that the positive (negative) velocity anomalies propagate downstream in the Agulhas Current at 44 $km.d^{-1}$ (23 $km.d^{-1}$). In this study, a regional HYCOM model is used to investigate the ability of a numerical model to resolve meanders and mesoscale variability in the Agulhas Current. It was found that a change in wind forcing, reduced the frequency of meander occurrences in the model and that in particular meanders smaller than 50km in size were more representative of meanders seen in the satellite data.

Many numerical models are unable to represent the observed eddy dissipation processes described above (Backeberg et al., 2014; Durgadoo et al., 2013; Loveday et al., 2014). In these models, eddies propagate from the source regions to the Agulhas retroflection as a train of successive eddies. Consequently, this may affect our understanding of the Agulhas Current system. Analysing two simulation experiments in HYCOM, one forced with absolute winds and the other forced with relative winds, the response of the model to current feedback was investigated. The results of this study suggest that the “mechanical dampening” process observed in coupled ocean-atmosphere models by Duhaut and Straub, 2006; Dawe and Thompson, 2006; Eden and Dietze, 2009; Renault et al., 2016a; Renault et al., 2016b and Renault et al., 2017 can also be caused by changing the wind forcing in the regional ocean only HYCOM model from absolute to relative winds.

Changing the wind forcing in the regional HYCOM has resulted in a reduction in wind stress from ABS to REL, particularly in the Mozambique Channel, south of Madagascar and the Agulhas Current and a 33% reduction in EKE in the regional HYCOM. A previous study by Renault et al. (2017) demonstrated a 25% reduction in energy of the Agulhas Current system. Results from REL are more representative of the EKE observed in the satellite product, AVISO compared to ABS. The MKE from ABS to REL is also significantly reduced, with the exception of an increase in MKE in the core of the Agulhas Current as well as the SEMC. Backeberg et al. (2008) shows that the velocities of the Agulhas Current in the HYCOM simulation are weaker than observed in the satellite product and the increase in the MKE from ABS to REL, whilst still too weak, indicates that the change in wind forcing has improved the representation of the Agulhas Current. The representation of mean velocities of the Agulhas Current across the ACT transect has improved from the simulation forced with absolute winds to the simulation forced with relative winds. The mean velocity of the Agulhas Current has increased, offshore velocities have decreased and the vertical extent of the current has increased from ABS to REL. The pattern of the EKE and MKE reductions from ABS to REL is strongly reflective of those seen in the wind stress, indicating the influence of the wind stress on the energy of the Agulhas Current system. It is acknowledged that Backeberg et al. (2009) demonstrated a significant improvement in the representation of the Agulhas Current using a fourth order momentum advection scheme and that changing the wind forcing of the regional model is not the only way to improve the regional HYCOM model. However, the fourth order advection scheme was not avialable for this study and it has been shown that the second order momentum scheme improved the representation of the mean circulation of version 2.2 of HYCOM Backeberg et al. (2014). Future studies would benefit from experiments using both the fourth order advection scheme and the change in wind forcing.

There is a reduction in energy within the eddies from ABS to REL in the Mozambique Channel, south of Madagascar and in the Agulhas Current of approximately 100 − 400 $cm^2.s^{-2}$. The difference in residual EKE between ABS and REL is approximately 2.5 times more than that of the difference in energy within the eddies. This suggests that the contribution of mesoscale eddies to the overall EKE is not as important as other forms of variability in the Agulhas Current system.

There are fewer westward propagating eddies in the region south of Madagascar in REL compared to ABS. One possible reason for this is the reduction in MKE south of

Madagascar, and thus a weaker SEMC which responsible for the formation of anti-cyclonic eddies in the region (de Ruijter et al., 2004; Halo, 2008; Siedler et al., 2009; Ridderinkhof et al., 2013; Halo et al., 2014b). This thesis also shows that there are fewer eddies propagating along the offshore edge of the Agulhas Current in REL compared to ABS. Results from this thesis suggest the simulation of the dissipation process of source region eddies improved by changing the wind forcing in the regional HYCOM.

In addition to this, an investigation into the eddy properties indicates that a change in wind forcing in the regional HYCOM has a significant dampening effect on the eddies. There is a reduction in eddy amplitudes, radii and circum-averaged speeds from ABS to REL as well as a decrease in anti-cyclonic eddy life-spans. Additionaly, there are significantly more eddies tracked in ABS than REL, which could suggest that eddy formation is linked with increased energy imparted on the ocean currents in HYCOM in the absolute winds simulation.

The barotropic and baroclinic energy conversion terms reveal a large reduction in energy from ABS to REL of 34.10% for the barotopic energy conversion term and 43.52% for the baroclinic energy conversion term. The effect here of the change in wind forcing in the regional HYCOM is much larger than in a previous study by Renault et al. (2017) which used a coupled ocean-atmosphere model. Because of the improvement in the representation of EKE in the regional HYCOM, the dampening coefficient (of approximately 0.7) used by Renault et al. (2017) was not applied to the change in wind forcing in the regional HYCOM. Had the dampening coefficient been applied, it is very likely that the resulting difference in EKE, eddy properties and the energy conversion terms between the two experiments would have been smaller. The results of the change in wind forcing in the regional HYCOM, without the dampening coefficient, were found to reduce EKE and be more agreeable to that of the AVISO EKE. As suggested by Renault et al. (2016a; 2017), a future study which includes the Indian Ocean Gyre into the model domain could further reduce the EKE and generation of Natal Pulses in the region.

The change in wind forcing from absolute to relative winds has improved the simulation of small meanders (less than 50 km in size) in the regional HYCOM. Whilst the change in wind forcing has resulted in a necessary decrease in the frequency of large meanders (greater than or equal to 50 km) from ABS to REL, the decrease is too large. If the dampening coefficient described by Renault et al. (2017) had been applied, it is likely that the change would have been smaller and that the frequency of larger, Natal Pulse type meanders in the Agulhas Current would be more accurate. The decrease in the frequency of larger meanders from the Port Edward to the ACT location in both HYCOM simulations as well as the satellite suggests that some meanders dissipated before reaching the southern location.

Whilst the inclusion of relative wind forcing in the regional HYCOM has greatly improved the simulation in many aspects, there are a few instances the dampening effect has been too large. For example, the sizes of cyclonic eddies which were already too small have become even smaller in the simulation forced with relative winds. An investigation into the effects of applying the dampening coefficient described by Renault et al. (2017) in the regional HYCOM could help to further improve the simulation. As suggested by Renault et al. (2017) future studies could also benefit from the inclusion of the entire Indian Ocean Gyre into the model domain. The EKE values in the regional HYCOM, although significantly improved, are still too large in some parts of the Agulhas Current System. It is likely that this would further reduce the wind work on the ocean, the mean circulation speed and the EKE over the Agulhas Current region. A multi-model comparison would also bring more robustness to this study. Whilst, HYCOM is often used in a data assimilative framework where it would be more difficult to apply a coupled model, it would also be interesting to investigate whether the results of this study are consistent with a coupled HYCOM model. Much of this study has been focused on the northern Agulhas Current, where the current is very stable. The effects of the change in wind forcing on the southern extent of the Agulhas Current, its retroflection and the Agulhas Leakage have yet to be investigated in the regional HYCOM.

REFERENCES

Abel, R., C. W. Böning, R. J. Greatbatch, H. T. Hewitt, and M. J. Roberts (2017), Feedback of mesoscale ocean currents on atmospheric winds in high-resolution coupled models and implications for the forcing of ocean-only models, *Ocean Science Discussions*, 1–22, doi:10.5194/os-2017-24 .

Azevedo, J. L. L. D., L. R. D Oliveira, J. F. A. D Souza, I. D. Soares, and M. M. Mata, (2008), Os processos de conversão de energia nos oceanos: uma revisão do Diagrama de Lorenz, *Revista Brasileira de Geofisica*, 26(2), 153–172.

Backeberg, B. C., J. A. Johannessen, L. Bertino, and C. J. Reason (2008), The greater Agulhas Current system: An integrated study of its mesoscale variability, *Journal of Operational Oceanogr*aphy, 1(1), 29–44.

Backeberg, B. C., L. Bertino, and J. A. Johannessen, (2009), Evaluating two numerical advection schemes in HYCOM for eddy-resolving modelling of the Agulhas Current, *Ocean Science,* 5(2), 173–190.

Backeberg, B. C., and C. J. Reason (2010), A connection between the South Equatorial Current north of Madagascar and Mozambique Channel eddies, *Geophysical Research Lett*ers, 37(4), L04604, doi:10.1029/2009GL041950.

Backeberg, B. C., F. Counillon, J. A Johannessen, and M. -I. Pujol (2014), Assimilating along-track SLA data using the EnOI in eddy resolving model of the Agulhas system, *Ocean Dyn*amics, 65, 1121–1136, doi:10.1007/s10236-014-0717-6.

Barnier, B., G. Madec, T.Penduff, J. –M. Molines, A. -M. Treguier, J. Le Sommer, A. Beckmann, , A. Biastoch, C. Böning, and J. Dengg (2006), Impact of partial steps and momentum advection schemes in a global ocean circulation model at eddy-permitting resolution, *Ocean Dynamics*, 56(5-6), 543–567.

Beal, L. M., W. P. de Ruijter, A. Biastoch, and R. Zahn (2011), On the role of the Agulhas system in ocean circulation and climate, *Nature*, 472(7344), 429–436.

Beal, L. M., S. Elipot, A. Houk, and G. M. Leber (2015), Capturing the transport variability of a Western Boundary Jet: Results from the Agulhas Current Time-series experiment (ACT), *Journal of Physical Oceanography*, 45(5), 1302–1324.

Bentsen, M., G. Evensen, H. Drange, and A. D. Jenkins (1999), Coordinate transformation on a sphere using conformal mapping, *Monthly Weather Review*, 127(12), 2733–2740.

Biastoch, A. and W. Krauss (1999), The role of mesoscale eddies in the source regions of the Agulhas Current, *Journal of Physical Oceanography,* 29, 2303-2317.

Biastoch, A., J. R. E. Lutjeharms, C. W. Boning, and M. Scheinert (2008), Mesoscale perturbations control inter-ocean exchange south of Africa, *Geophysical Research Letters*, 35, L20602, doi:10.1029/2008GL035132.

Bleck, R. (2002), An oceanic general circulation model framed in hybrid isopycnic-Cartesian coordinates, *Ocean Modelling*, 37:55–88.

Bouffard, J., A. Pascual, S. Ruiz, and Y. Faugere (2010), Coastal and mesoscale dynamics characterization using altimetry and gliders: A case study in the Balearic Sea, *Journal of Geophysical Research*, 115, C10029, doi:10.1029/2009JC006087.

Braby, L., B. C. Backeberg, I. Ansorge, M. J. Roberts, M. Krug, and C. J. C. Reason (2016), Observed eddy dissipation in the Agulhas Current, *Geophysical Research Letters*, 43, 8143–8150, doi:10.1002/2016GL069480.

Browning, G. L. and H. O. Kreiss (1982), Initialization of the shallow water equations with open boundaries by the bounded derivative method, *Tellus*, 34:334–351.

Browning, G. L. and H. O. Kreiss (1986), Scaling and computation of smooth atmospheric motions, *Tellus*, 38:295–313.

Bryden, H. L., L. M. Beal, and L. M. Duncan (2005), Structure and Transport of the Agulhas Current and Its Temporal Variability, *Journal of Oceanography*, 61:479–492.

Chelton, D. B., R. A. deSzoeke, M. G. Schlax, K. E. Naggar, and N. Siwertz (1998), Geographical variability of the first-baroclinic Rossby radius of deformation, *Journal of Physical Oceanography*. 28, 433–460.

Chelton, D. B., M. G. Schlax, M. H. Freilich, and R. F. Milliff (2004), Satellite measurements reveal persistent small-scale features in ocean winds, *Science*, 303(5660), 978–983.

Chelton, D. B., M. G. Schlax, and R. M. Samelson (2007), Summertime coupling between sea surface temperature and wind stress in the California Current System, *Journal of Physical Oceanography*, 37(3), 495–517.

Chelton, D. B., M. G. Schlax, and R. M. Samelson (2011), Global observations of non-linear mesoscale eddies, *Progress in Oceanography*, 91, 167–216.

Chen, H., E. K. Schneider, and Z. Wu (2016) Mechanisms of internally generated decadal- to- multidecadal variability of SST in the Atlantic Ocean in a coupled GCM, *Climate Dynamics*, 46(5-6), 1517–1546.

Colas, F., J. C. McWilliams, X. Capet, and J. Kurian (2012). Heat balance and eddies in the Peru-Chile current system, *Climate dynamics*, *39*(1-2), 509-529.

Collins, C., J. C. Hermes, and C. J. C. Reason (2014), Mesoscale activity in the Comoros Basin from satellite altimetry and a high resolution ocean circulation model, *Journal of Geosphysical Research: Oce*ans, 119, 4570–4760, doi:10.1002/2014JC010008.

Cornillon, P., and K. Park (2001), Warm core ring velocities inferred from NSCAT, *Geophysical Research Letters*, 28(4), 575–578.

Cronin, M., and D. R. Watts (1996), Eddy–mean flow interaction in the Gulf Stream at 68 W. Part I: Eddy energetics, *Journal of Physical Oceanography*, *26*(10), 2107-2131.

Danielson, R. E., J. A. Johannessen, G. D. Quartly, M. H. Rio, B. Chapron, F. Collard, and C. Donlon (2018). Exploitation of error correlation in a large analysis validation: GlobCurrent case study, *Remote Sensing of Environment*, *217*, 476-490.

Davies, H. C. (1983), Limitations of some common lateral boundary schemes used in NWP models, *Monthly Weather Review*, 111:1002–1012.

Dawe, J. T., and L. Thompson, (2006), Effect of ocean surface currents on wind stress, heat flux, and wind power input to the ocean, Geophysical Research Letters, 33(9), L09604.

Dee, D. P., S. M. Muppala, A. J. Simmons, P. Berrisford, P. Poli, S. Kobayashi, U. Andrae, M. A. Balmaseda, G. Balsamo, P. Bauer, and P. Bechtold (2011), The ERA-Interim reanalysis: configuration and performance of the data assimilation system, *Quarterly Journal of the Royal Meteorological Society*, 137, 553–597.

de Ruijter, W. P. M., P. J. van Leeuwen, and J. R. E. Lutjeharms (1999), Generation and evolution of natal pulses: Solitary meanders in the Agulhas Current, *Journal of Physical Oceanography*, 29, 3043–3055.

de Ruijter, W. P. M., H. Ridderinkhof, J. R. E. Lutjeharms, M. W. Schouten & C. Veth (2002), Observations of the flow in the Mozambique Channel, *Geophysical Research Letters*, 29(10), 140-1−140-3.

de Ruijter, W. P. M., H. M. van Aken, E. J. Beier, J. R. E. Lutjeharms, R. P. Matano, and M. W. Schouten (2004), Eddies and dipoles around South Madagascar: Formation, pathways and large-scale impact, *Deep-Sea Research*, 51, 383–400.

de Vos, M. (2016), The impact of assimilating along-track SLA data on simulated eddy characteristics in the Agulhas System. *M.Sc. Thesis, University of Cape Town.*

de Vos, M., B. Backeberg, and F. Counillon (2018), Using an eddy-tracking algorithm to understand the impact of assimilating altimetry data on the eddy characteristics of the Agulhas system, *Ocean Dynamics*, 68, 1071–1091, https://doi.org/10.1007/s10236-018-1174-4.

Dewar, W. K., and G. R. Flierl (1987), Some effects of the wind on rings, *Journal of Physical Oceanography*, 17(10), 1653–1667.

Drange, H., and K. Simonsen (1996), Formulation of air-sea fluxes in the ESOP2 version of MICOM, *Nansen Environmental and Remote Sensing Center*.

Duhaut, T. H., and D. N. Straub (2006), Wind stress dependence on ocean surface velocity: Implications for mechanical energy input to ocean circulation, *Journal of Physical Oceanography*, 36(2), 202–211.

Durgadoo, J., B. Loveday, C. Reason, P. Penven, and A. Biastoch (2013), Agulhas leakage predominantly responds to the Southern Hemisphere westerlies, *Journal of Physical Oceanography,* 43(10), 2113–2131, doi:10.1175/JPO-D-13-047.1.

Eden, C., and H. Dietze (2009), Effects of mesoscale eddy/wind interactions on biological new production and eddy kinetic energy, *Journal of Geophysical Research: Oceans*, 114(C5), C05023.

Elipot, S., and L. M. Beal (2015), Characteristics, energetics, and origins of agulhas current meanders and their limited influence on ring shedding, *Journal of Physical*

Oceanography, 45(9), 2294–2314.

Escudier, R., L. Renault, A. Pascual, P. Brasseur, D. Chelton and J. Beuvier (2016), Eddy properties in the Western Mediterranean Sea from satellite altimetry and a numerical simulation, *Journal of Geophysical Research: Oceans*, *121*(6), 3990-4006.

Gaube, P., D. B. Chelton, R. M. Samelson, M. G. Schlax, and L. W. O'Neill, (2015), Satellite observations of mesoscale eddy-induced Ekman pumping. *Journal of Physical Oceanography*, 45(1), 104–132.

George, M. S., L. Bertino, O. M. Johannessen, A. Samuelsen (2010), Validation of a Hybrid Coordinate Ocean Model for the Indian Ocean, *Journal of Operational Oceanography*, 3, 25–38.

Gordon A. L., K. –I. Horai, and M. Donn (1983), Southern hemisphere western boundary current variability revealed by GEOS 3 altimeter, *Journal of Geophysical Research*, 88, 755-762.

Gordon, A. L. (1986), Inter-ocean exchange of thermocline water, *Journal of Geophysical Research: Oceans*, 91, 5037–5046.

Gordon, A. L., K. T. Bosley, and F. Aikman (1995), Tropical Atlantic water within the Benguela upwelling system at 27S, *Deep Sea Research Part I: Oceanographic Research Papers*, *42*(1), 1-12.

Griffies, S. M., F. O. Bryan, E. P. Chassignet, R. Gerdes, H. Hasumi, and D. Webb (2000). Developments in ocean climate modelling, *Ocean Modelling, 2*(3), 123-192.

Grundlingh, M. L. (1980), On the volume transport of the Agulhas Current, *Deep-Sea Research*, 27, 557–563.

Gründlingh, M. L. (1983), On the course of the Agulhas Current. *South African*

Geographical Journal, 65:49–57.

Gründlingh, M. L. (1985). Features of the circulation in the Mozambique Basin in 1981, *Journal of Marine Research*, *43*(4), 779-792.

Halo, I. F. M. (2008), Influence of the Madagascar Ridge on the flow to the south of Madagascar and the Mozambique Channel, *M.Sc. Thesis,* University of Cape Town.

Halo, I., B. Backeberg, P. Penven, I. Ansorge, C. Reason, and J. Ullgren (2014a), Eddy properties in the Mozambique Channel: A comparison between observations and two numerical ocean circulation models, *Deep Sea Research*, Part II, 100, 38–53, doi:10.1016/j.dsr2.10.015.

Halo, I., P. Penven, B. Backeberg, I. Ansorge, and F. Shillington (2014b), Mesoscale eddy variability in the southern extension of the East Madagascar Current: Seasonal cycle, energy conversion terms, and eddy mean properties, *Journal of Geophysical Research: Oceans,* 119, 7324–7356, doi:10.1002/2014JC009820.

Hancke, L., M. J. Roberts, and J. F. Ternon (2014), Surface drifter trajectories highlight flow pathways in the Mozambique Channel, *Deep Sea Research Part II: Topical Studies in Oceanography*, *100*, 27-37.

Harlander, U., H. Ridderinkhof, M. W. Schouten, and W. P. M. de Ruijter (2009), Long-term observations of transport, eddies, and Rossby waves in the Mozambique Channel, *Journal of Geophysical Research*, 114, C02003, doi:10.1029/2008JC004846.

Hughes, C. W., and C. Wilson (2008), Wind work on the geostrophic ocean circulation: An observational study of the effect of small scales in the wind stress, *Journal of Geophysical Research: Oceans*, (1978–2012), 113(C2).

Hutchings, L., L. E. Beckley, M. H. Griths, M. J. Roberts, S. Sundby, and C. van der Lingen (2002), Spawning on the edge : spawning grounds and nursery areas around the southern African coastline, *Marine Freshwater Research*, 53 (1996), 307–318, doi:10.1071/MF01147.

Isern-Fontanet, J., E. Garcia-Ladona, and J. Font (2003), Identification of marine eddies from altimetric maps, *Journal of Atmospheric and Oceanic Technology*, 20, 772–778.

Isern-Fontanet, J. E., J. Font, E. Garcia-Ladona, M. Emelianov, C. Millot, and I. Taupier- Letage (2004), Spatial structure of anticyclonic eddies in the Algerian basin (Mediterranean Sea) analyzed using the Okubo–Weiss parameter, *Deep-Sea Research*, 51, 3009–3028.

Isern-Fontanet, J., E. Garcia-Ladona, and J. Font (2006a), Vortices of the Mediterranean Sea: an altimetric perspective, *Journal of Physical Oceanography,* 36, 87–103.

Isern-Fontanet, J., E. Garcia-Ladona, J. Font, and A. Garcia-Olivares (2006b), Non-Gaussian velocity probability density functions: an altimetric perspective of the Mediterranean Sea, *Journal of Physical Oceanography,* 36, 2153–2164.

Jackett, D. R., and T.J Mcdougall (1995), Minimal adjustment of hydrographic profiles to achieve static stability, *Journal of Atmospheric and Oceanic Technology*, *12*(2), 381-389.

Jackson, J. M., L. Rainville, M. J. Roberts, C. D. McQuaid, and J. R. Lutjeharms (2012), Mesoscale bio-physical interactions between the Agulhas Current and the Agulhas Bank, South Africa, *Continental Shelf Research*, 49, 10–24.

Jury, M. R., H. R. Valentine, and J. R. E. Lutjeharms (1993), Influence of the Agulhas Current on summer rainfall along the southeast coast of South Africa, *Journal of Applied Meteorology*, 32(7), 1282-1287.

Kara, A. B., P. A. Rochford, and H. E.Hurlburt (2000), Efficient and accurate bulk parameterizations of air-sea fluxes for use in general circulation models, *Journal of Atmospheric and Oceanic Technology*, 17, 1421–1438.

Kelly, K. A., S. Dickinson, M. J. McPhaden, G. C. Johnson (2001). Ocean currents evident in satellite wind data. *Geophysical Research Letters*, *28*(12), 2469-2472.

Kundu, P. K. (1990), Fluid Mechanics, *Academic*, San Diego, California, 1, 638.

Krug, M., and J. Tournadre (2012), Satellite observations of an annual cycle in the Agulhas Current, *Geophysical Research Letters*, 39(15).

Krug, M., J. Tournadre, and F. Dufois (2014), Interactions between the Agulhas Current and the eastern margin of the Agulhas Bank, *Continental Shelf Research*, 81, 67–79.

Krug, M., D. Schilperoort, F. Collard, M. W. Hansen, M. and Rouault (2018), Signature of the Agulhas Current in high resolution satellite derived wind fields, *Remote Sensing of Environment*, 217, 340-351.

Large, W. G., J. C. McWilliams, and S. C. Doney (1994), Oceanic vertical mixing: A review and a model with a nonlocal boundary layer parameterization, *Reviews of Geophysics*, 32(4), 363–404.

Leber, G. M., and L. M. Beal (2014), Evidence that Agulhas Current transport is maintained during a meander, *Journal of Geophysical Research: Oceans*, 119, 3806–3817, doi:10.1002/2014JC009802.

Liu, Y., X. S. Liang, and R. H. Weisberg (2007), Rectification of the bias in the wavelet power spectrum. *Journal of Atmospheric and Oceanic Technology*, 24(12), 2093-2012.

Loveday, B., J. Durgadoo, C. Reason, A. Biastoch, and P. Penven (2014), Decoupling of the Agulhas leakage from the Agulhas Current, *Journal of Physical Oceanography*, 44(7), 1776–1797, doi:10.1175/JPO-D-13-093.1.

Loveday, B. R., P. Penven, and C. J. C. Reason (2015), Southern Annular Mode and westerly-wind-driven changes in Indian-Atlantic exchange mechanisms, *Geophysical Research Letters*, 42(12), 4912-4921.

Lutjeharms, J. R. E. (1988), On the role of the East Madagascar current as a source of the Agulhas current, *South African Journal of Science*, 84, 236-238.

Lutjeharms, J. R. E. and H. R. Roberts (1988), The Natal Pulse: An extreme transient on the Agulhas Current, *Journal of Geophysical Research*, 93, 631–645.

Lutjeharms, J. R. E., and R. C. van Ballegooyen (1988), Anomalous upstream retroflection in the Agulhas Current, *Science*, 240, 1770–1772.

Lutjeharms, J., and D. Webb (1995) Modelling the Agulhas current system with FRAM (fine resolution antarctic model), *Deep Sea Research Part I: Oceanographic Research Papers*, 42(4), 523–551.

Lutjeharms, J. R. E., and J. Cooper (1996), Interbasin leakage through Agulhas Current filaments.,*Deep Sea Research Part I: Oceanographic Research Papers*, *43*(2), 213-238.

Lutjeharms, J. R. E., and I. J. Ansorge (2001), The Agulhas Return Current, *Journal of Marine Systems*, 30(1-2), 115–138.

Lutjeharms, J. R. E. (2006), Three decades of research on the greater Agulhas Current, *Ocean Science Discussions*, 3, 939–995.

Lutjeharms, J.R.E. (2006), *The Agulhas Current*, Berlin: Springer.

Malan, N., B. Backeberg, A. Biastoch, J. V. Durgadoo, A. Samuelsen, C. Reason, and J Hermes (2018), Agulhas Current meanders facilitate shelf-slope exchange on the Eastern Agulhas Bank, *Journal Geophysical Research: Oceans*, 123, 4762–4778, https://doi.org/10.1029/2017JC013602.

Maltrud, M. E., and J. L. McClean, (2005), An eddy resolving global 1/10 ocean simulation, *Ocean Modelling*, 8(1), 31–54.

Mason, E., A. Pascual, and J. C. McWilliams (2014), A new sea surface height–based code for oceanic mesoscale eddy tracking, *Journal of Atmospheric and Oceanic Technology*, *31*(5), 1181-1188.

Marchesiello, P., J. C. McWilliams, and A. Shchepetkin (2003), Equilibrium structure and dynamics of the California Current System, *Journal of physical Oceanography*, *33*(4), 753-783.

McClean, J. L., D. C. Bader, F. O. Bryan, M. E. Maltrud, J. M. Dennis, A. A. Mirin, P. W. Jones, Y. Y. Kim, D. P. Ivanova, and M. Vertenstein (2011), A prototype two- decade fully-coupled fine-resolution CCSM simulation, *Ocean Modelling*, 39(1), 10–30.

Meyer, I., L. Braby, M. Krug, and B. Backeberg (2017), Mapping the ocean current strength and persistence in the Agulhas to inform marine energy development, *Marine Renewable Energy: Resource Characterization and Physical Effects*, 179-215. Springer, Cham.

Middleton, W. (2015), Investigating the Sea Surface Height bias and effects of utilising a Relative wind forcing scheme on the Agulhas Return Current in the regional HYCOM model, *B.Sc (Hons) Thesis,* University of Cape Town.

Minobe, S., A. Kuwano-Yoshida, N. Komori, S. –P. Xie, and R. J. Small (2008) Influence of the Gulf Stream on the troposphere, *Nature*, 452(7184), 206–209.

Nof, D. (1999), Strange encounters of eddies with walls, *Journal of Marine Research*, 57, 739–761.

Ou, H. W. and W. P. W. de Ruijter (1986) Separation of an inertial boundary current from a curved coast, *Journal of Physical Oceanography*, 16: 280-289.

Oki, T. and Y. C. Sud, (1998), Design of Total Runoff Integrating Pathways (TRIP) - A global river channel network, *Earth Interactions*, 2, 1–37.

Okubo, W., (1970), Horizontal dispersion of floatable particles in the vicinity of velocity singularities such as convergencies, *Deep Sea Research*, 17, 445–454.

Park, H., D. Lee, W. –P. Jeon, S. Hahn, J. Kim, J. Kim, J. Choi, and H. Choi (2006), Drag reduction in flow over a two-dimensional bluff body with a blunt trailing edge using a new passive device, *Journal of Fluid Mechanics*, 563, 389–414.

Penven, P., V. Échevin, J. Pasapera, F. Colas, J. Tam, (2005), Average circulation, seasonal cycle and mesoscale dynamics of the Peru Current System: a modelling approach, *Journal of Geophysical Research*. 110, C10021.

Penven, P., J. R. E. Lutjeharms, P. Florenchie, (2006), Madagascar: a pacemaker for the Agulhas Current system? *Geophysical Research Letters*, 33, L17609.

Pivan, X., M. Krug, and S. Herbette (2016), Observations of the vertical and temporal evolution of a Natal Pulse along the Eastern Agulhas Bank, *Journal of Geophysical Research: Oceans*, 121(9), 7108-7122.

Ponsoni, L., B. Aguiar-González, H. Ridderinkhof, and L. R. Maas (2016), The East Madagascar Current: Volume transport and variability based on long-term observations, *Journal of Physical Oceanography*, *46*(4), 1045-1065.

Putrasahan, D., B. P. Kirtman, and L. M. Beal, (2015), Modulation of SST interannual variability in Agulhas leakage region associated with ENSO, *Journal of Climate*, 29.

Quartly, G. D., and M. A. Srokosz (2002), SST observations of the Agulhas and East Madagascar retroflections by the TRMM Microwave Imager, *Journal of Physical Oceanography*, *32*(5), 1585-1592.

Quartly, G. D. and M. A. Srokosz (2004), Eddies in the Southern Mozambique Channel, *Deep-Sea Research II*, 51(1 - 3), 69-83.

Reason, C. J. C., and H. Mulenga (1999), Relationships between South African rainfall and SST anomalies in the southwest Indian Ocean, *International Journal of Climatology: A Journal of the Royal Meteorological Society*, *19*(15), 1651-1673.

Reason, C. (2001), Evidence for the influence of the Agulhas Current on regional atmospheric circulation patterns, *Journal of Climate*, 14(12), 2769–2778.

Renault, L., M. J. Molemaker, J. Gula, S. Masson, and J. C. McWilliams (2016a), Control and Stabilization of the Gulf Stream by Oceanic Current Interaction with the Atmosphere, *Journal of Physical Oceanography*, 46(11), 3439–3453.

Renault, L., M. J. Molemaker, J. C. Mcwilliams, A. F. Shchepetkin, F. Lemarie, D. Chelton, S. Illig, and A. Hall (2016b), Modulation of Wind Work by Oceanic Current Interaction with the Atmosphere. *Journal of Physical Oceanography*, 46(6), 1685–1704.

Renault, L., J. C. McWilliams, and P. Penven (2017), Modulation of the agulhas current retroflection and leakage by oceanic current interaction with the atmosphere in coupled simulations, *Journal of Physical Oceanography*, *47*(8), 2077-2100.

Rennell, J. (1832), *An investigation of the currents of the Atlantic Ocean, and of those which prevail between the Indian Ocean and the Atlantic*, London: J.G. and F. Rivington.

Richardson, P. L., (2007), Agulhas leakage into the Atlantic estimated with subsurface floats and surface drifters, *Deep Sea Research Part I: Oceanographic Research Papers*, 54(8), 1361–1389.

Ridderinkhof, H. and W. P. M. de Ruijter (2003), Moored current observations in the Mozambique Channel, *Deep-Sea Research II,* 50 (12-13): 1933-1955.

Ridderinkhof, W., D. Le Bars, A. S. von der Heydt, and W. P. M. de Ruijter (2013), Dipoles of the South East Madagascar Current, *Geophysical Research Letters,* 40, 558–562, doi:10.1002/grl.50157.

Rio, M. -H., S. Mulet, and N. Picot (2014), Beyond GOCE for the ocean circulation estimate: Synergetic use of altimetry, gravimetry, and *in-situ* data provides new insight into geostrophic and Ekman currents, *Geophysical Research Letters*, *41.* doi: 10.1002/2014GL061773.

Roberts, M. J. (2005), Chokka squid (Loligo vulgaris reynaudii) abundance linked to changes in South Africa's Agulhas Bank ecosystem during spawning and the early life cycle, *ICES Journal of Marine Science*, 55, doi:10.1016/j.icesjms.2004.10.002.

Roberts, M. J., C. D. van der Lingen, C. Whittle, and M. van den Berg (2010), Shelf currents, lee-trapped and transient eddies on the inshore boundary of the Agulhas Current, South Africa: their relevance to the KwaZulu-Natal sardine run, *African Journal of Marine Science*, 32(2), 423–447, doi:10.2989/1814232X.2010.512655.

Rouault, M., A. M. Lee-Thorp, and J. R. E. Lutjeharms (2000), The atmospheric boundary layer above the Agulhas Current during alongcurrent winds, *Journal of Physical Oceanography*, *30*(1), 40-50.

Rouault, M., S. A. White, C. J. C. Reason, J. R. E. Lutjeharms, and I. Jobard (2002), Ocean–atmosphere interaction in the Agulhas Current region and a South African extreme weather event, *Weather and Forecasting*, *17*(4), 655-669.

Rouault, M., and J. R. E. Lutjeharms (2003), Estimation of sea-surface temperature around southern Africa from satellite-derived microwave observations. *South African Journal of Science*, 99:489–494.

Rouault, M. J., and P. Penven (2011), New perspectives on Natal Pulses from satellite observations, *Journal of Geophysical Research*, 116, C07013, doi:10.1029/ 2010JC006866.

Saetre, R. and J. Da Silva (1984) The circulation of the Mozambique Channel, *Deep-Sea Research.* 31: 508-585.

Sasaki, H., Y. Sasai, S. Kawahara, M. Furuichi, F. Araki, A. Ishida, Y. Yamanaka, Y. Masumoto and H. Sakuma (2004), A series of eddy-resolving ocean simulations in the world ocean-OFES (OGCM for the Earth Simulator) project, In *OCEANS'04. MTTS/IEEE TECHNO-OCEAN'04*, 3, 1535-1541.

Schouten, M. W., W. P. M. de Ruijter, and P. J. van Leeuwen (2002), Upstream control of Agulhas ring shedding, *Journal of Geophysical Research*, 107(C8), 3109, doi:10.1029/2001JC000804.

Schouten, M. W., W. P. M. de Ruijter, P. J. van Leeuwen, and H. Ridderinkhof (2003), Eddies and variability in the Mozambique Channel, *Deep Sea Research II*, 50:1987–2003.

Scott, R. B., and Y. Xu, (2009), An update on the wind power input to the surface geostrophic flow of the World Ocean, *Deep Sea Research Part I: Oceanographic Research Papers*, 56(3), 295–304.

Seo, H., A. J. Miller, and J. R. Norris (2015), Eddy-wind interaction in the California Current System: dynamics and impacts, *Journal of Physical Oceanography*, 46(2015), 439–459.

Shi, C., and D. Nof (1993), The splitting of eddies along boundaries, *Journal of Marine Research*, 51, 771–795.

Shi, C., and D. Nof (1994), The destruction of lenses and generation of wodons, *Journal of Physical Oceanography*, 24, 1120–1136.

Siedler, G., M. Rouault, A. Biastoch, B. Backeberg, C. J. C. Reason, and J. R. E. Lutjeharms (2009) Modes of the southern extension of the East Madagascar Current, *Journal of Geophysical Research,* 114(C1), DOI: 10.1029/2008JC004921.

Steele, M., R. Morley, and W. Ermold (2001), PHC: A global ocean hydrography with a high-quality Arctic Ocean, *Journal of Climate*, *14*(9), 2079-2087.

Stramma, L. and J. R. E. Lutjeharms (1997), The flow field of the subtropical gyre in the South Indian Ocean, *Journal of Geophysical Research*, 99, 14053- 14070.

Thoppil, P. G., J. G. Richman, and P. J. Hogan (2011), Energetics of a global ocean circulation model compared to observations, *Geophysical Research Letters,* 38(15).

Torrence, C. and G. P. Compo (1998), A practical guide to Wavelet Anaylsis *Bulletin of American Meteorological Soceity*,79, 61–78.

Tsugawa, M., and H. Hasumi (2010), Generation and growth of the Natal Pulse, *Journal of Physical Oceanography*, 40, 1597–1612.

Van der Vaart, P. C. F., and W. P. M. de Ruijter (2001), Stability of western boundary currents with an application to pulse like behavior of the Agulhas Current, *Journal of*

Physical Oceanography, 31(9), 2625–2644.

van Leeuwen, P. J., W. P. M. de Ruijter, and J. R. E. Lutjeharms (2000), Natal Pulses and the formation of Agulhas rings, *Journal of Geophysical Research*, 105, 6425–6436, doi:10.1029/1999JC900196.

Vermeulen, E. A., B. Backeberg, J. Hermes and S. Elipot (2019), Investigating the relationship between volume transport and sea surface height in a numerical ocean model, Ocean Science, 15(3).

Walker, N. D. (1990), Links between South African summer rainfall and temperature variability of the Agulhas and Benguela Current systems, *Journal of Geophysical Research: Oceans*, *95*(C3), 3297-3319.

Wallcraft, A. J., H. E. Hurlburt, E. J. Metzger, R. C. Rhodes, J. F. Shriver, and O. M. Smedstad (2002), Real-time ocean modelling systems, *Computing in Science & Engineering*, *4*(2), 50-57.

Wallcraft, A. J., E. J. Metzger, and S. N. Carroll (2009), *Software design description for the hybrid coordinate ocean model (HYCOM), Version 2.2* (No. NRL/MR/7320--09-9166), Naval Research Lab Stennis Space Center MS Oceanography Div.

Weijer, W., W. P. de Ruijter, H. A. Dijkstra, and P. J. van Leeuwe (1999), Impact of inter- basin exchange on the Atlantic overturning circulation, *Journal of Physical Oceanography*, 29(9), 2266–2284.

Weiss, J. (1991), The dynamics of enstrophy transfer in two-dimensional hydro-dynamics*, Physica D,* 48, 273–294.

Zamudio, L., E. J. Metzger, amd P. Hogan (2011), Modelling the seasonal and interannual variability of the northern Gulf of California salinity, *Journal of Geophysical Research: Oceans*, *116*(C2).

Zhai, X., H. L. Johnson, and D. P. Marshall (2010), Significant sink of ocean-eddy energy near western boundaries, *Nature Geoscience*, 3, 608–612, doi:10.1038/NGEO943.